JPL PUBLICATION 82-13

Stirling Laboratory Research Engine: Preprototype Configuration Report

Frank W. Hoehn

February 15, 1982

NASA
National Aeronautics and
Space Administration

Jet Propulsion Laboratory
California Institute of Technology
Pasadena, California

TECHNICAL REPORT STANDARD TITLE PA

1. Report No. JPL Pub.82-13	2. Government Accession No.	3. Recipient's Catalog No.
4. Title and Subtitle STIRLING LABORATORY RESEARCH ENGINE: PREPROTOTYPE CONFIGURATION REPORT		5. Report Date February 15, 1982 6. Performing Organization Code
7. Author(s) Frank W. Hoehn		8. Performing Organization Report N
9. Performing Organization Name and Address JET PROPULSION LABORATORY California Institute of Technology 4800 Oak Grove Drive Pasadena, California 91109		10. Work Unit No. 11. Contract or Grant No. NAS 7-100 13. Type of Report and Period Covere JPL Publication
12. Sponsoring Agency Name and Address NATIONAL AERONAUTICS AND SPACE ADMINISTRATION Washington, D.C. 20546		14. Sponsoring Agency Code

15. Supplementary Notes

(RTOP : 778-35-05-050)

16. Abstract

A NASA sponsored project to validate the concept of a simple Stirling research engine that could be used by industrial, university and government laboratories has been completed at the Jet Propulsion Laboratory (JPL). Accomplishments include the conceptual and final designs, hardware fabrication and the experimental validation of a preprototype Stirling Laboratory Research Engine (SLRE). The engine design is based entirely on technical information openly available, without proprietary restrictions. Also completed was a task to identify the potential markets for research engines of this type. An analytical effort was conducted to provide a Stirling Cycle Computer Model. The versatile engine is a horizontally opposed, two-piston, single-acting Stirling engine with a split crankshaft drive mechanism; special instrumentation is installed at all component interfaces. Results of a thermodynamic energy balance for the system are reported. Also included are the initial engine performance results obtained over a range of speeds, working pressures, phase angles and gas temperatures. Efforts to date with the preprototype SLRE have demonstrated the potential for a Stirling research engine to support the laboratory requirements of educators and researchers.

17. Key Words (Selected by Author(s))	18. Distribution Statement
	Unclassified - Unlimited

19. Security Classif. (of this report)	20. Security Classif. (of this page)	21. No. of Pages	22. Price
Unclassified	Unclassified	92	

JPL 0184 1M

JPL PUBLICATION 82-13

Stirling Laboratory Research Engine: Preprototype Configuration Report

Frank W. Hoehn

February 15, 1982

NASA

National Aeronautics and
Space Administration

Jet Propulsion Laboratory
California Institute of Technology
Pasadena, California

ABSTRACT

A NASA sponsored project to validate the concept of a simple Stirling research engine that could be used by industrial, university and government laboratories has been completed at the Jet Propulsion Laboratory (JPL). Accomplishments include the conceptual and final designs, hardware fabrication and the experimental validation of a preprototype Stirling Laboratory Research Engine (SLRE). The engine design is based entirely on technical information openly available, without proprietary restrictions. Also completed was a task to identify the potential markets for research engines of this type. An analytical effort was conducted to provide a Stirling Cycle Computer Model. The versatile engine is a horizontally opposed, two-piston, single-acting Stirling engine with a split crankshaft drive mechanism; special instrumentation is installed at all component interfaces. Results of a thermodynamic energy balance for the system are reported. Also included are the initial engine performance results obtained over a range of speeds, working pressures, phase angles and gas temperatures. Efforts to date with the preprototype SLRE have demonstrated the potential for a Stirling research engine to support the laboratory requirements of educators and researchers.

ACKNOWLEDGMENTS

Many people within the Jet Propulsion Laboratory (JPL) as well as outside consultants and vendors have made significant contributions to successfully complete the design, fabrication and experimental evaluation of a preprototype Stirling Laboratory Research Engine (SLRE). The project was sponsored by the NASA Office of Aeronautics and Space Technology. The NASA Program Manager was John L. Anderson, Energy Systems Division.

This report was written by Frank W. Hoehn, JPL Task Manager. Special thanks are extended to Allan McDougal for the preliminary analysis and engineering design and to Howard Miller for translating this effort into engine hardware. Thanks is given to Fred Vote and Gerry Meisenholder of JPL, for their individual contributions and helpful managerial suggestions.

Appreciation is also expressed to the following technical specialists who were retained as consultants during the design and analysis phases of the program: Dr. Graham Walker, Professor of Mechanical Engineering at the University of Calgary; Mr. Hans Hermann, Chief Engineer, Drake Engineering Corporation; and Dr. Michael J. Maurer, Professor of Mechanical Engineering at the California State University at Los Angeles.

CONTENTS

Tables

Figures

I. INTRODUCTION

This report was prepared for the National Aeronautics and Space Administration (NASA), Office of Aeronautics and Space Technology, Energy Systems Division. The work was conducted by the Propulsion Systems Section, Control and Energy Conversion Division of the Jet Propulsion Laboratory (JPL). The report presents a summary of work accomplished under NASA Contract NAS7-100 from May 1976 through September 1981.

Stirling engines offer the potential of high conversion efficiency, wide fuel tolerances and low emissions. The basic engine technology, however, resides largely in Europe. To enhance the possibility of Stirling engines making significant contributions to U.S. energy conservation, the research and technology base in the U.S. must be broadened.

The overall objective of this program is to validate the concept of a simple, Stirling Laboratory Research Engine (SLRE) that could be used by academic, industrial and government laboratories to gain an understanding of Stirling principles and to conduct research investigations. The approach was to design, build, operate and characterize a Stirling research engine which would serve as a preprototype engine.

The SLRE was designed through an analytical effort based on non-proprietary analytical and technical information. The computer model developed for this purpose was subsequently refined and verified through an iterative process based on experimental data from the SLRE tests. In addition, a survey of potential laboratory users of the SLRE was conducted by JPL in an effort to determine the interest and needs for this type of engine.

This report describes the preprototype SLRE design and the experimental results obtained during operation of the SLRE over a range of engine speeds, working pressures, gas temperatures and phase angles.

The SLRE is currently being used at JPL for an experimental research study to characterize the performance of Stirling cycle regenerators. Results of this task, being undertaken in cooperation with a university researcher, will be reported separately.

II. SUMMARY

A preprototype Stirling Laboratory Research Engine was successfully designed and fabricated, then experimentally tested at JPL over a wide range of operating conditions. The preliminary design was based on first-order analytical techniques using a modified Schmidt theory. This work represents a significant first step of validating the concept of a simple laboratory engine, one that is completely free of proprietary constraints and restrictions.

High engine efficiency was not a basic requirement for this first design. However, tests conducted after less than five hours of engine operation showed a brake thermal efficiency of about 18%, and an indicated thermal efficiency of 32%. These figures are expected to increase, because system losses can be reduced as more operating experience is accumulated.

As might be expected for the first engine design, a number of problems where encountered. For example, various types of heater heads were evaluated and the indirect resistance type was finally chosen. Successful development and operation of this heater verified the correctness of that choice.

Prior to operating the engine, both fluid and mechanical friction were accurately measured and characterized through engine motoring tests. Analysis of these results showed positive engine operation could be expected. That was verified by successful engine starting and the demonstration of net brake horsepower output.

Next came a series of performance validation tests. Although the engine was run within a limited speed range, its operation was at or near the design-rated levels of gas temperature, phase angle, and pressure conditions. Some of the major technical achievements which resulted from these tests were:

(1) System indicator diagrams were obtained from both the compression and expander spaces.

(2) Transient pressure and mean temperature were measured and recorded at all component interfaces.

(3) Steady-state data were taken from 34 separate test points over a wide range of working pressures, engine speeds, phase angles, and gas temeratures.

(4) Thermodynamic energy balance was derived for the total engine systems.

(5) Reliability and effectiveness of the redesigned electric heater was demonstrated.

(6) Engine control strategy was tested and validated over a variety of operating conditions.

These tests have clearly identified several areas where improvement could be made to achieve increases in both engine power and efficiency. However, optimization of the engine design was beyond the scope of this program.

A Stirling Cycle Computer Model (SCCM) has been developed using experimental test data for a number of the inputs. However, several areas have been identified where significant improvement and refinement in the model are possible. These refinements deal with changes in the heat transfer modeling procedures, and the regenerator model appears to be the most significant area of potential improvement.

Predominantly favorable results plus many positive comments and suggestions have come from a survey conducted by mail to identify potential SLRE users, and to determine their requirements regarding such a research tool. Questionnaires returned to JPL were received from academic, industrial and government areas worldwide. Many respondents expressed a genuine interest in acquiring a future and more advanced version of a commercially produced SLRE. Desired key attributes were well defined as were potential uses for the SLRE and Stirling engines in general.

III. ENGINE DESIGN PHASE

A. BACKGROUND

The fully developed Stirling engine can perform most of the functions that are currently being done by internal combustion engines, and with generally higher efficiencies. In addition to their excellent thermodynamic efficiency, Stirling engines have several characteristics which make them suitable for solar energy conversion, for multifuel use, for use where low noise levels are required, and for regions where low environmental pollution levels are mandatory. Potential applications include the generation of electricity from solar insolation, auxiliary power supplies for the military, underground propulsion, marine propulsion, and as the propulsion source for conventional ground transportation vehicles. The reader is referred to G. Walker (Ref. 1) of the University of Calgary for a theoretical and complete discussion of the Stirling cycle and its applications.

Interest at JPL in a laboratory-type Stirling cycle engine which could support basic research began in 1976. This interest was stimulated to a large degree by the then ongoing Ford/ERDA/NASA development program to adapt Stirling engines for automotive use. One phase of this work utilized a Philips 4-215 double-acting (DA) Stirling engine installed in a 1973 Ford Torino passenger car. Details of this engine related work have been described by van Giessel (Ref. 2) of N. V. Philips Gloeilampenfabrieken. This earlier engine development activity had some influence in selecting the basic design specifications for the SLRE.*

It was desireable for the SLRE to have bore and stroke dimensions typical of "real" Stirling engines. Several comparisons can be made showing similarities between the laboratory engine design and the Ford/Philips 4-215 swash-plate drive automotive engine. These comparisons are presented in Table 1.

In a very general sense, the SLRE engine represents approximately a one-twelfth scale version of the Ford/Philips 4-215 engine (i.e., it operates at one-third the pressure level and has one-fourth the number of active cylinders). The approach used to develop the preliminary engine design is described in the next section.

B. PREPROTOTYPE ENGINE DESIGN

The engine design approach is diagrammed in Figure 1. The fundamental approach used was consistent with preliminary design philosophy of any new heat engine development which utilizes basic theory and known component characteristics.

*The approach was to base estimates, projections, and scalings on actual engine data whenever possible. At that time, the Ford/Philips 4-215 engine was the only Rinia-type Stirling engine for which an experimental performance data map was available in open literature.

Table I. Comparison of Engine Design Specifications

Parameters	JPL SLRE	Ford 4-215 (Ref)
Design Power, hp (kW)	12 (9)	170 (127)
Design Pressure, psia (N/mm^2)	1000 (7)	2844 (20)
Working Gas	Hydrogen	Hydrogen
Cylinder Bore, in (mm)	2.87 (73)	2.87 (73)
Piston Stroke, in (mm)	2.12 (54)	2.05 (52)
Number Cylinders	2 (SA)	4 (DA)
Number Regenerators	1	8
Number Coolers	1	8
Hot Gas Temperature, °F(°C)	1400 (760)	1382 (750)
Cold Gas Temperature, °F (°C)	150 (65)	148 (64*)
Drive System	Split C'shaft	Swashplate
Technology Base	Original Design	Philips

* Cooling Water Temperature

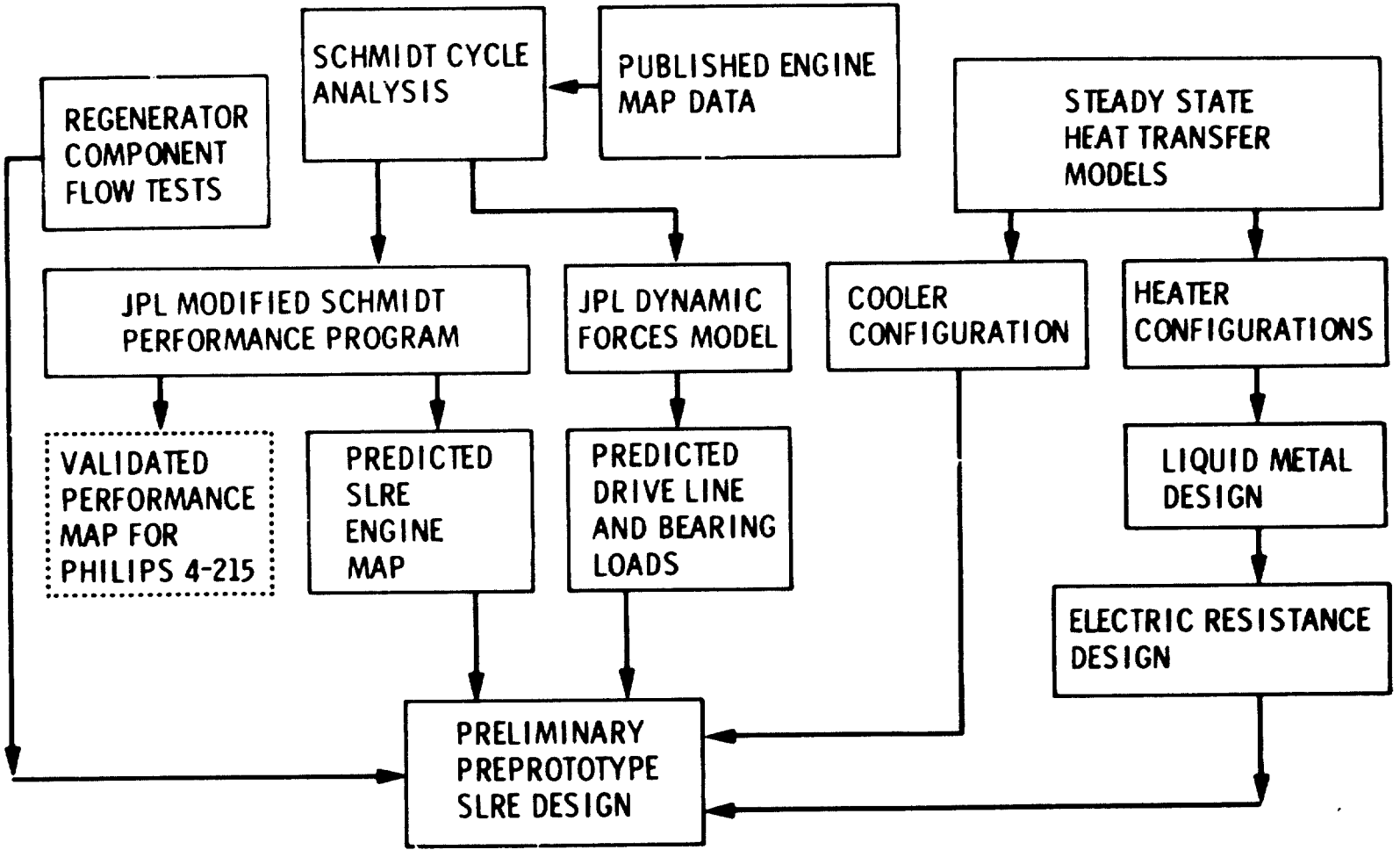

Figure 1. Preprototype Engine Design Approach

1. Analytical Performance Model

The primary analytical tool used in the design was that developed much earlier by Schmidt (Ref. 3). This is a highly idealized analysis technique which assumes isothermal compression and expansion, and perfect regeneration. The principal assumptions used in the analysis have been identified by Walker (Ref. 1) and are listed below:

(1) The regenerative process is perfect.

(2) The instantaneous pressure is the same throughout the system.

(3) The working fluid obeys the characteristics gas equation, $PV = \rho RT$.

(4) There is no leakage, and the mass of working fluid remains constant.

(5) The volume variations in the working space occur sinusoidally.

(6) There are no temperature gradients in the heat-exchangers.

(7) The cylinder wall and piston temperatures are constant.

(8) There is perfect mixing of the cylinder contents.

(9) The temperature of the working fluid in the ancillary spaces is constant.

(10) The speed of the machine is constant.

(11) Steady-state conditions exist.

One major limiting feature of the Schmidt analysis is that the calculated thermal efficiency is always equal to the Carnot efficiency:

$$\eta_{Thermal} = \eta_{Carnot} = 1 - \frac{Tc}{Th} \qquad (1)$$

where T_c = Cold (compression) gas temperature,

and T_h = Hot (expansion) gas temperature.

The only engine operating conditions which affect the calculation are the two constant temperature reservoirs and therefore thermal efficiency is always overestimated. A computer program based on the Schmidt analysis was written by Finegold (Ref. 4) for this effort. The program uses scaling factors and was reasonably accurate in predicting brake horsepower and thermal efficiency at the maximum efficiency point of the Ford/Philips 4-215 engine. The scaling factors were calculated in a bivariant linear interpolation subroutine as a function of engine speed and mean pressure level. Accuracy of the modified

Schmidt performance program was checked by comparing predicted values with actual published performance results for the Ford/Phillips 4-215 engine (Ref. 5).

When confidence in the analytical procedure was established, the program was used to predict the performance of the SLRE. Prediction accuracy is contingent on future optimization of the preprototype SLRE to the same level of development as the Ford/Philips 4-215 engine. The experimental results reported herein for the SLRE represent only the initial performance data obtained with the first engine assembly.

As shown in Figure 1, the Schmidt program provided the basic framework for another analytical tool - the JPL Dynamic Forces Model. A detailed description of this analysis technique has been presented by Hoehn (Ref. 6). A brief summary of the work follows.

2. Analytical Dynamics Model

The total dynamic engine forces are produced by an unbalanced pressure loading on the pistons and by inertia of the reciprocating parts. They are computed by the model as a function of crank angle for various engine operating conditions. These two forces combine to produce a net force on the piston that is transmitted along the connecting rod to the crankshaft. The resultant force also produces loads in the piston pin and bearing, main rod bearing, and engine crankshaft bearings. This information was needed to design these critical engine components with an adequate margin of safety.

Gas pressure in the working space of the engine varies about the base (mean) pressure due to cyclic changes in the working volume. The back side of each piston is pressurized to base (buffer) pressure. The differential pressure produces a total force which must be combined algebraically with the inertia forces. The inertia forces depend upon the reciprocating mass and velocity of the moving engine parts. As shown in Figure 2, the velocity of the expander piston is zero at the beginning of the stroke, reaches a maximum near the middle, and decreases to zero again at the end of the stroke. By convention, the velocity has a positive sign when the piston is moving towards the crankshaft. The motion of the two pistons represented by the example of Figure 2 is displaced by a 1.6 rad (90°) phase angle relationship. For a given engine geometry, the piston velocity varies linearly with engine speed.

The calculated gas pressure and inertia forces, shown in Figure 3, for one complete cycle for a given set of engine operating conditions. Unlike conventional internal combustion engines, the gas-pressure forces reverse direction during each cycle depending upon the magnitude of the instantaneous working pressure relative to buffer pressure. The results of Figure 3 were used to compute the internal stresses of the reciprocating engine parts as well as bearing loads.

3. Analytical Heat Exchanger Models

Component designs critical to the operation of the SLRE include those for the heating and cooling heat exchangers. Each consists of tube bundles through which the working fluid flows to either gain or to lose heat. Thermo-

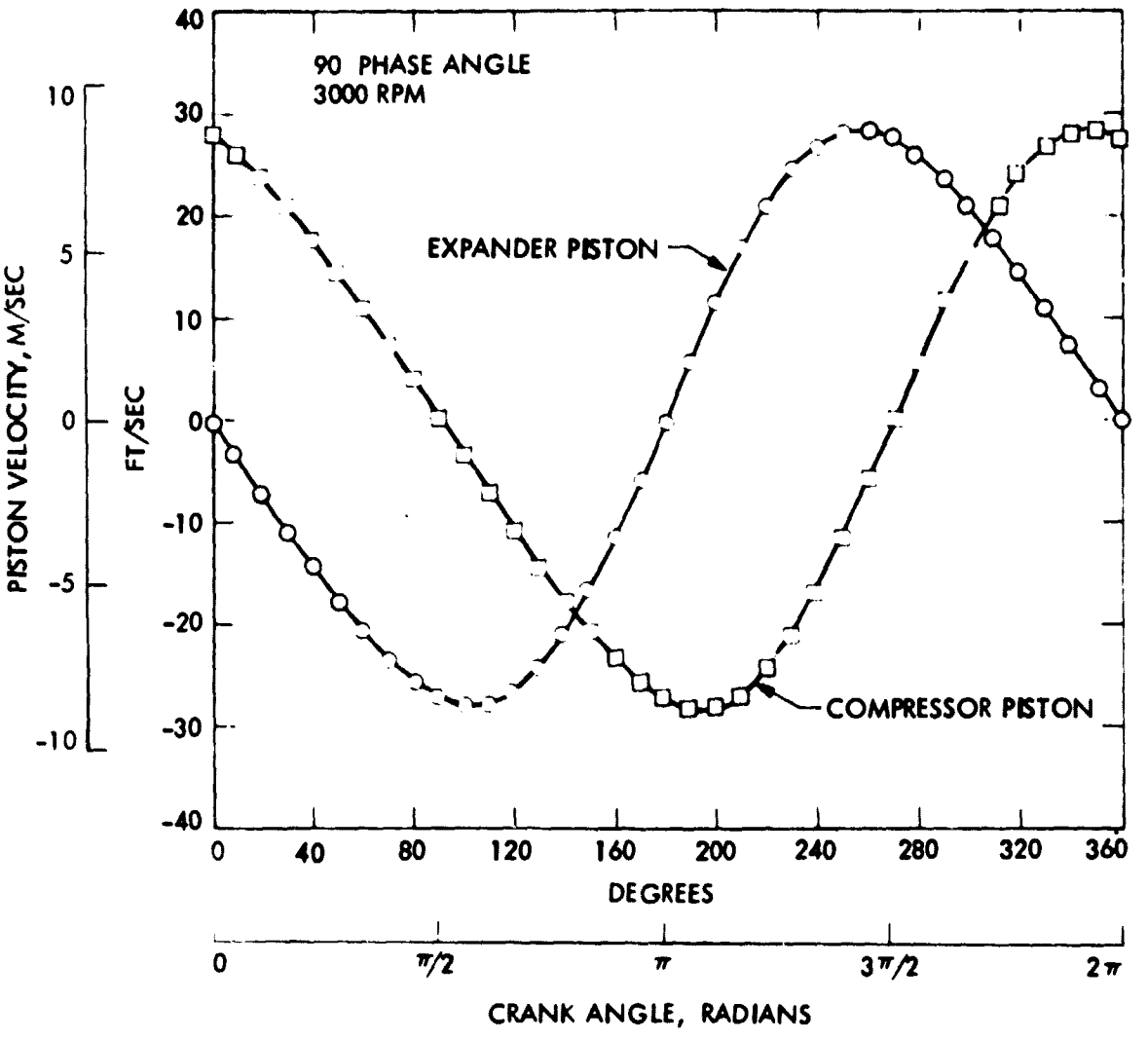

Figure 2. Calculated Variations in Piston Speed

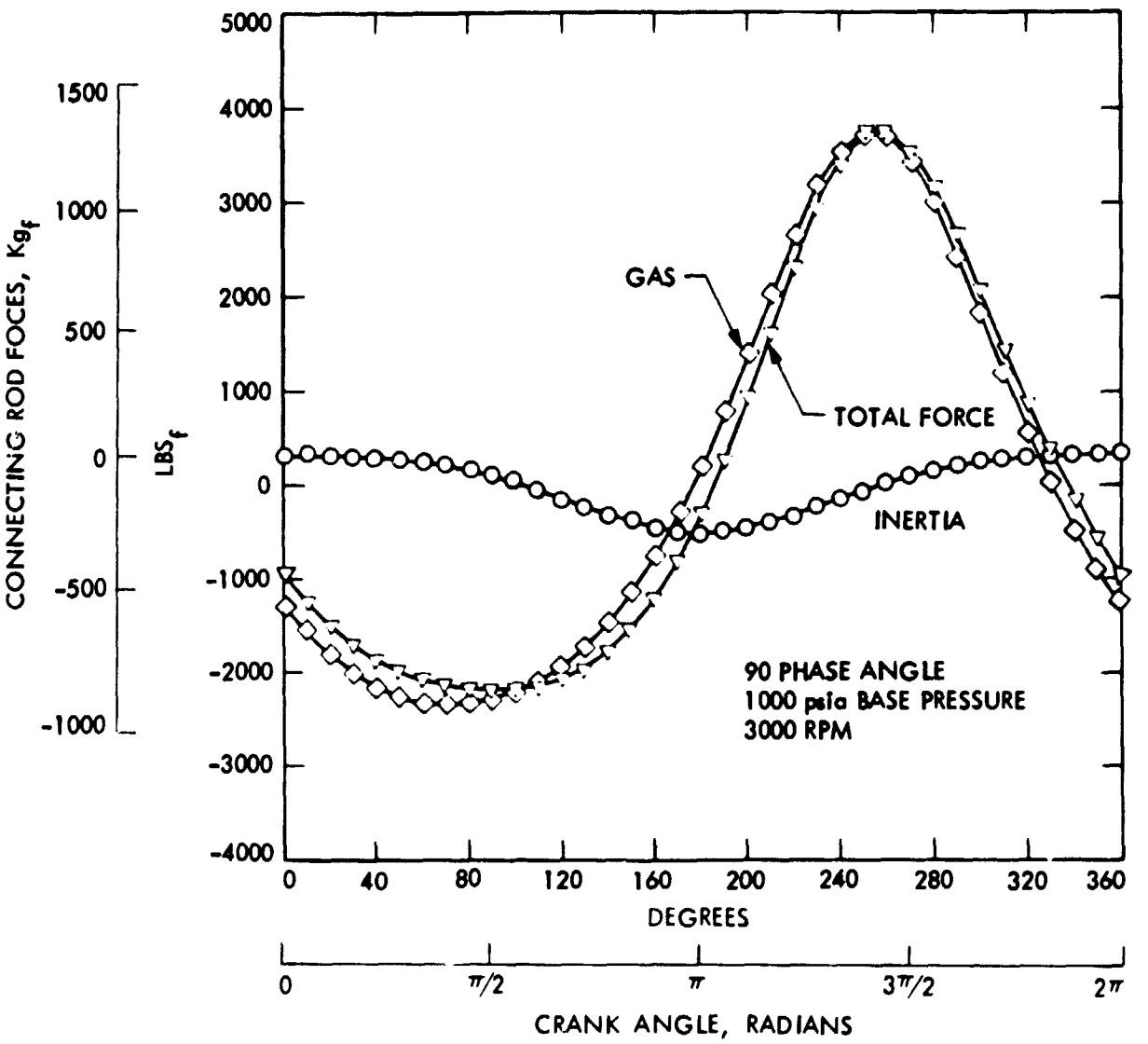

Figure 3. Calculated Combined Rod Forces

dynamic cycle analysis shows that optimum engine performance is obtained when the internal volume of these components is zero and the pressure drop required to cause the working fluid to shuttle back and forth through the tubes is also zero. These attributes can only be approached simultaneously if the tube length is made infinitesimally small. On the other hand, the fluid heat transfer coefficients and the surface area available for heat exchange are dependent upon the number, length, and internal diameter of the tubes. These parameters, in turn, determine the required internal tube volume. The product of the surface area and heat transfer coefficient must not be too small or the temperature difference required to drive heat at the required rate to (or from) the working fluid becomes excessive. So, for practical engine design, a compromise must be made between internal tube volume, acceptable pressure drop, and heat transfer rate between the tube and fluid.

To aid in the design of the heater and cooler sections, two computer programs were written specifically for the purpose of predicting pressure drop for hydrodynamically and thermally developing flow of a compressible fluid in a tube, one for uniform wall heat flux, and the other for uniform wall temperature. Depending on the method used to heat or cool the tubes, one of these two thermal boundary conditions apply. It was quickly recognized that the level of effort required to solve the system of non-linear partial differential equations which truly describe the reciprocating (transient), two-dimensional, developing flow of a compressible fluid was very complex and probably not justifiable. Instead, it was assumed that the pressure drop calculated by "equivalent" steady, one-dimensional, compressible flow theory would yield information adequate for preliminary design purposes. A detailed description of this analytical design procedure has been reported by Hoehn (Ref. 6).

4. Regenerator Selection

The regenerator separates the hot and cold working spaces of the engine. It also serves the important function of storing heat as the working gas flows from the hot to the cold space of the engine, then returns this heat to the gas as it passes in the reverse direction. The optimization of a regenerator matrix is a difficult task because the Stirling engine regenerator must satisfy a number of conflicting requirements. Some of these requirements have been identified by Walker (Ref. 1) and are repeated below:

(1) To improve overall effectiveness of the regenerator, the ratio of the heat capacity of the matrix to that of the gas should be a maximum. This can be achieved with a large, dense matrix.

(2) A large pressure drop across the regenerator results in a decrease in engine power and engine thermal efficiency. The gas friction loss is minimized by a highly porous matrix.

(3) The regenerator dead space must be made as small as possible, since its size influences the ratio of maximum-to-minimum volume of working space, which in turn directly affects the ratio of maximum-to-minimum pressure. A small dead space is achieved by a dense matrix.

(4) To improve performance, the maximum surface area must be exposed for heat transfer between the working gas and the matrix. Therefore, the matrix should be finely divided, with preferential thermal conduction at a maximum normal to the flow, and a minimum in the direction of the flow.

All of these conflicting requirements could not be satisfied with a single regenerator design. A compromise was therefore made in the selection of a matrix for the preprototype SLRE. In the absence of a simulation test apparatus, where a given matrix could be tested under cyclic conditions, the selection was based on the results of steady state, cold flow tests of several candidate matrices. Based upon these gaseous nitrogen flow tests, a parallel plane type matrix was selected. Additional details of the regenerator design are presented in Section IV.A.

C. PROBLEM AREAS AND SOLUTIONS

Approximately 80 engineering drawings were made and released for component fabrication. Component parts of the SLRE were machined by both the JPL Fabrication Services Division as well as numerous outside vendors. The initial preprototype engine assembly was completed and proof tested to 17.2×10^6 N/m^2 (2500 psia) using nitrogen gas.

This section of the report discusses several problem areas identified during the initial test effort and the solutions devised to correct them. Two major problems, low starting torque and heater head developments, caused a significant impact on the planned scheduled and will be decribed first.

1. Engine Cranking/Starting Problems

The motoring dynamometer provides the engine cranking function to start the SLRE. During cranking, the gas working pressure and temperature are gradually increased until self-sustaining operation is achieved. A problem was encountered during early attempts to start the engine because of high motoring torque requirements during the cranking cycle. This caused an overload condition on the dynamometer motor.

Several contributing factors were identified. First, the preprototype engine was observed to exhibit higher friction characteristics than originally estimated.* The second factor contributing to the engine cranking problem relates to the limited torque capacity of the motoring dynamometer during low speed operation. When the dynamometer was selected, it was assumed that its 11.2 kW (15 hp) rated electric motor would have no problem in turning and starting a 8.9 kW (12 hp) Stirling engine. However, this was not the case, and the problem is graphically illustrated by the example in Figure 4 and explained below.

---

*Results of subsequent experimental tests to characterize both the mechanical and fluid friction for the SLRE are presented in Section V.A. These tests were made to identify those sources of friction which could possibly be reduced by engine design changes.

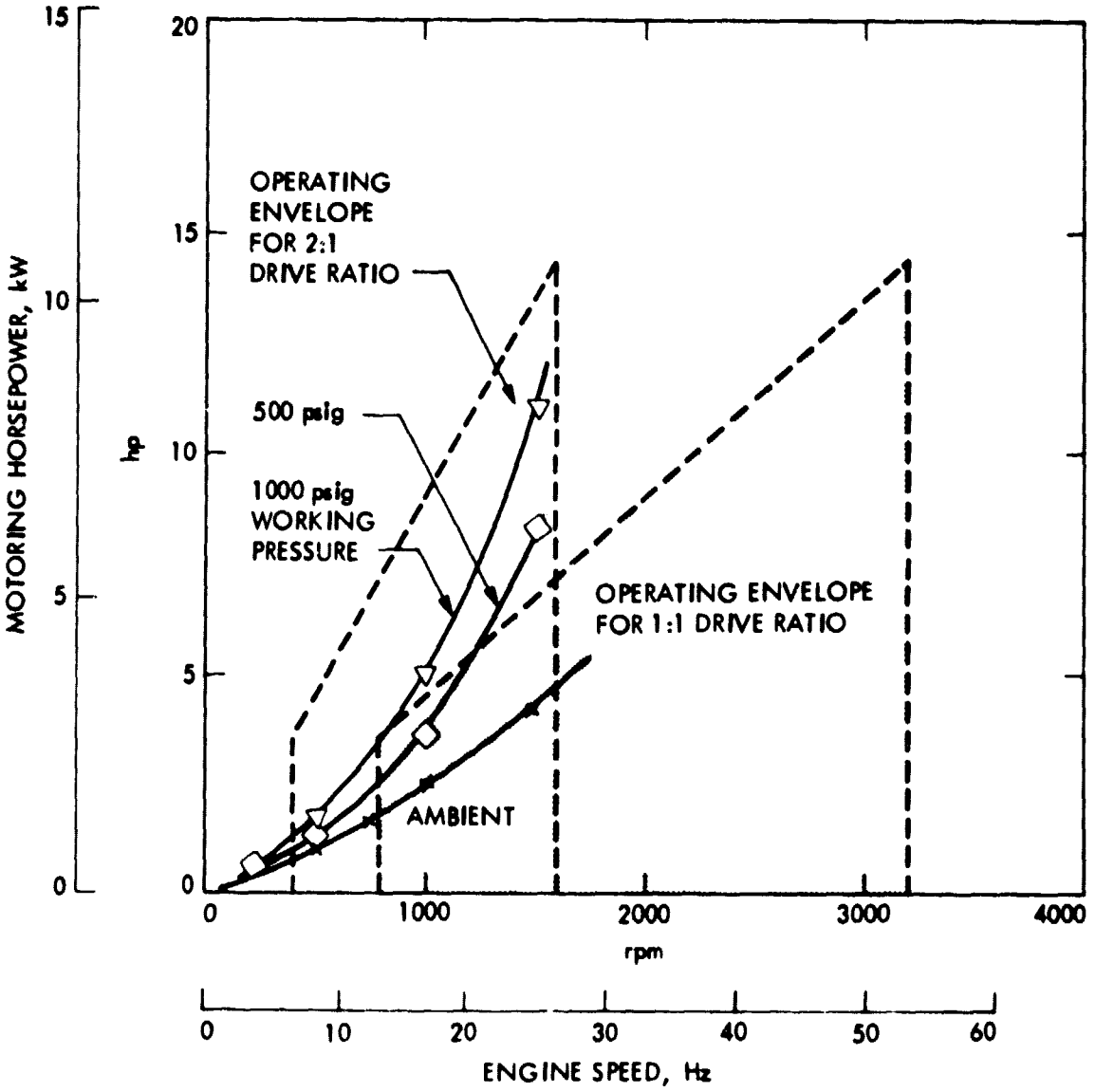

Figure 4. Motoring Characteristics for Two Different Drive Ratios

The original engine design specified equal diameter pulleys for both the engine flywheels and the common dynamometer input shaft. This 1:1 drive line ratio produced a system operating range shown in Figure 4 and resulted in equal speeds for both the engine and dynamometer. The operating range is restricted on the high side by the maximum design speed of the electric motor and on the low side by the limitations of the electronic speed control device used to regulate engine speed. The diagonal line represents the maximum deliverable motoring power (speed dependent) which, if exceeded, results in excessive field current and eventual circuit overloading.

Several data points obtained over a range of engine speeds during three different constant pressure motoring tests are also shown Figure 4. These data were obtained at ambient temperature. No cranking problems were observed at ambient pressure since adequate reserve power is available from the electric motor. However, tests made at 3.4×10^6 N/m^2 (500 psig) demonstrate only marginal operation in terms of motoring capability but added margin is available as the cycle indicated power rises with increasing hot gas temperatures.

The problem of marginal cranking power was resolved by modifying the drive line system. This was accomplished by incorporating a 2:1 speed ratio between the engine and dynamometer so that the dynamometer turns twice the engine speed. The new operating range of the dynamometer is also shown in Figure 5. The result of this change was to double the deliverable motoring power for a given speed at the sacrifice of halving the attainable top speed of the SLRE. As shown, the SLRE can now be motored at its mean design pressure of 6.9×10^6 N/m^2 (1000 psig) without overloading the electrical circuits. As discussed later, this modification permitted the preprototype Stirling engine to be cranked and successfully started (i.e., the indicated cycle power exceeds the internal system losses).

2. Engine Heater Head Problems

The second major problem involved the design of the preprototype heater. The original electric heater head was designed to operate using the reflux boiler principle using liquid sodium as the heat transfer medium. Although this heater performed as expected during several engine motoring tests, sodium containment problems developed after repeated high temperature operations. The cost and schedule impact of redesigning this heater for leakproof operation was judged to be unacceptable, so an alternate, resistance type electric heater head was designed and fabricated for use with the SLRE. The following paragraphs give a more complete description of the heater configurations and discusses the specific problems associated with each of them.

a. Liquid Metal Heater. The original heater design was based on the reflux boiler principle using sodium as the two-phase fluid transport medium. This design had the potential of providing near-isothermal conditions between the sodium and heat exchanger tubes. Heat was supplied to the working gas by the condensation of sodium vapors on the outside surface of the heat exchanger tubes. The sodium was heated to its equilibrium boiling point using ten immersion heaters located in the bottom of the reflux boiler. The condensing vapor returned to the liquid pool by gravity. The condensed liquid reheated

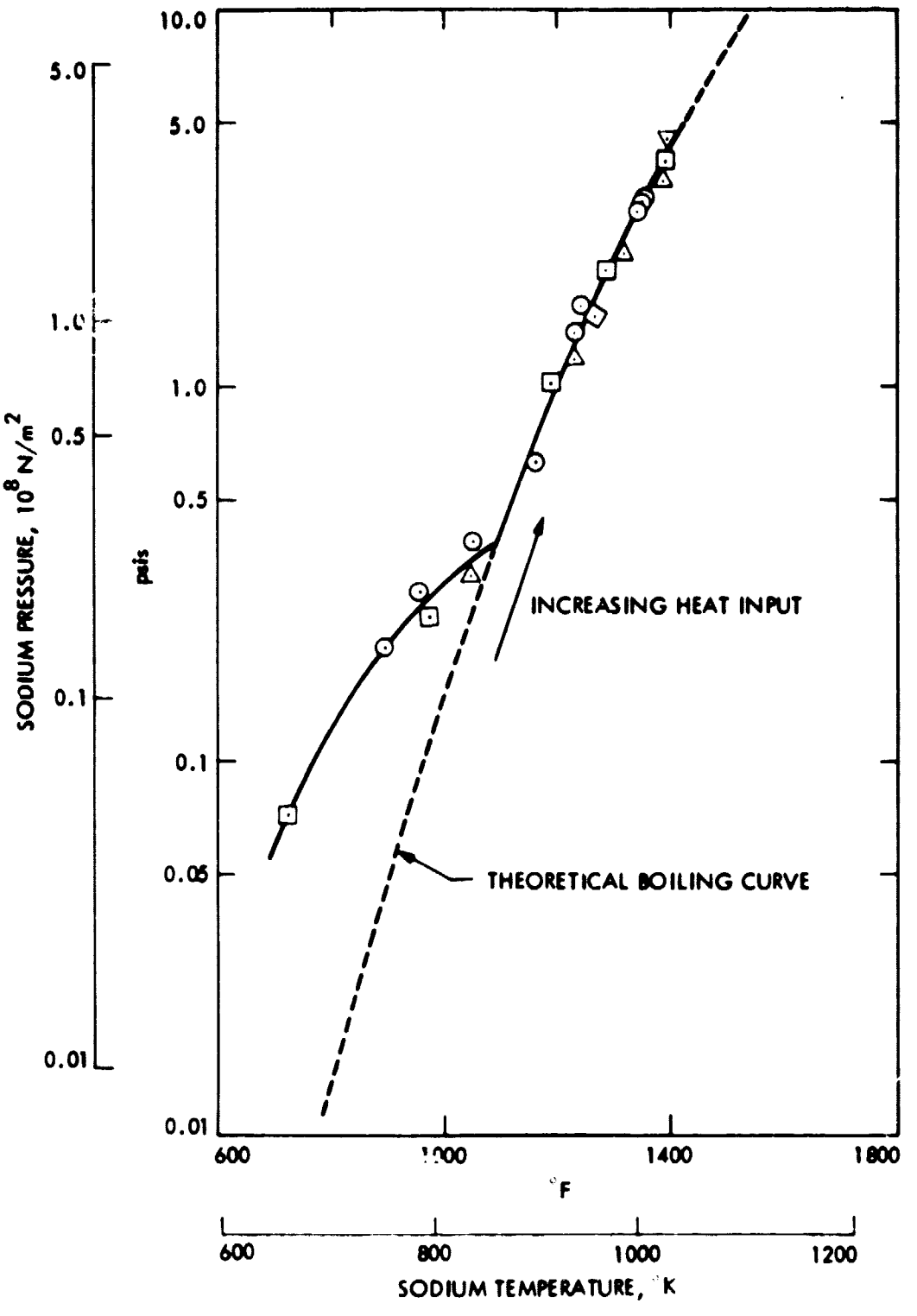

Figure 5. Liquid Metal Heater Operating Characteristics

to the boiling point by the electric heaters, thus achieving the continuous "refluxing" action. The actual temperature achieved with the device was dependent on the equilibrium pressure within the sodium containment vessel. The system was initially evacuated to less than 1 kN/m^2 (0.05 psia) using a commercial vacuum pump. The vapor-to-liquid phase change provides an effective heat transfer method due to the high latent heat of vaporization for sodium.

As part of the original design procedure, calculations were made to ensure that the heat generated by the electric immersion elements could be adequately transferred to the liquid sodium without exceeding the predicted burnout heat flux. Burnout could occur if the predominant heat transfer mechanism at the heater sheath surface changed from nucleate to film boiling. However, these design calculations showed that this condition should not occur and therefore present no problem.

The experimentally measured operating characteristics of the liquid metal heater are shown in Figure 5. The dashed line represents the theoretical boiling curve for sodium when in equilibrium with its own vapor. The boiling temperature is seen to increase with increasing heat addition and produces a corresponding increase in vapor pressure. At the rated power condition of the engine, the sodium was calculated to reach 1089°K (1500°F) at 55.1 kN/m^2 (8.0 psia). A series of experimental data points are plotted on this same figure. The sodium temperatures represent the average measurements from two thermocouples installed in thermowells located below the sodium liquid level. Pressure was measured with a special 0-690 kN/m^2 (0-100 psia) Statham transducer located in the vapor space of the sodium reflux vessel.

The experimental data plotted presents the transient warm-up characteristics of the system as measured during four separate engine motoring tests. The point at which the experimental data coincides with the theoretical boiling curve represents the liquid-to-boiling transition. As shown, the highest sodium temperature achieved during these early tests was about 1034°K (1400°F).

One operational difficulty was observed with the refluxing system. Following shut-down of the heater power supply, some portion of the liquid sodium solidified and formed a metal coating on individual heater tubes. This coating affected heat transfer on subsequent tests and significantly extended the time required to re-establish the refluxing action.

During one of the checkout tests with the liquid metal heater head, a leak developed in the sodium containment vessel, causing a small fire. Post-test inspection of the engine revealed a crack in one of the braze joints between a heater tube and one end-flange. A small amount of helium working gas escaped into the sodium space during the test, causing overpressurization of the sodium containment vessel. This type of failure was anticipated. The resulting overpressure condition was sensed by the Statham transducer which initiated the instantaneous shutdown of the engine. As part of the emergency shutdown procedures, fast venting of the engine working gas immediately relieved the sodium overpressure condition.

A second leak was found in the braze joint between the end-flange and the sodium containment vessel. This leak, in combination with the temporary overpressurization condition described above, caused a small amount of sodium to escape into the test cell which then spontaneously ignited. The ensuing

fire caused no damage to the engine and/or test facility, other than local destruction of wiring in the immediate vicinity of the sodium leak.

A failure analysis revealed the probable cause to be related to thermal distortion of the sodium containment vessel with subsequent stress concentrations occurring in several of the assembly braze joints. The distortion was believed to be a result of nonuniform temperature distributions in the sodium vessel during engine start-up and shutdown transients. Rather than pursue this approach of using liquid sodium, alternate heater head designs were considered. The results of this study are briefly discussed in the next paragraph.

b. Alternate Heater Head Designs. Several characteristics were identified as desirable for any future SLRE heater head design. The list is presented below. The specific order does not imply priority in terms of relative importance.

(1) Simple measurement of input energy.

(2) Uniform tube wall temperature.

(3) Low internal (dead) volume.

(4) Low pressure drop.

(5) High surface area for heat transfer.

(6) Safety of operation.

(7) Quantifiable heat losses.

(8) Compatible with low cost power supply.

Each of these characteristics was considered in evaluating the alternative heater types shown in Table 2. The advantages and disadvantages are listed for each of these possible types of heater head configurations. As previously stated, the indirect resistance type was selected for the second-generation heater head design. A discussion of this particular heater head follows.

c. Indirect Resistance Heater. The indirect resistance type heater provides heat by means of externally wrapped heater elements brazed onto the heater tubes. Circuit resistance is controlled by the diameter and length of Nichrome heater wires, hence the name "indirect resistance" is used. One similiarity between this design and the previously described liquid metal version is that they are both electrically powered.

An alternative electric heater head design uses voltage applied directly to the heat exchanger tubes so that each tube becomes an electrical resistance element. However, the direct resistance type design requires an electric current of thousands of amperes to generate sufficient resistance heating.

Table 2. Alternate Heater Head Types

TYPE	ADVANTAGES	DISADVANTAGES
1. Direct Resistance	Low Voltage Measure Power Input Simple Concept Previous Experience	High Amperage Requirements Bus Bar Losses Special Power Supply Needed Dual Function of Tubes Electrical Resistance vs Temp Non-Uniform Temperatures
2. Indirect Resistance	Conventional Power Supply Uniform Tube Temperature Single Tube Function Measure Power Input	Difficult Fabrication Electrical Short Circuits
3. Conduction	Simple Concept Measure Power Input Conventional Power Supply	Low Thermal Conductivity
4. Liquid Sodium	Uniform Tube Temperature Conventional Power Supply High Heat Flux Measure Power Input Heat Pipes Used	Containment Problems Vacuum System Required Difficult Fabrication
5. Radiation	Simple Concept Measure Power Input	High Temperature High Vacuum Required Geometry Sensitive
6. Induction	Fast Warmup High Heat Flux	Geometry Sensitive Measure Power Input Expensive Power Supply Long Delivery Time Shielding Required
7. Catalytic Combustion	Uniform Tube Temperature	Exhaust Gas Disposal Measure Power Input Long Development Time High Surface Area High Reaction Temperature
8. Conventional Combustion	Commonly Used Uniform Tube Temperature	Exhaust Gas Disposal Measure Power Input Development Time High Surfce Area High Reaction Temperature

Also, because the temperature coefficient of many high-performance alloys reverses at high temperatures, instabilities of the heater power supply could be induced, followed by burnout of one or more heater tubes. In addition, safety must be considered when applying voltage directly to an exposed engine component. For these reasons, the indirect resistance approach was selected for the SLRE.

The heating elements were fabricated by Temcom Inc. starting with a large diameter tubular sheath that contains the insulated Nichrome wire. It is then swaged and drawn to a very small diameter, and in the process, the insulation becomes highly compacted. The heater element is flexible enough to be wound spirally and then furnace-brazed to the heat exchanger tubes.

With the indirect resistance heater, total circuit resistance is selected independently of the tube geometry by simply changing the size of the wires and/or the number of wire wraps around each tube. The heater head contains a total of 18 double-turn coils of tubing, through which the working gas flows. As shown in Figure 6, these coils form a toroid about the periphery of the heater head body. A computer analysis was used to optimize the configuration in terms of the electrical properties, heat transfer characteristics and internal volume requirements. Specifications for the indirect resistance type heater are given in Table 3.

Component bench tests were made with several of the individual heat exchanger elements to ensure reliability of the design. Each element was checked at the maximum design temperature under cyclic (5000 + cycles) conditions using full line voltages. No failures of the component parts were observed.

For comparison, Figure 7 shows cutaway drawings of the SLRE with both the liquid sodium and the indirect resistance heater heads. The later configuration is approximately 8 in. shorter than the original assembly which graphically illustrates the versatility of the engine design concept. A total of 33 experimental data points were recorded with the engine using the resistance-type heater head. The maximum output hp of 1.0 kW (1.4 bhp) was measured during this time.

A problem soon developed with the connections between the Nichrome resistance elements and nickel lead wires due to electrical shorting. This failure was attributed to insufficient compaction of the magesium oxide insulation in the connectors. This allowed electrical contact between the Nichrome and/or nickel wires and the grounded metal sheath. Subsequent discussions with the manufacturer led to the improved (and final) version discussed below.

For the improved design, the transition sections were formed earlier in the fabrication cycle. The connections for each of the Nichrome/nickel joints were made prior to the drawing and swaging operations, thus ensuring adequate compaction of the magnesium oxide insulation. Prior to brazing the new heater elements into the body, additional component tests were run. This time, in addition to repeating the above component qualification tests, selected elements were also subjected to vibration testing. For these tests, the expected temperature, electrical power and the vibrational environment were simulated. Again, no bench test failures of any heat exchanger components were observed.

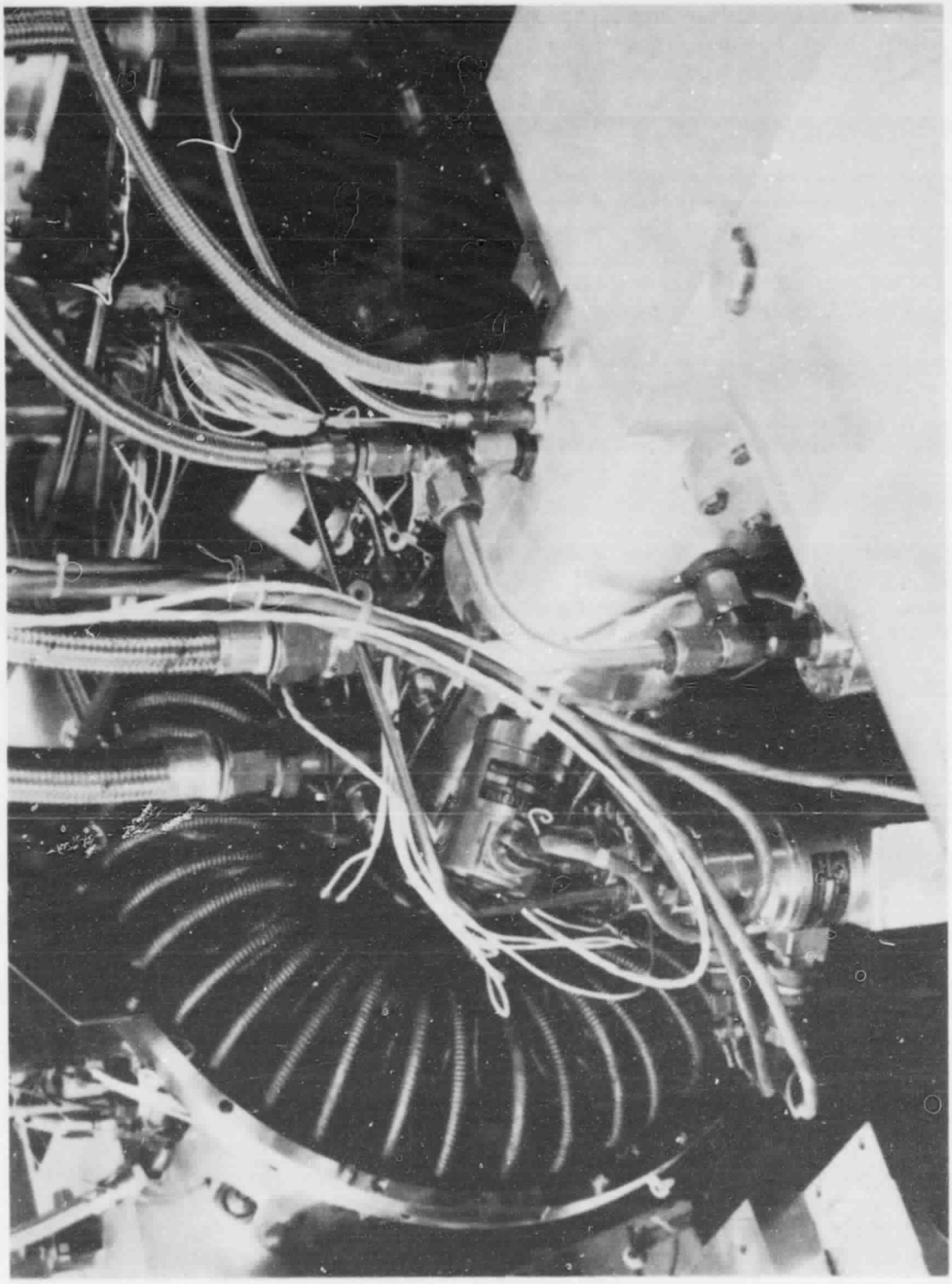

Figure 6. Photograph of Installed Indirect Resistance Heater

Table 3. Specifications for Indirect Resistance Type Heater

Heater Type	Electric
Maximum Rating	40 kW
Number of Elements	18
Element Type	Nichrome
Wire Resistance	2.1 ohms/m (0.63 ohms/ft)
Maximum Power Density	328 w/m (1000W/ft)
Operating Voltage	208V, 3-phase
Sheath Diameter	2.03 mm (0.080 in.)
Sheath Length	8.29 m (27.2 ft)
Tube Size	6.52 OD x 1.02 wall mm (0.257 OD x 0.040 in.)
Tube Heated Length	67.3 cm (26.5 in.)
Power Supply	SCR Thyristor Controlled
Power Measurement	Digital Wattmeter

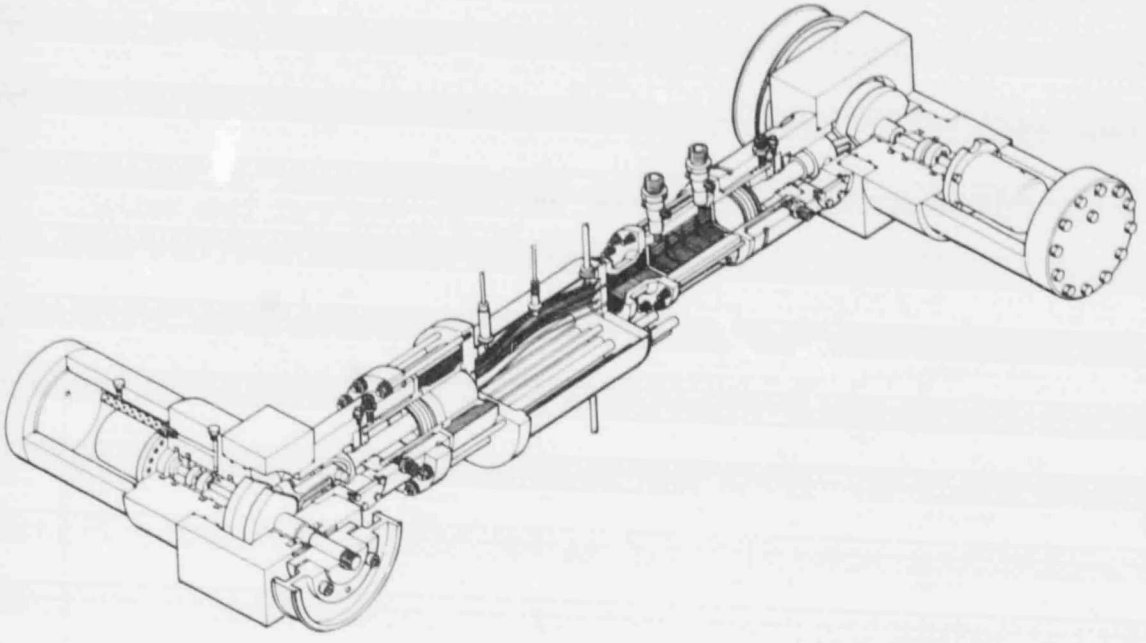

A. LIQUID SODIUM HEATER HEAD

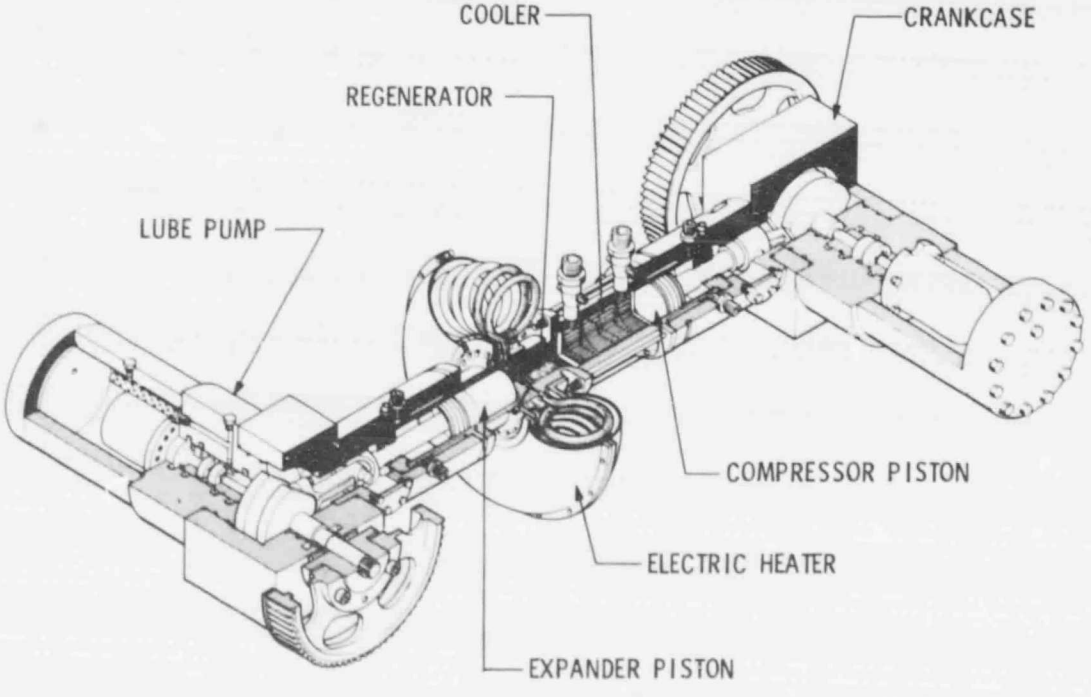

B. ELECTRIC HEATER HEAD

Figure 7. Cutaway View of Two Preprototype Engine Versions

The final assembly of the preprototype engine was then completed using the improved heater design.

The problems described thus far obviously impacted the project schedule. This was mostly caused by procurement lead times and fabrication difficulties associated with the super alloy materials. In addition, other problems were encountered, the more significant of which are described in the next section.

3. Miscellaneous Problems and Solutions

Additional hardware related problems were discovered as the project developed, but most did not cause a major impact on the overall schedule. The more serious of these are tabulated in Table 4 with the resulting solutions.

In addition to the first-order analytical techniques developed in support of the engine design, considerable time was expended in formulating a more comprehensive Stirling computer model. Results of this effort are described in the following sub-sections.

D. STIRLING CYCLE COMPUTER MODEL

A generalized computer program was formulated to analyze engine systems operating on the Stirling cycle. The purpose of the Stirling cycle computer model (SCCM) was to provide steady-state cyclic performance predictions for real engine components, accounting for irreversibilities and external losses. The present SCCM model is based on the work of Finegold and Vanderbrug (Ref. 4).

1. General Description of Model

The technical approach used in the SCCM is based on lumped parameter numerical integration to obtain the cyclic transient response of the working fluid at various points in the engine. The integration method assumes that the thermodynamic processes are quasi-static during the small time interval of integration for each control volume. This approach is commonly used by others in Stirling cycle models to avoid the direct integration of the many non-linear coupled differential equations.

The lumped parameter method is desirable for several other reasons besides the avoidance of the non-linearity problem. The method allows the use of a modular program structure offering a variety of user-specified options. Discontinuities such as those produced by the transition from laminar to turbulent flow, or flow discontinuities resulting from choked flow, for example, are readily simulated. In addition, intermediate calculations can be performed between integration steps to simulate real component effects such as heat transfer.

The SCCM program differs from other Stirling models described in the literature in that it attempts to determine the pressure distribution and mass flow dynamics analytically during the integration interval. In order to avoid potential numerical instabilities inherent in this approach, an iterative

Table 4. Miscellaneous Problem Areas and Solutions

Problem Description	Solution
Crosshead seizure on compressor side	Increased running clearance
Low oil pressure on expander side	Changed flow-restrictor
Low oil pressure on both pumps	Modified assembly torque procedures
Excessive vibration in drive belts	Adjusted tension of idler pulley and pinned expansion side of engine to test stand
Hot gas leakage between heater and regenerator housing	New heater assembly has integral body and regenerator housing
Shaft seal leakage	Incorporated a vented seal cavity system, partially successful
Partial loss of power when crankcases are pressurized	Unknown
Crankcase stud failures	Changed material specifications
Collapse of oil filter case and loss of pressure	Installed heavier case
Loss of working gas on compressor end	Reworked piston ring gap to prevent failure of backup "O" ring
Excessive piston ring leakage	Reworked piston ring grooves

procedure is used. The SCCM program also predicts the pressure distribution within the engine based upon the actual mass flow rates between engine components. Any numerical approach suffers from the disadvantage of requiring extremely small computing time intervals to satisfy the quasi-static assumption for mass flow dynamics. For the SCCM program, this interval was chosen as the time required for one degree of engine rotation. Unfortunately, this relatively small computing interval translates into high computer costs. It should be pointed out that the total required computing time cannot be inferred solely from the total number of cycles required but is also dependent on the number of iterations per cycle.

Although the technical approach of the SCCM program is similar to other Stirling cycle programs, it offers greater user flexibility due to its modular structure and the variety of input options. The SCCM consists of a library of individual modeling routines. Each routine contains the logic and generalized equations required to simulate the mass flow dynamics of the component. This allows the user to select components from the library and assemble them into a functional loop representative of the physical system being modeled.

The user specifies the initial conditions, boundary conditions, and other key parameters describing known relational characteristics for each component. The input parameters can be either constants or tabulated curve data stated as functions of time, temperature or some other control value such as crank angle. The modular approach of the SCCM is therefore flexible and generalized, allowing transient simulation of most mass flow dynamics of Stirling engines, as well as other heat engines. In addition, the modular program structure allows the user to add new component routines to the library as required.

2. Model Status

The SCCM program has been run using both air and helium as the working fluid while varying the heat transfer and flow resistance factors from zero to estimated maximums. In all cases, the program was observed to be numerically stable for an integration interval of one crankshaft degree.

The SCCM program has been only partialy successful in achieving the goal of simulating the mass flow dynamics of the preprototype SLRE. Nevertheless, it is believed this objective should remain as an essential goal for any computer simulation model that aspires to yield practical design data for a Stirling engine. Budgetary and schedule considerations did not permit this analytical effort to be completed.

E. STIRLING ENGINE USER SURVEY

It was considered important at an early stage in the SLRE project to determine the needs of potential users so that future engine designs could be configured to support actual requirements. For this reason, JPL conducted a survey to determine the potential market for a laboratory engine and the technical requirements of Stirling engine researchers. The results have been reported by Anderson and Hoehn (Ref. 7) and a brief summary of the survey is given below.

A questionnaire was prepared and mailed to 358 people representing a broad cross-section of the technical community within the United States and 12 foreign countries. The overall response to the questionnaire was considered significant because approximately one-third were returned with appropriate comments.

A total of 57 respondants expressed interest in acquiring some type of Stirling test engine and 45 believed that the SLRE could fulfill their specific technical requirements. Furthermore, 39 indicated that their current budgets could include funds which could be applied towards the purchase of such an engine. The academic community listed acceptable cost as the most important consideration for such a procurement. Several institutions indicated that a subsidy or some form of grant would be sought in order to permit acquisition of this type of laboratory test equipment. On the other hand, those responding from industrial and government laboratories believed engine reliability to be the most important attribute for any test engine. This was followed, in order, by safety, versatility, performance and engine maintenance considerations.

The predominance of university interest in an SLRE, smaller than 10 kW (13.4 hp), can perhaps be attributed to two factors; first, its primary use as a teaching tool, and second, the expected lower cost of a smaller engine. Greater interest was shown in larger test engines by industrial and government laboratories, probably because their concerns include component developments for ground transportation and stationary power applications. Relative to the types of possible engine heat sources, a slight preference for combustor heating was indicated, followed closely by electric, with the potential for solar heating a distant third.

In general, the high cycle efficiency and multi-fuel capability of Stirling engines were listed as the most important attributes. These opinions undoubtedly reflect the growing concern for the conservation of petroleum-derived fuels. On an overall basis, there is widespread interest in the Stirling engine since it can fulfill a wide variety of potential roles. These roles are, of course, predicated on the successful development of commercially available engines in a variety of sizes. Composite ratings derived from the survey placed air conditioning/refrigeration as the most promising use in both the near-term (1980-1990) and far-term (>1990) periods. Solar thermal-electric energy conversion and surface transportation were also considered as possible areas of use for Stirling cycle machines.

IV. DESCRIPTION OF TEST HARDWARE

A. PREPROTOTYPE ENGINE

The SLRE is a horizontally-opposed, two-piston, single-acting engine with a split crankshaft drive mechanism. The engine is assembled with an in-line arrangement to provide for the interchangeability of all seals and heat exchanger components. A cross-sectional side view of the assembled engine showing the significant design features is presented in Figure 8. A detailed description of the preprototype engine design has been reported by Hoenn (Ref. 6). A brief summary of the principle features follows.

1. Mechanical Assembly

The crankcase and cylinder assemblies used in both the expansion and compression sections of the engine are identical. Each lower-end assembly contains a single crankshaft and the reciprocating parts of the engine. The aluminum crankcase is designed to operate over a range of pressures, from atmospheric up to the maximum working pressure of the engine. The cylinder assembly consists of the aluminum cylinder block and liner. The liner and the sliding surface for the crosshead are both chrome plated and diamond honed to close tolerances. Two separate annular cavities are formed between each of the cylinder blocks and liners to provide a water cooling jacket and gas manifold passage for the engine buffer space.

The engine pistons and shafts are machined from a single billet of aluminum alloy. The expander piston is fitted with a hollow Inconel dome to minimize heat transfer to the uncooled rings. Rulon piston ring seals are used in combination with Viton backup "O" rings to maintain radial cylinder pressure.

With an arrangement of timing belts and a common idler shaft, the engine brake horsepower is measured by coupling the two engine flywheels to a single dynamometer output shaft. Figure 9 is a photograph of the SLRE mounted on the stand ready for testing. An overall view of the test-cell showing the dynamometer installtion can be seen in Figure 10.

2. Seals

The primary high pressure gas seal for the engine is achieved by a pressure-balanced, rotary-face seal installed on the crankshaft, inboard of each flywheel. A secondary sliding piston shaft seal assembly separates the lubricating oil from the working gas. The heater-regenerator assembly and cooler heat exchanger components can be identified in Figure 8. A brief description for each of these components follows.

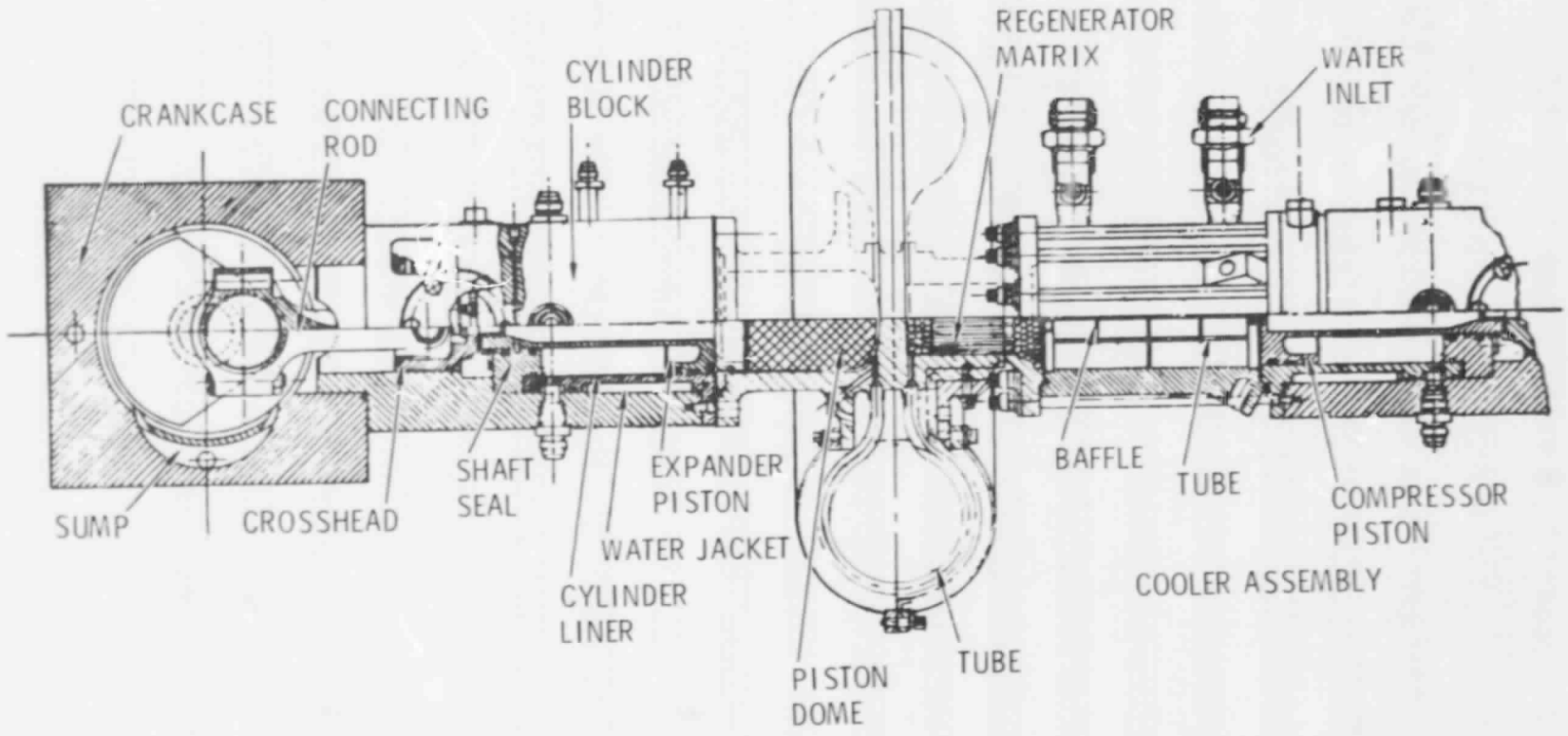

Figure 8. Cross-Sectional View of SLRE Showing Internal Details

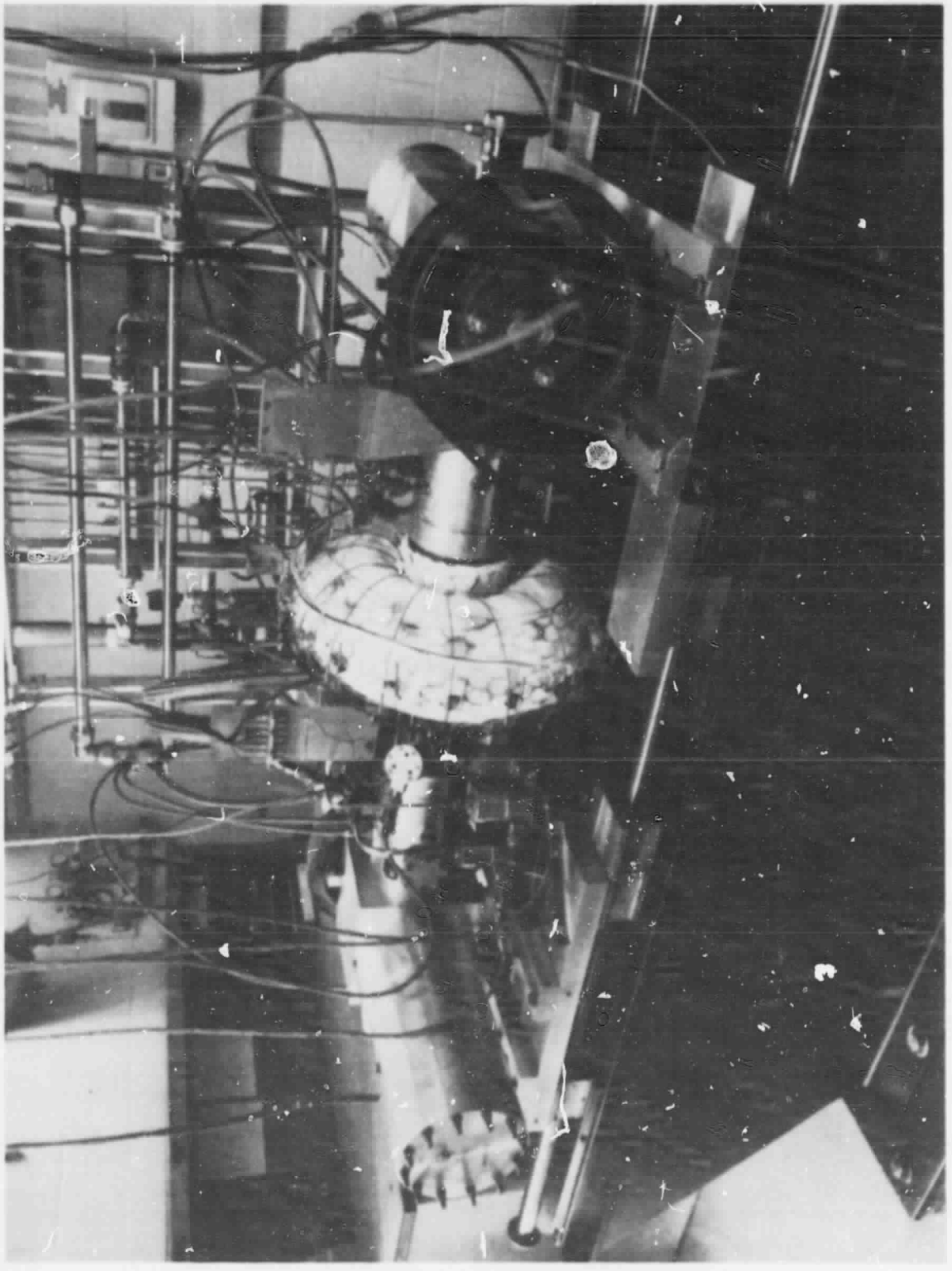

Figure 9. Photograph of Preprototype SLRE in Test Configuration

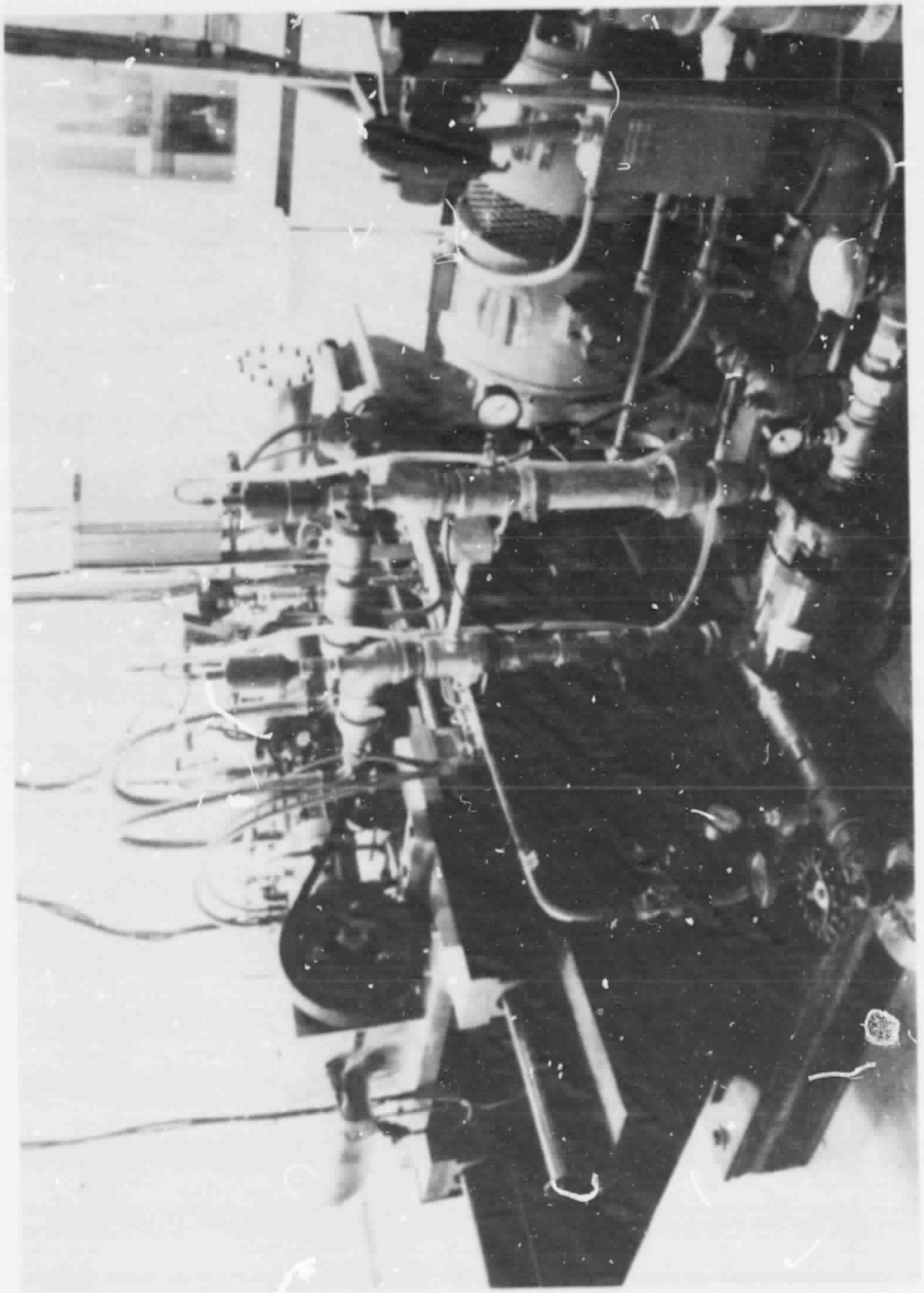

Figure 10. Test Cell Installation

3. Heat Exchangers

The parallel plane type regenerator matrix was constructed from a single strip of stainless steel shim stock. The strip was embossed with a series of parallel indentations, each approximately 0.20 mm (0.008 in.) high, then wound on a mandrel and inserted into the regenerator housing. The indentations provide separation between adjacent layers that result in semi-rectangular flow passages which approximate parallel infinite planes. Flow characteristics of the matrix were determined by steady-state component flow tests using nitrogen gas. An end-view of the matrix is shown in Figure 11.

The cooler for the preprototype engine is a conventional cross-flow heat exchanger consisting of 109 copper tubes, furnace-brazed into end plates which are welded to a stainless steel housing. The 40 kW heater is of the electrical resistance type containing 18 individual Inconel heat exchanger tubes wrapped with special Nichrome elements. As discussed previously, the resistance elements are encapsulated in highly compacted magnesium oxide insulation.

4. Lubrication System

The engine lubrication system consists of two identical, positive displacement pump mechanisms. The pump rotors are internally driven through couplings attached to one end of each crankshaft. Flywheels are installed at the opposite end of the two crankshafts. A cross sectional view of a typical lubrication system is shown in Figure 12.

B. TEST INSTRUMENTATION

A digital data acquisition system was available for the real-time recording and engine data reduction requirements. In addition, special high-speed instrumentation has been provided to record the required fast response, cyclic measurements.

The digital acquisition system capacity is large enough to allow real-time output of not only transducer data, but also key calculated parameters in engineering units. Brake thermal efficiency, for example, was displayed in real-time as one indicator of engine thermal equilibrium. In addition to the digital and analog recorders, video displays of critical control parameters were provided at the operator's console. A photograph of the console is shown in Figure 13. Cyclic pressure and mean temperature recordings were taken at each of the major component interfaces. Shock-tube bench tests were conducted earlier to ensure that the measured frequency response was adequate to track engine pressure on a cycle-by-cycle basis.

The cyclic pressure data were also recorded on high-speed magnetic tape and subsequently computer processed to produce the pressure-volume plots used to determine indicated horsepower. The technique developed at JPL to produce experimental indicator diagrams for the engine expansion space is shown graphically in Figure 14. A brief description of the technique follows.

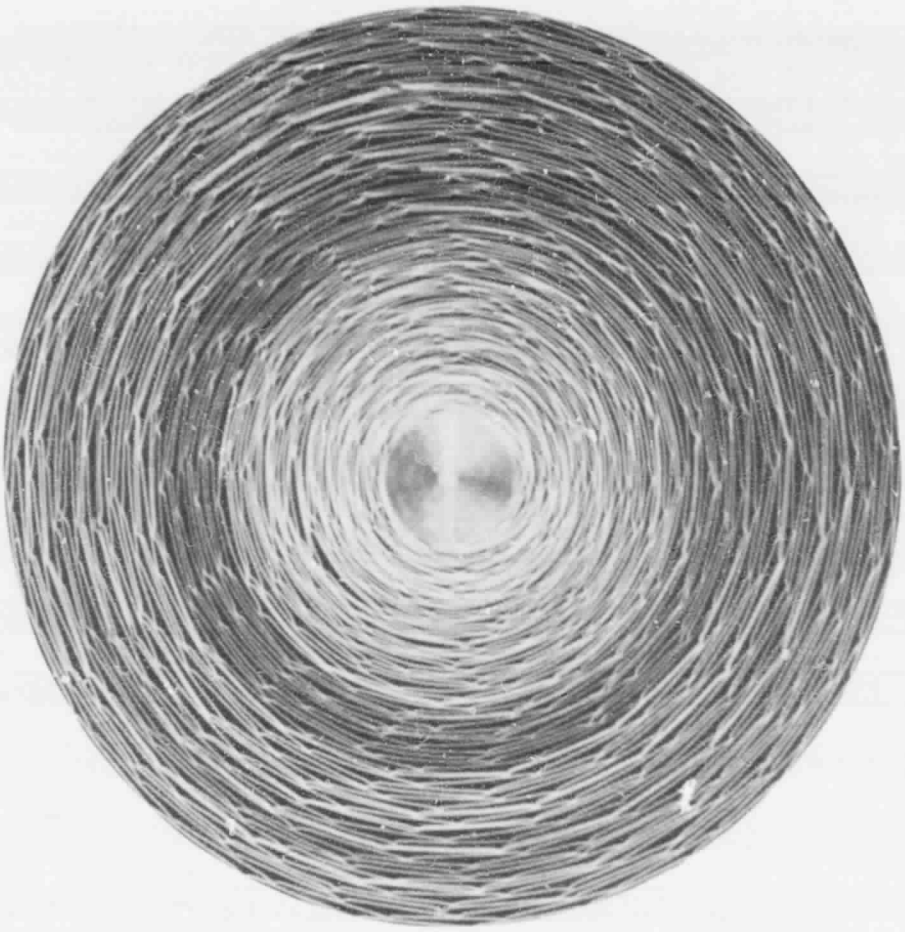

Figure 11. End-View of Parallel Plane-Type Regenerator Matrix

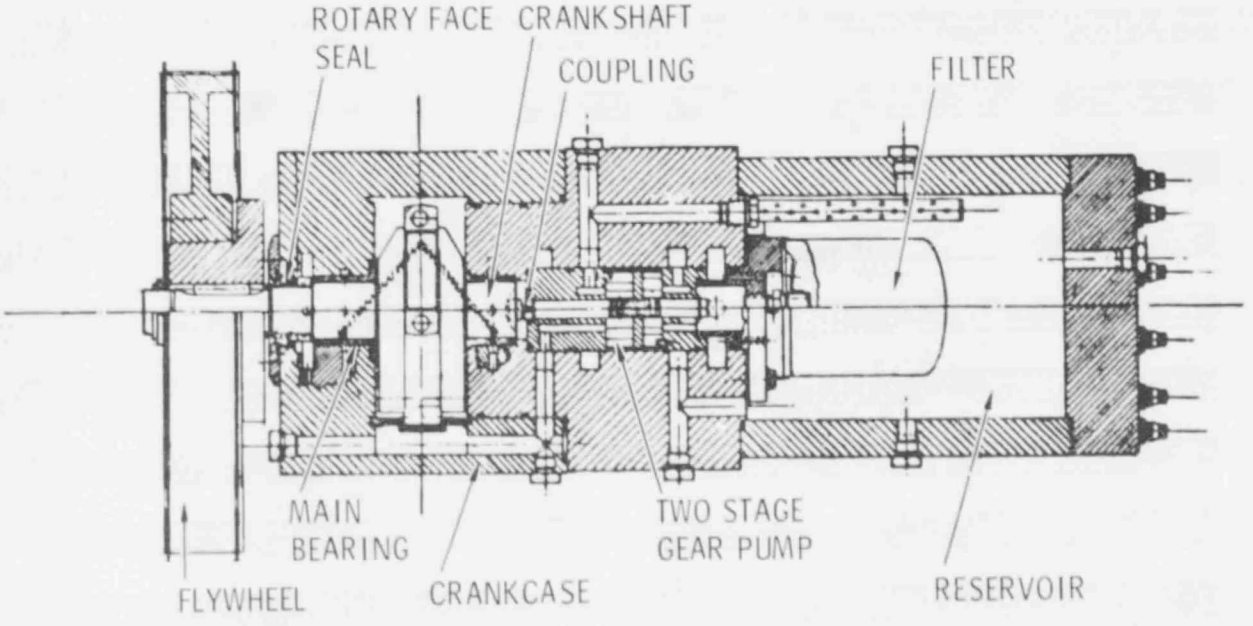

Figure 12. Design Details of the Lube Pump Assembly

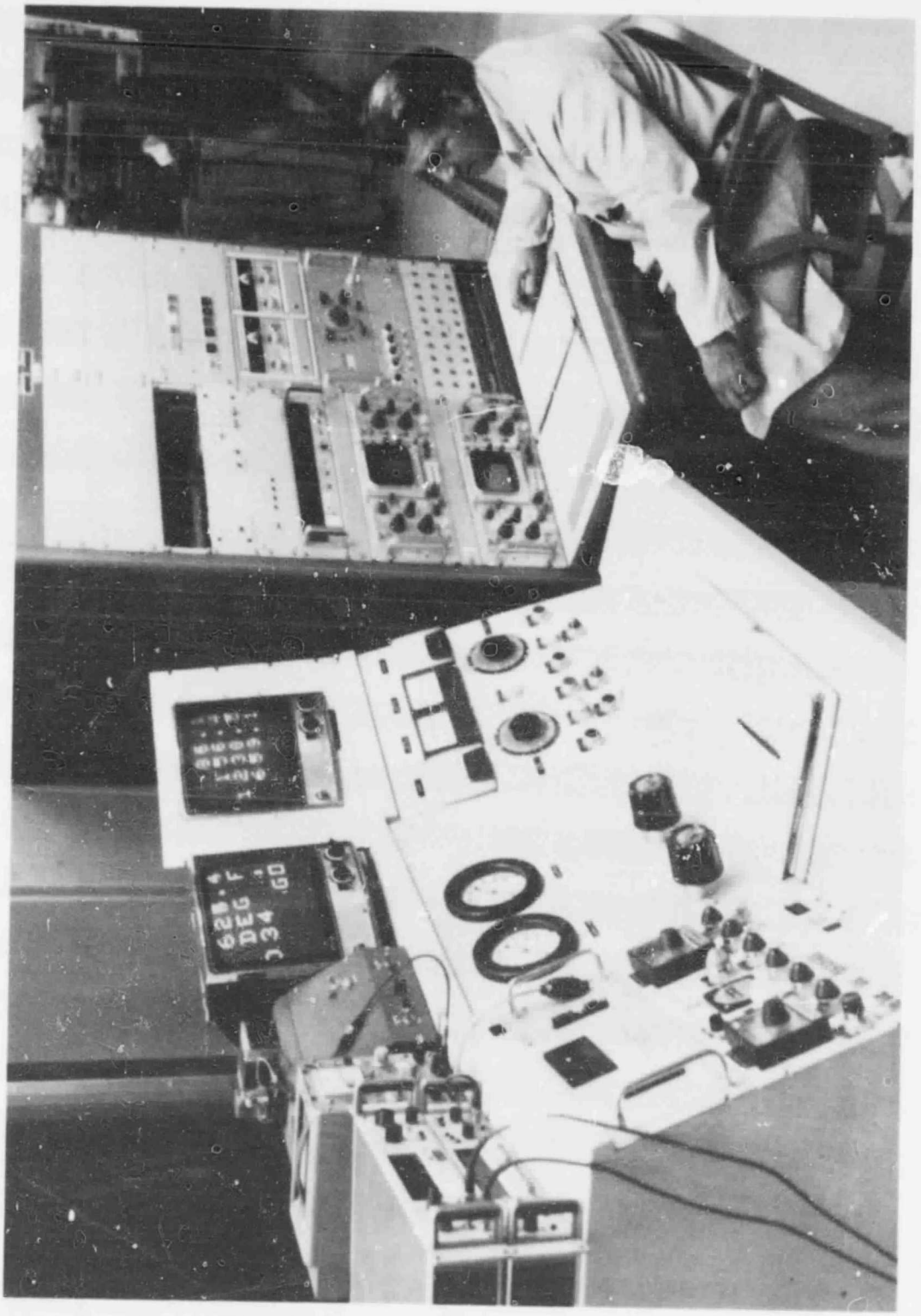

Figure 13. Operator's Console

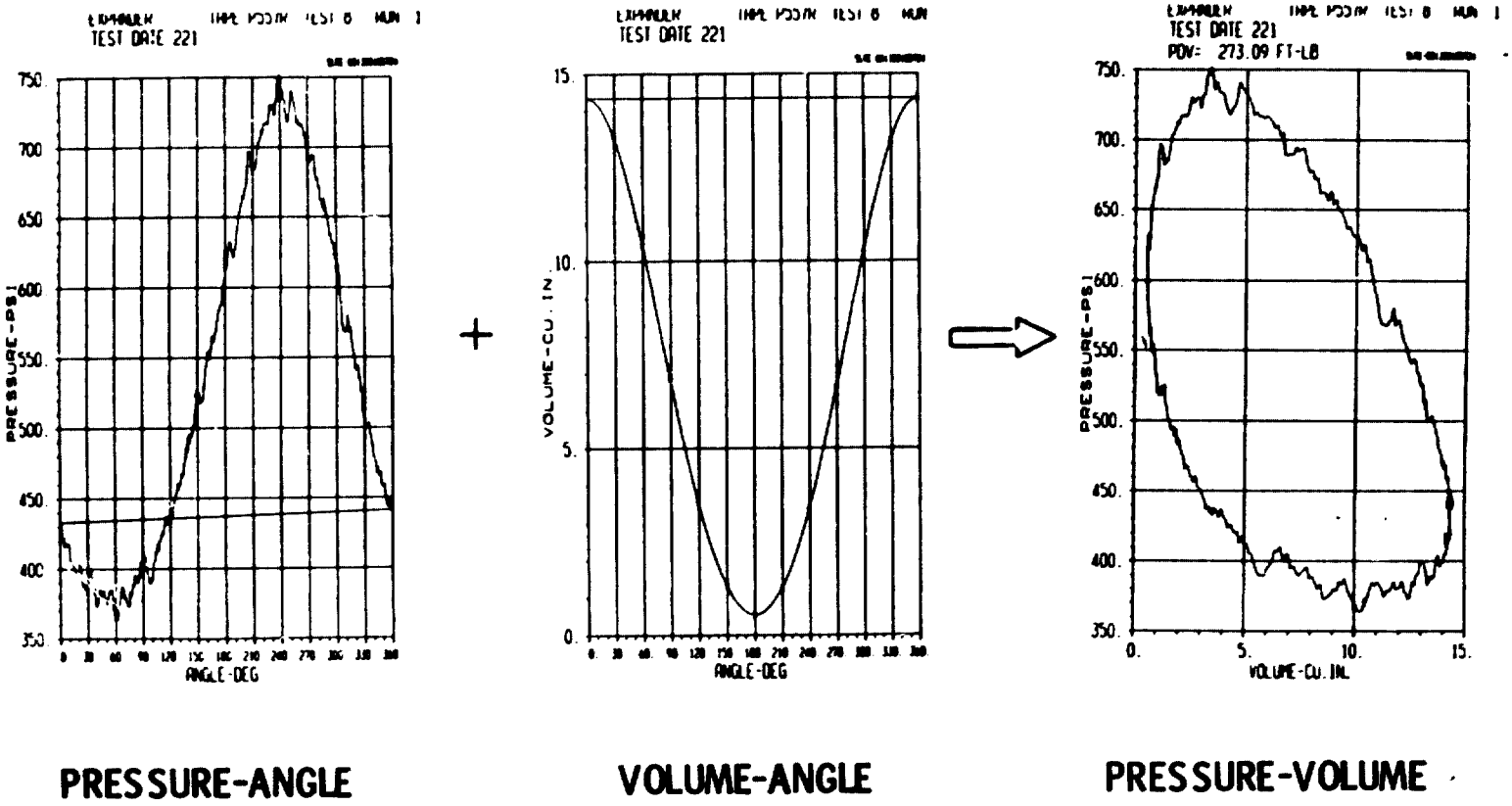

Figure 14. Development of a Typical Expander Indicator Diagram

Crankshaft angular position is determined from fiber optic sensors which view flywheel timing marks synchronized to the top-dead-center position of each piston. This information is combined with the cyclic pressure-data to give the pressure-angle plot shown in Figure 14. A computer program converts this angular position into the respective engine working space volume using known piston movement/swept volume relationships. Finally, the pressure-angle and volume-angle information is combined into a pressure-volume indicator diagram also shown in Figure 14. An identical process is followed for the compression space and the data average from six (or more) cycles into a single indicator diagram for the given test condition. The computer program then performs an integration of the diagram, and using engine speed, calculates the indicated horsepower. In addition, angular position is measured simultaneously for both pistons and converted in real time to engine phase angle, which is displayed at the operator's console for direct read-out.

An Eaton Model A-15U universal dynamometer serves the engine cranking function and also provides motoring capability for measuring engine friction characteristics. The dynamometer has an electronic controller for automatic speed and load control.

The engine cooling water system is instrumented with turbine-type flowmeters, while three-element thermopiles provide precise calorimetric temperature measurements. A three-phase digital wattmeter is connected to the electrical leads of the heater for measuring total input energy. Additional instrumentation has been provided such that a total energy balance can be made for the overall thermodynamic system. Other recorded parameters include engine speed, oil pressures and coolant temperatures to ensure proper engine operation. The present instrumentation list is given in Appendix A, and shows symbol, location, units and range of each parameter.

C. ENGINE CONTROLS

The SLRE was designed to operate over a wide range of engine test conditions. Five different control functions are provided to maintain the various test parameters during a given test. A brief description of the control methods used for maintaining the desired pressure, speed, phase angle, and the working gas temperatures follows.

1. Engine Pressure Control

A separate pressurization system is available for each of the three control volumes of the engine. Included are the crankcase, buffer, and the working spaces. The method of pressure control consists of three individual hand loader and pressure regulator systems mounted on the operator's console. The control systems are compatible with both helium and hydrogen gases. The engine tests reported were made using helium gas in the SLRE working and buffer spaces. Both crankcases were vented to atmospheric pressure.

2. Engine Speed Control

Engine speed is maintained by the electronic control circuits of the dynamometer which also provides overspeed protection. As explained previously, the dynamometer rotates twice the engine speed to provide increased low-end motoring torque. Engine speed is set with a vernier potentiometer located on the console.

3. Engine Phase Angle

Phase angle is defined as that angle by which the expander piston leads the compression piston. Phase angle is now changed for the SLRE by shifting the relative position of one of the gear-tooth timing belts used to couple an engine flywheel to the dynamometer shaft. Although not implemented during the present investigation, a remotely operated phase change mechanism was designed by McDougal (Ref. 8) for use while the engine is running. The device consists of a pair of coaxially aligned bevel gears mounted on the dual crankshafts which mesh with a controllable third gear. A hydraulic coupler interconnects the crankshafts in a variable phase relationship. In this manner, the reciprocating motion of the two pistons is synchronized to operate with any desired phase relationship. The engine typically operates at 1.6 rad (90°) phase angle, although, special motoring friction tests have been conducted using a 3.2 rad (180°) phase relationship.

4. Hot Gas Temperature Control

The hot gas temperature is an important control parameter for the Stirling engine. Temperature control is maintained by the amount of electrical energy supplied to the heater head. This is accomplished by a thermocouple sensor which measures heater outside wall temperature. This signal provides input to a 208-volt, 3-phase SCR power supply, which in turn modulates the input voltage to the electric heater elements. Heater wall temperature is selected at the operater's console. Direct readout is also available for the mean working gas temperature. The digital wattmeter is used to measure the input energy and these signals are integrated over a 30-second time interval to average out power transients.

5. Cold Gas Temperature Control

The temperature of the working gas in the compressor side of the SLRE is also maintained automatically by controlling the cooling water flow through the engine cooler. The coolant is supplied by a closed-loop facility system with provisions for fresh makeup water. A three-way proportioning valve selects the correct amount of fresh cold water and thereby maintains the proper temperature mix of the coolant. This ultimately establishes the gas side temperature in the engine heat exchanger. With the system operating in the full open-loop mode, a minimum cold gas temperature of about 310°K (100°F) can be achieved.

V. EXPERIMENTAL RESULTS

The experimental data reported here represent the initial test results for the preprototype SLRE. Although the engine was fully operational, the performance results do not represent those of a totally optimized Stirling cycle engine. These early test results were obtained to demonstrate validity of the design concept and were recorded during the first five hours of operation of the preprototype engine. A total of 34 quasi-steady-state data points were obtained over a range of engine speeds, pressures, phase angles and working gas temperatures. A summary of the engine performance results is shown in Tables 5 and 6. Examples of engine data reduced from the high speed magnetic tapes are presented in Appendix B.

Prior to these operational engine tests, a series of motoring tests was conducted to determine the preprototype SLRE friction characteristics. The results of these earlier experiments will be described first, followed by a discussion of the engine performance tests.

A. ENGINE FRICTION STUDIES

Motoring an engine is the usual technique employed for measuring the internal friction losses of an internal combustion engine. However, this procedure produces a unique set of problems for the Stirling cycle engine. In order to determine friction power of a Stirling engine, precautions must be taken to minimize pumping effects, since motoring in the normal direction of rotation results in a refrigeration cycle which absorbs additional power. An example of SLRE operation as a refrigerator is illustrated in Figure 15. For this case, the complete engine assembly was motored without the electric heater being energized. Depending on engine speed, the working gas experienced a temperature decrease during the cyclic expansion process. The motoring power measured for these tests obviously represent more than the frictional losses. The technique developed at JPL for isolating the engine friction measurement is discussed below. The information was needed to analyze the engine starting (self-sustaining power) requirements and to optimize the mechanical design of future prototype engines.

1. Mechanical Friction Results

A series of motoring tests were conducted using the mechanical assembly of only one-half of the SLRE, the cogged belt was removed from the engine expander for this purpose. In addition, the engine heat exchangers were not installed for these tests. The compressor lower-end assembly was connected to the motoring dynamometer using a single drive belt, resulting in a configuration similar to that shown in Figure 16 (less cooler). These tests were run (by necessity) at ambient pressure. As shown by the plotted results in Figure 17, data were obtained over a range of engine speeds to about 42 Hz (2500 rpm). The total friction measured for this configuration is shown in Figure 17 as the compressor-side total and the friction power is seen to be about 2.2 kW (3 hp) at 33 Hz (2000 rpm). The total mechanical friction (in-

Table 5. Engine Performance Summary - Test 9

TEST POINT	RPM	AVG GAS PRESS	T COLD (TCC) °F	T HOT (THE) °F	BHP	PHASE ANGLE Ø, DEG	BRAKE THERMAL EFF, %	PREDICTED BHP[b]
1	1008	728	98	880	- .80	89.6		1.73
2	1012	733	99	984	- .09	89.6		1.87
3	1017	734	99	1083	0.53	89.7	1.7	1.81
4	1022	667	100	1193	1.13	89.8	3.5	1.79
5	1025	654	102	1183	1.53	89.9	4.5	1.73
6	751	655	99	1065	1.39	89.8	8.6	1.15
7	755	722	101	1179	1.97	89.8	8.9	1.18
8	756	668	100	1209	2.21	90.0	8.7	1.25
9	508	634	95	1052	1.56	(90)[a]	14.3	0.67
10	508	633	94	1163	1.81	(90)	12.5	0.68
11	877	715	107	1127	1.43	90.0	6.2	1.60
12	1003	680	110	1203	1.19	89.9	4.8	1.77
13	753	1017	113	1082	2.66	89.6	10.4	2.24
14	755	1080	115	1169	3.61	89.1	11.3	2.62
15	757	1091	115	1216	4.01	89.2	12.6	2.53
16	501	1117	105	1060	3.06	(90)	17.8	1.70
17	502	995	103	1181	3.35	(90)	15.6	1.50
18	1004	961	122	1095	0.91	89.4	3.1	2.66
19	1010	986	120	1188	1.43	89.9	3.9	3.01
20	756	953	114	1209	3.63	89.6	11.4	2.11
21	746	501	103	1034	0.97	90.1	11.3	0.66
22	749	460	99	1172	1.18	90.3	6.8	0.59

a. Estimated, based upon known set point

b. Based upon modified Schmidt cycle analysis

Table 6. Engine Performance Summary - Test 10

TEST POINT	RPM	AVG GAS PRESS	T COLD (TCC) °F	T HOT (THE) °F	BHP	PHASE ANGLE Ø, DEG	BRAKE THERMAL EFF	PREDICTED BHP[b]
1	502	635	92	1035	1.36	(90)[a]	11.0	0.67
2	405	645	89	1058	1.30	(90)	11.1	0.47
3	310	630	84	1081	1.16	(90)	10.7	0.39
4	747	683	108	1083	1.22	(90)	6.6	1.20
5	751	592	106	1071	1.01	89.7	6.6	0.98
6	759	667	101	1098	0.81	70.0	3.7	1.09
7	753	758	106	1094	0.24	(110)	1.3	1.44
8	750	684	104	1081	1.54	90.5	9.5	1.07
9	740	684	173	1060	0.69	90.3	4.2	0.93
10	734	793	205	1063	0.41	90.2	2.5	0.99
11	405	617	94	1056	1.44	(90)	11.6	0.51
12	501	626	96	1065	1.63	(90)	14.2	0.69

a. Estimated, based upon known set point

b. Based upon modified Schmidt cycle analysis

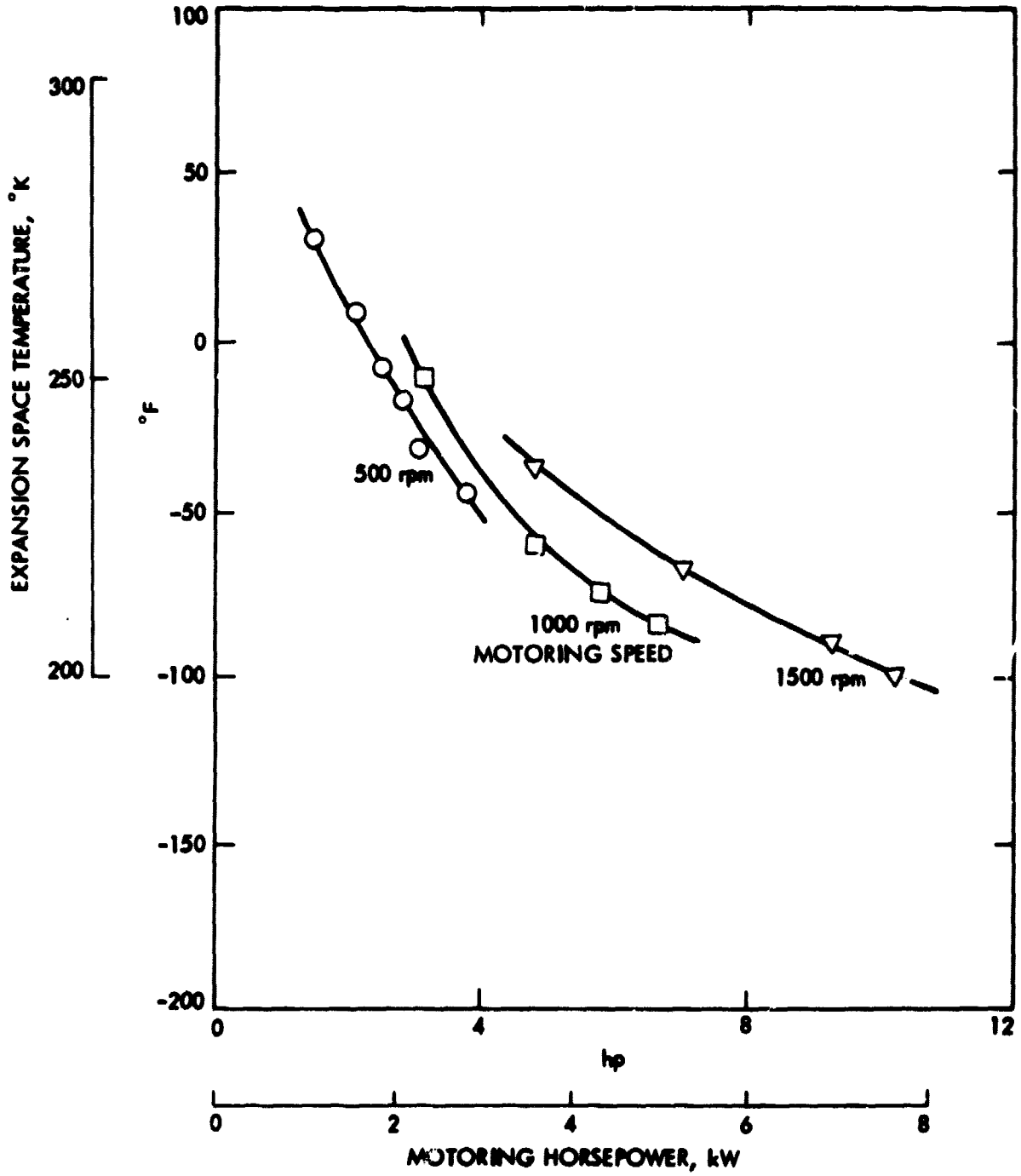

Figure 15. Example of SLRE Operating as a Refrigerator

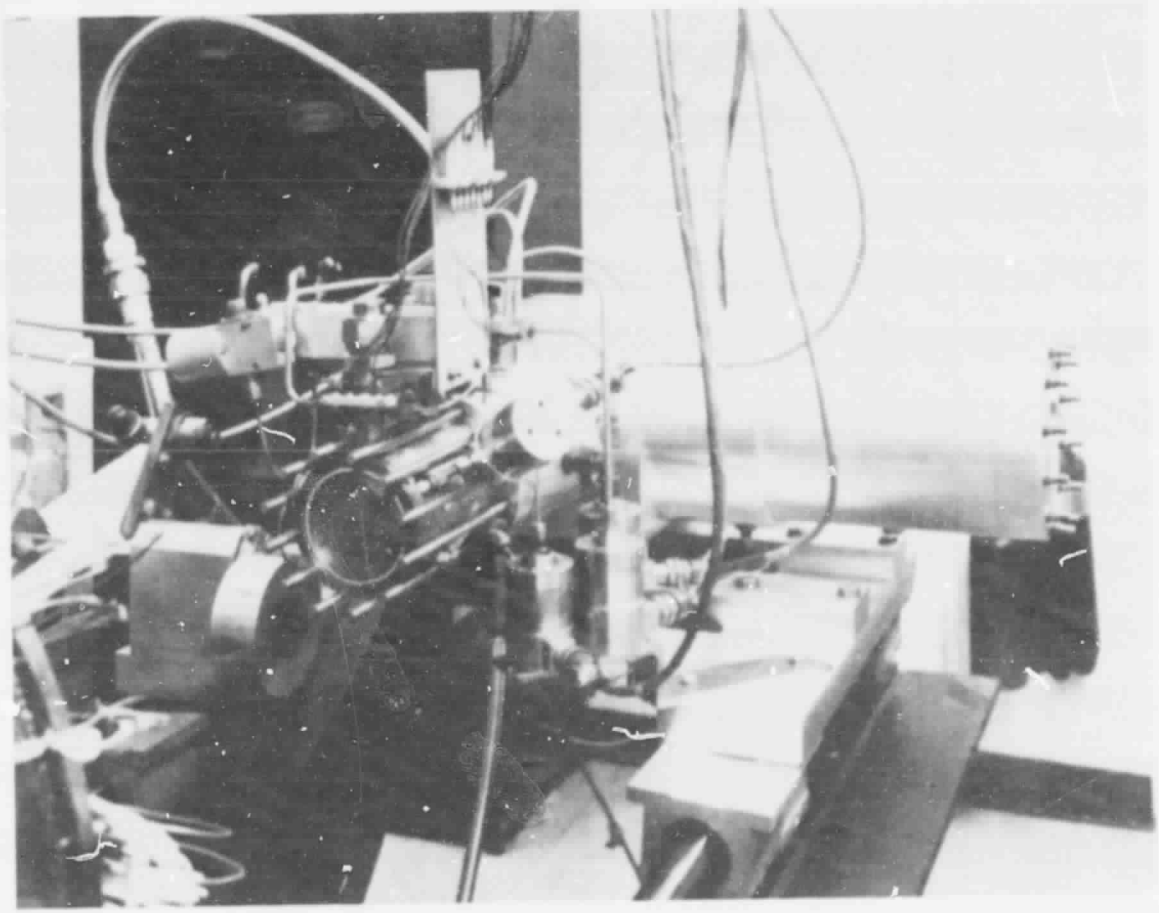

Figure 16. Configuration of Compressor Assembly for Mechanical Friction Motoring Tests (Less Cooler)

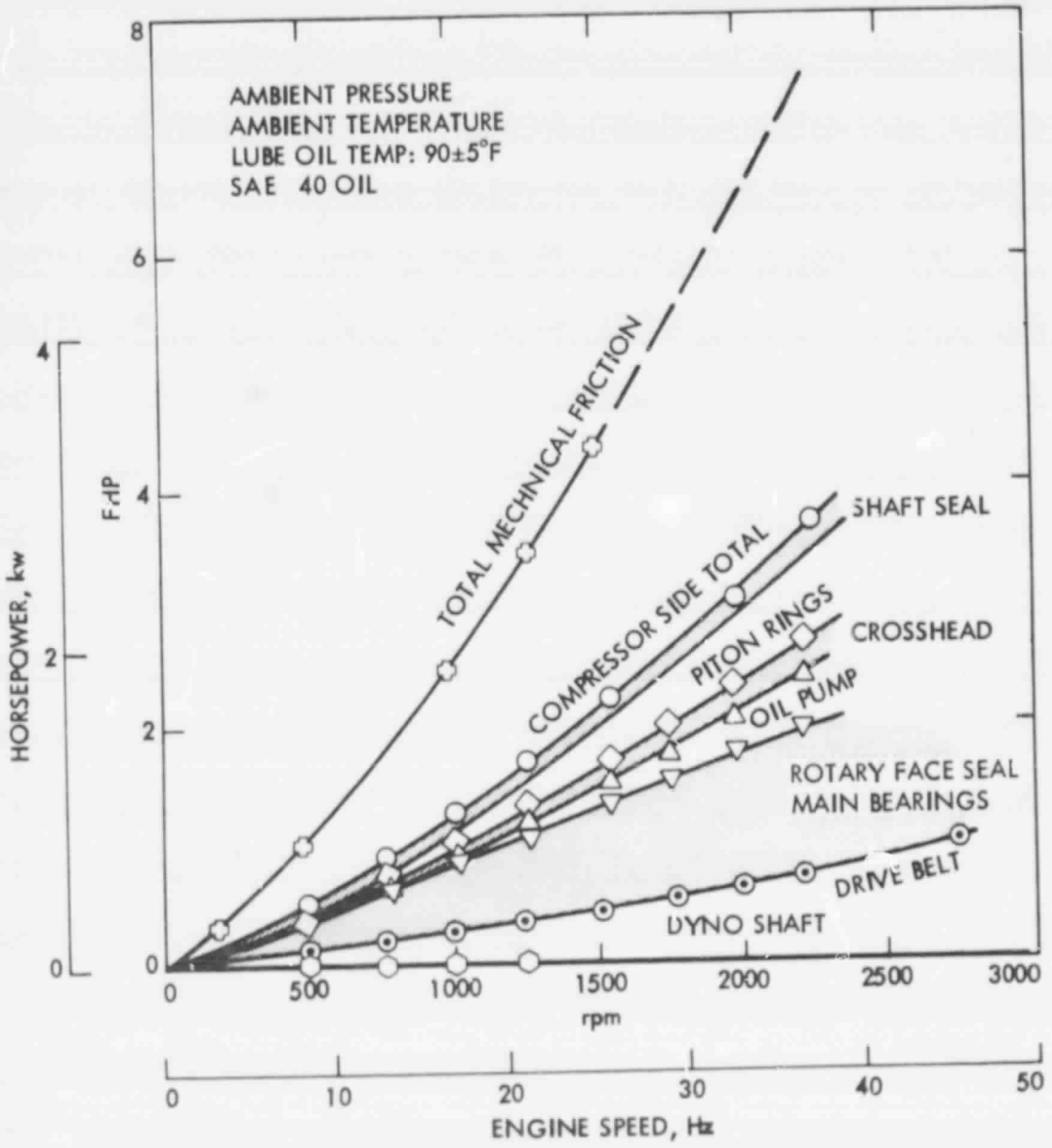

Figure 17. Distribution of Mechanical Friction by Component

cluding the expander-end losses) for the SLRE at ambient temperature and pressure is represented by the curve drawn through the uppermost data points.

Special motoring tests were also made to assess the separate contribution to friction of the individual components in the mechanical drive line. The various mechanical components comprising the drive line system were systematically disassembled on the compressor-end and the motoring tests repeated. Using this technique, the separate frictional effects were determined for the (1) sliding shaft seal assembly, (2) piston rings, (3) crosshead, (4) oil pump assembly, (5) main crankshaft bearings and rotary face seal, (6) gear tooth drive belts, and (7) the dynamometer drive shaft. The results of these motoring tests are shown in Figure 17. In addition, the data are summarized in Table 7. The largest contributors to mechanical friction is that caused by the engine main bearings and drive belts. These particular bearings were machined from solid aluminum (alloyed with tin) and are designed to handle loads in excess of 13.8×10^6 N/m^2 (2000 psi). The main bearings, which are surface-plated with tin, are pressure lubricated by oil supplied through eight radially drilled passages. Photographs showing the main reciprocating parts of the engine are given in Figures 18 and 19. It was concluded from these tests that friction could not be reduced significantly without a major engine redesign.

Table 7. Summary Results of Component Friction Tests*

Engine Component	hp	kW	Percent of Total
Main Bearings and Rotary Seal	1.2	0.9	41
Drive Belts	0.7	0.6	22
Rulon Fitted Piston Rings	0.6	0.5	18
Sliding Shaft Seal	0.2	0.1	6
Crosshead	0.2	0.1	6
Oil Pump	0.3	0.2	6

* Tests made at ambient conditions using SAE-40 engine oil, 33 Hz (2000 rpm)

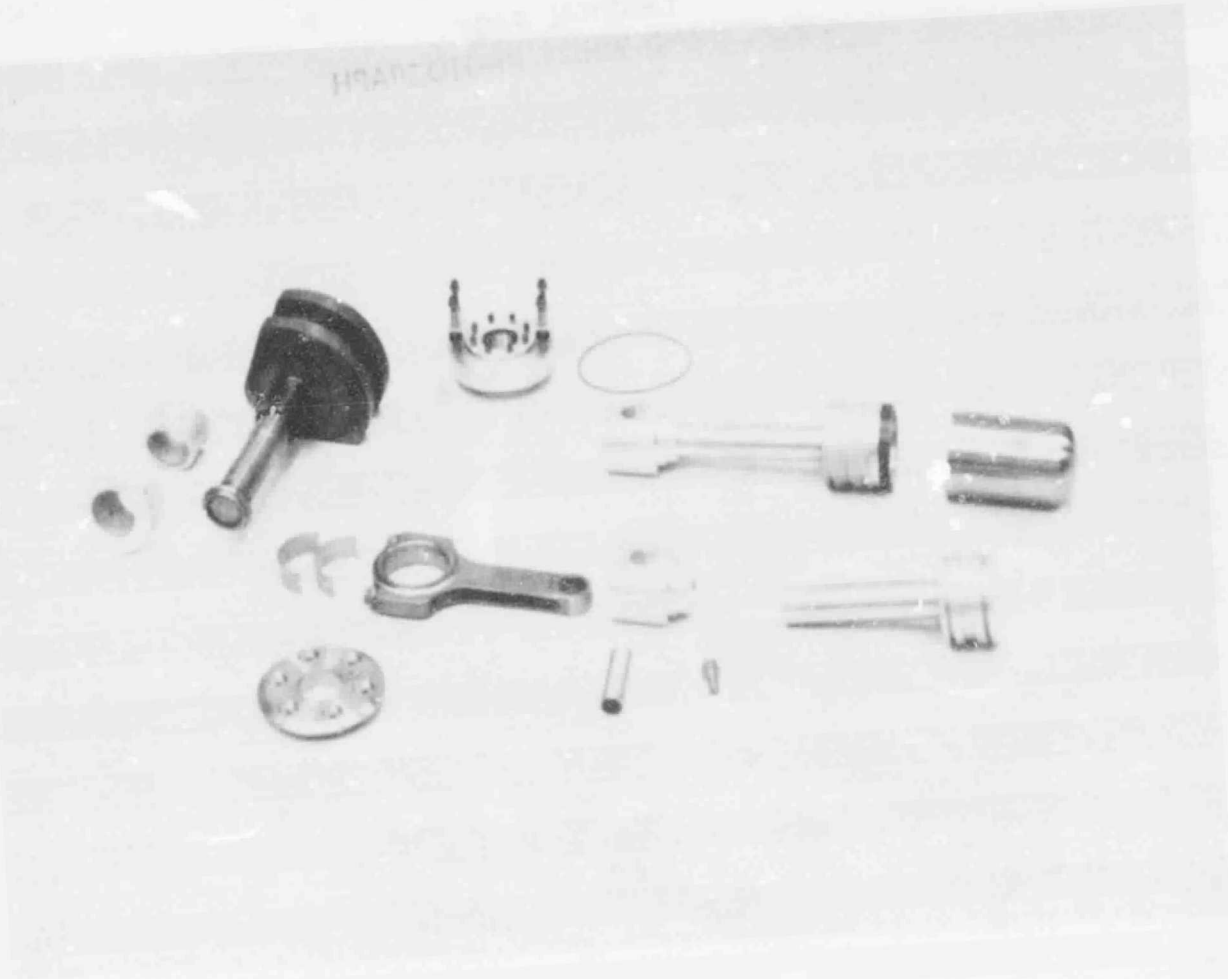

Figure 18. Drive Line Components for Preprototype SLRE

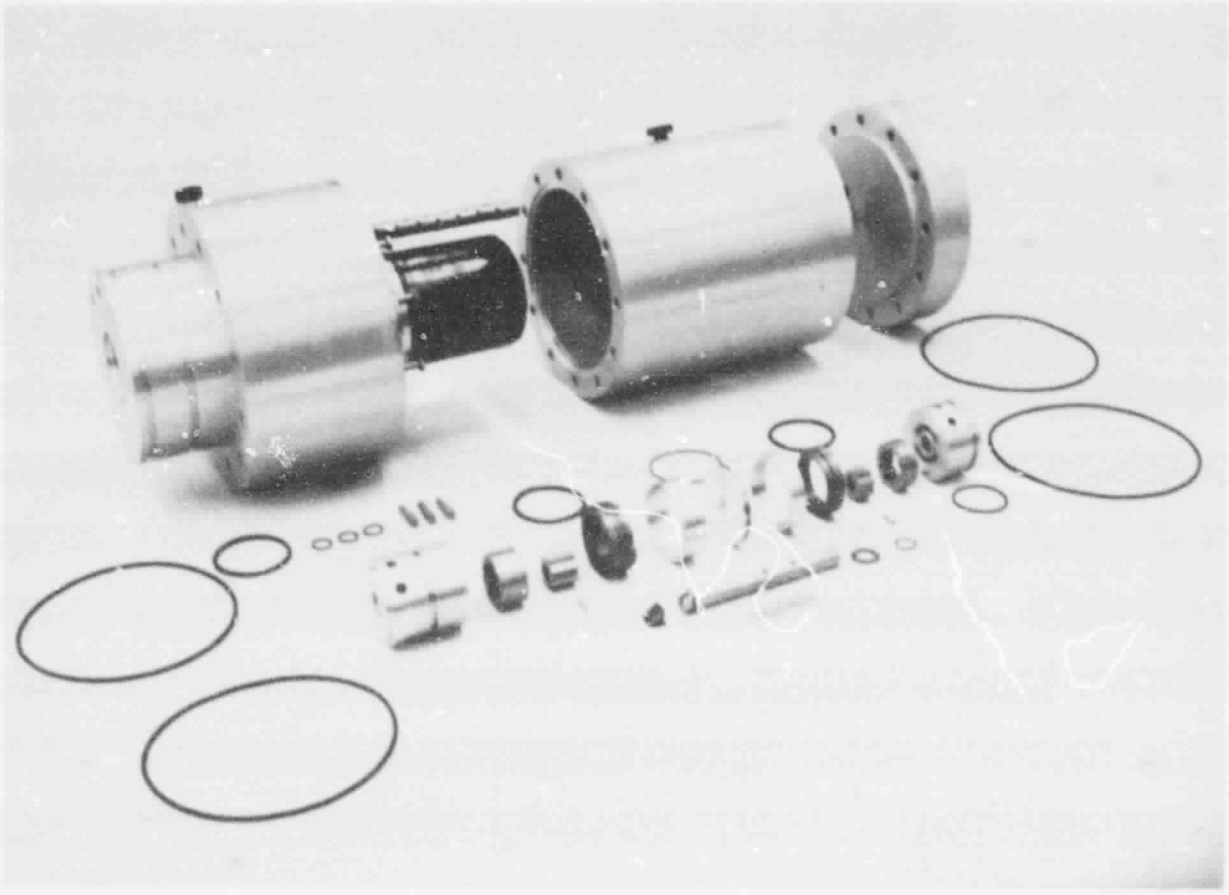

Figure 19. Typical Lubrication Pump Assembly

The objective of the next series of motoring tests was to determine the effect of working gas pressure on total mechanical friction, since bearing loads are known to change with varying pressure loads. The results of this investigation are shown in Figure 20. The lower curve (ambient pressure) is the same test data as that represented in the previous figure for the total mechanical friction. Pumping effects, normally associated with the Stirling cycle, were essentially eliminated during these tests by incorporating a large working space volume. This change effectively decreased the cycle pressure ratio and hence minimized cycle work normally associated with the compression and expansion processes. A photograph of this particular test configuration is shown in Figure 21.

Following these tests, the engine was reassembled with all components in place and additional motoring tests run. The purpose was to measure fluid friction caused by pressure drop in the three engine heat exchangers. The results of this investigation are presented in the next section of this report.

2. Fluid Friction Results

Engine pumping effects were eliminated for these tests by setting the phase angle at 3.2 rad (180°), thereby operating the cycle as a constant volume process. The additional dynamometer load required to compensate for the flow losses in the cooler, regenerator and heater components represent the fluid friction losses. The results of these tests are plotted in Figure 22.

The lower curve has been included for reference and represents the same data previously shown in Figure 21 for the 6.9×10^6 N/m^2 (1000 psig) working pressure test. Data for the upper curve was obtained at the same pressure level using the engine configuration just described. The difference between these two sets of data represents the motoring power necessary to pump the helium working gas back and forth through the three SLRE heat exchanger components. The difference between the upper curve and the dashed line represents the fluid friction for the regenerator, since the matrix was removed for this series of motoring tests. The difference between this data and the lower curve represents the fluid friction associated with the heater and cooler components. Similar results were obtained at other pressure levels. Only the 6.9×10^6 N/m^2 (1000 psig) data are presented for reasons of clarity.

The final motoring tests measured the effect of working gas composition on fluid friction. The motoring tests discussed thus far employed helium gas as the working fluid, although several other working fluids may be used in Stirling engines. Therefore, a series of tests was made using hydrogen, and the results are shown in Figure 23. Both sets of data were obtained with the regenerator matrix removed. The dashed line was obtained with helium and is the same data shown in Figure 22. The solid curve represents the hydrogen data, a significant reduction in fluid friction can be noted. This result relates to the lower molecular weight and density for the hydrogen working fluid. This is a primary reason for the use of hydrogen as the working gas in commercial Stirling engines where high specific power is needed.

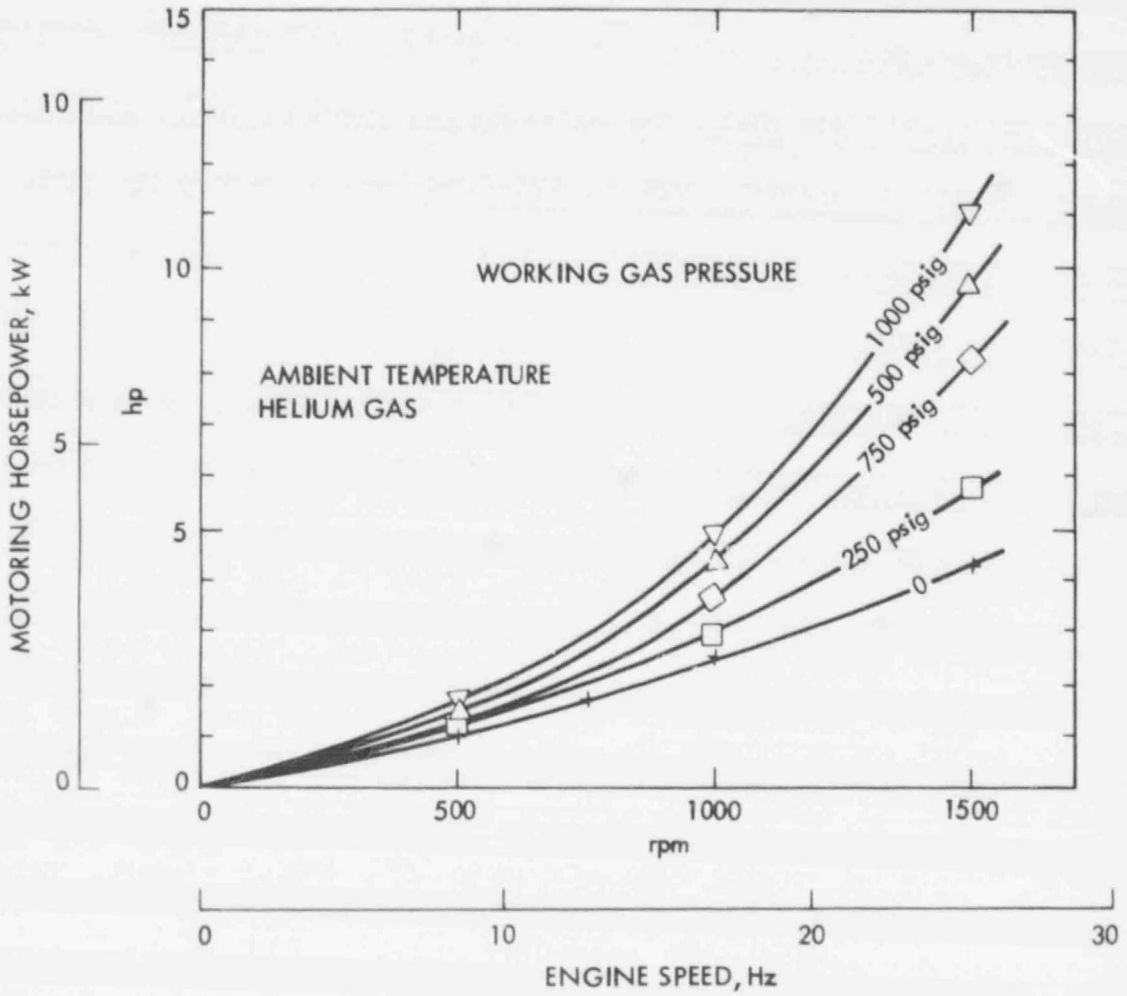

Figure 20. Experimental Mechanical Friction Results

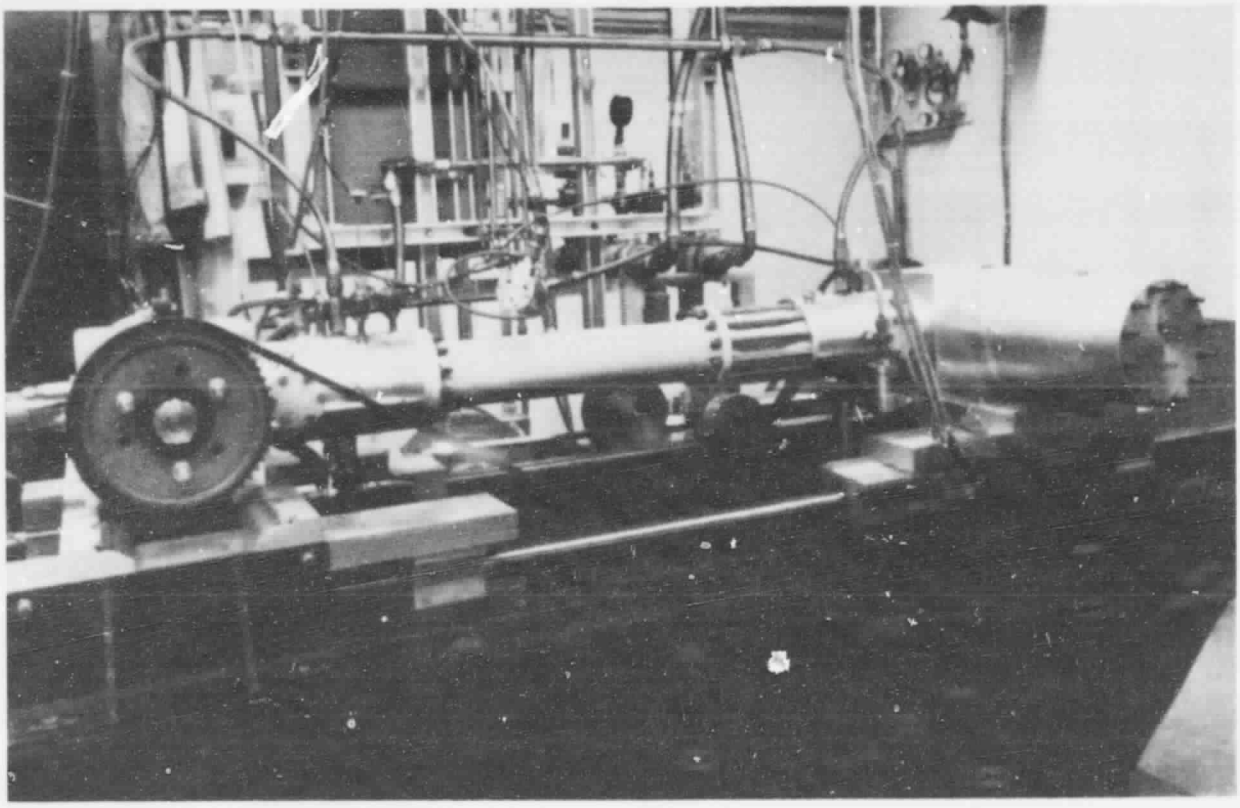

Figure 21. Test Configuration for Mechanical Friction Studies at Elevated Pressures

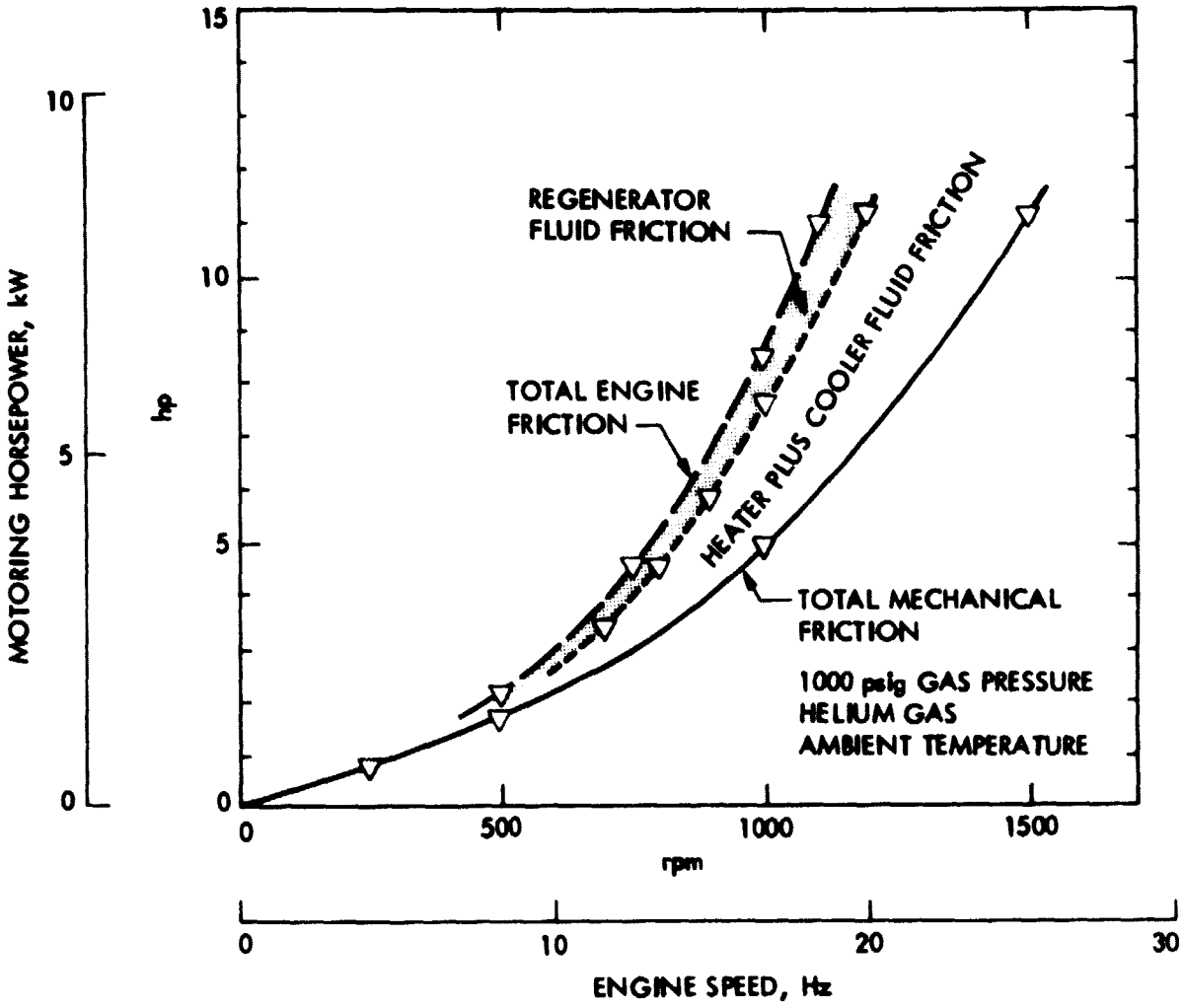

Figure 22. Experimental Fluid Friction Test Results

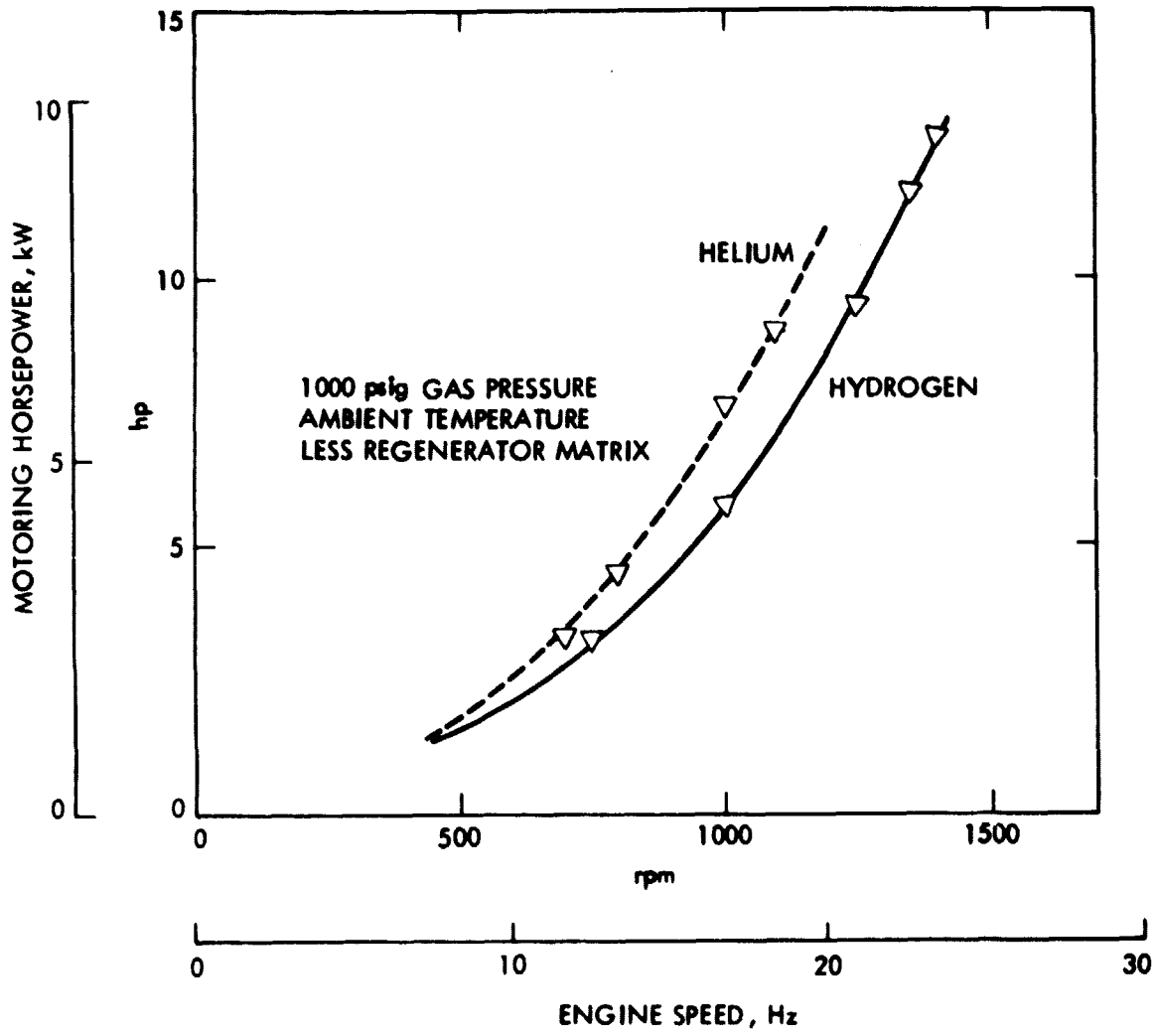

Figure 23. Fluid Friction Test Results for Hydrogen

All of the motoring tests discussed in this report were made using ambient temperature gases, with no attempt made to measure directly the effects of elevated temperatures on engine friction.

B. ENGINE STARTING CHARACTERISTICS

In general, self-sustaining engine operation is achieved whenever the indicated cycle power exceeds the internal losses (fluid plus mechanical friction). This is illustrated for the SLRE by the example shown in Figure 24. The predicted indicated horsepower (IHP) curve was obtained for this case using the classical Schmidt analysis described previously. The friction power has been graphically substracted from the Schmidt IHP to yield the predicted brake horsepower (BHP) curve. This predicted curve shows agreement with the actual measured data obtained while operating the SLRE at constant speed and working pressure. The five data points were taken while motoring the engine and gradually increasing the temperature of the working gas (plotted along the abscissa.) As shown in Figure 24, the engine was predicted to start (when IHP>FHP) as the gas temperature reached 733°K (860°F), but self-sustaining operation was actually achieved at about 810°K (1000°F). The largest source of error using this prediction technique probably stems from the fact that the experimental engine friction data were obtained at ambient rather than elevated temperature conditions. Engine friction could be expected to decrease with increasing gas temperature because of gas density and oil viscosity effects.

C. EXPERIMENTAL HEAT BALANCE

A calculation of the heat balance for the engine was made for each of the experimental test points. Some confidence in steady-state operation was achieved by observing the brake thermal efficiency in real-time, which represents the ratio of output and input energies. Engine operation was considered as "steady" and the performance stabilized when this calculated ratio remained constant within $\pm$ .01% during a 30-second time interval. However, this criteria does not imply temperature equilibrium in all of the various engine components.

The output energy is represented by the sum of the brake (net) horsepower and the heat transferred to the cooling water. The latter is measured for both the engine cooler and jacket expansion cylinder. The accuracy to which the overall system heat balance was achieved is shown in Figure 25. If all of the heat losses were accounted for, then:

$$Q_{INPUT} = Q_{HTR} = BHP + Q_{COOLANT} = Q_{OUTPUT} \quad (2)$$

where

$$Q_{COOLANT} = Q_{COOLER} + Q_{JACKET} \quad (3)$$

and the two different methods of calculating the brake thermal efficiency in Figure 25 would be identical. In actuality, those data points which fall above this ideal correlation line represent test data in which not all of the system losses were measured. The opposite is true for those points below the

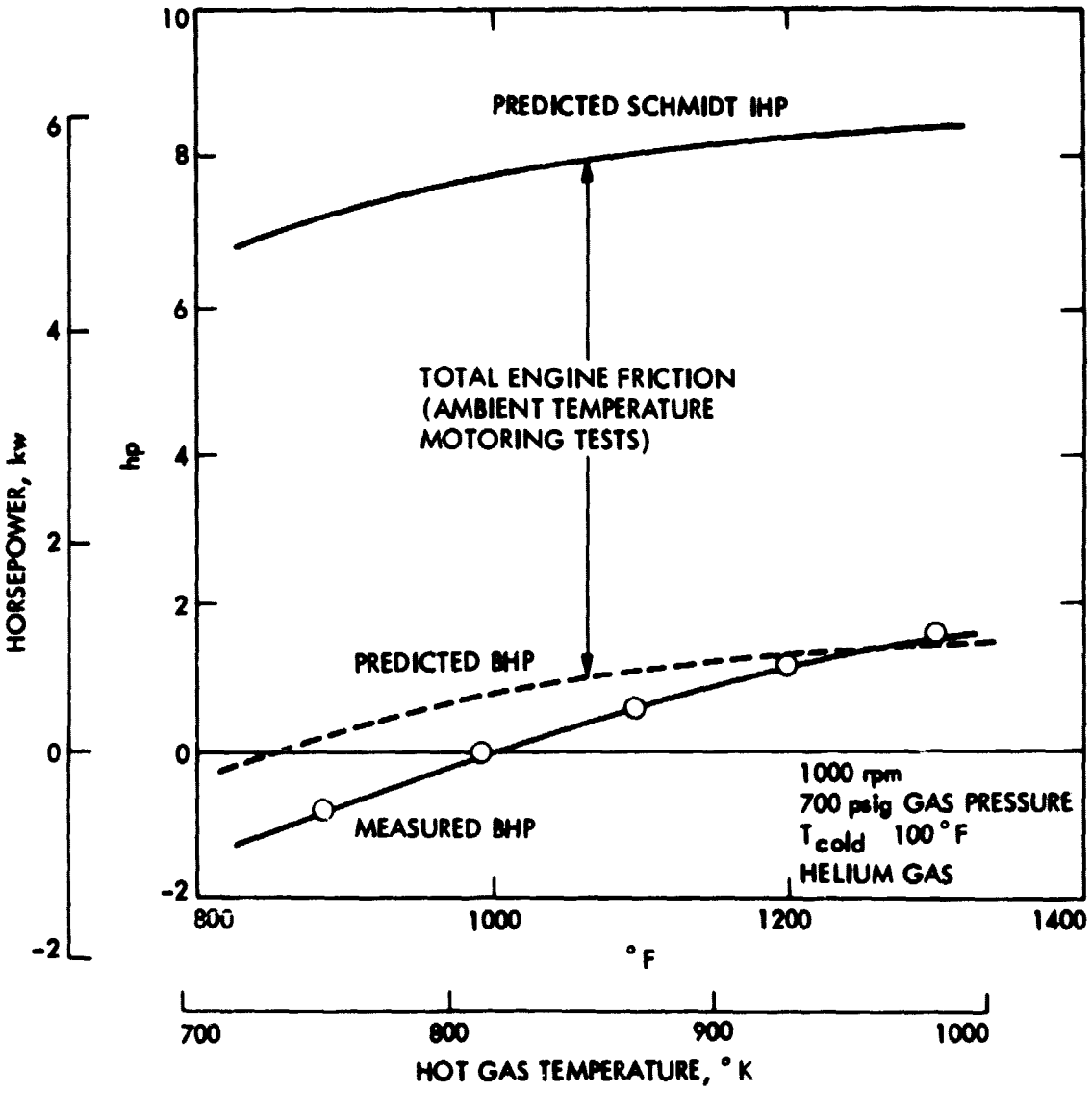

Figure 24. Typical SLRE Starting Characteristics

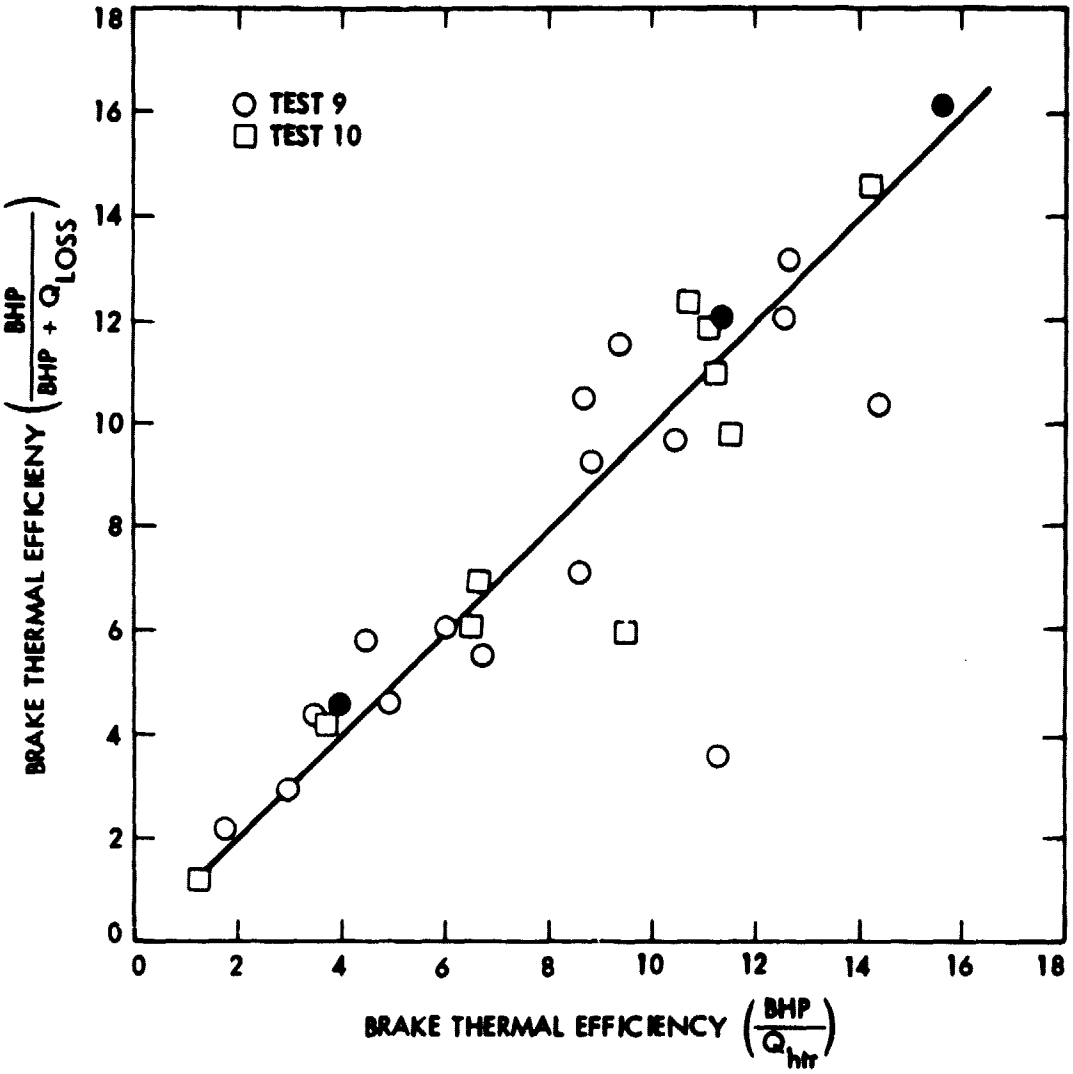

Figure 25. Experimental Heat Balance

line. For these cases, the engine is apparently operating on both heater and energy thermally stored.

The distribution of energy is shown in Figure 26 for the same three tests identified by the solid symbols in the previous figure. These are typical results obtained at constant working gas pressure and gas temperatures over a range of engine speeds. As shown in Figure 26, the largest energy consumer for for this case is the engine cooler which utilizes (as sensible heat to the cooling water) 66 to 71 percent of the available input energy. An additional 10 to 13 percent is transferred to the coolant flowing through the jacketed expansion cylinder. This latter heat flow undoubtedly represents excess cooling capacity in maintaining allowable temperature limits on the Rulon piston rings. No attempt was made to adjust any of the coolant flows in relation to engine performance during the limited test program.

A maximum of about 16 percent of the input heater energy was converted to net power during these particular tests. For the example of Figure 26, the unaccountable heat losses (shaded zone) ranged from about 4 to 12 percent. It is interesting to speculate that if the expansion cylinder could be run uncooled, then the engine brake horsepower should nearly double. This is one area which obviously requires further experimental investigation to optimize the SLRE energy distribution in terms of net output.

D. PERFORMANCE TEST RESULTS

An experimental test plan was devised so that an individual series of data points could be obtained with only a single change in the test variable. The independent variables studied included: (1) engine speed; (2) working gas pressure; (3) working gas temperatures (hot and cold); and (4) phase angle The initial performance results are discussed below.

1. Variable Engine Speed

Typical test results obtained over an 8-17 Hz (500 - 1000 rpm) speed range with constant temperature gas at two different pressure levels are shown in Figure 27. The lower part of the figure shows the brake (net) horsepower performance. As expected, horsepower increased with working pressure. The brake output power decreased with increasing engine speed since total engine friction increased at a faster rate than indicated horsepower (dashed line). These results suggest that further effort is required to optimize the regenerator and/or heater performance. Thermal efficiency data are plotted on the upper half of Figure 27, maximum efficiency is obtained at the lowest engine speed conditions.

Engine brake torque and heater input power are shown in Figure 28. Torque is shown to increase with decreasing speeds, which is a fundamental characteristic (good part-load performance) of Stirling engines of this type. Heater power, which represents the total input energy to the SLRE, increased with speed in order to maintain constant hot gas temperature conditions.

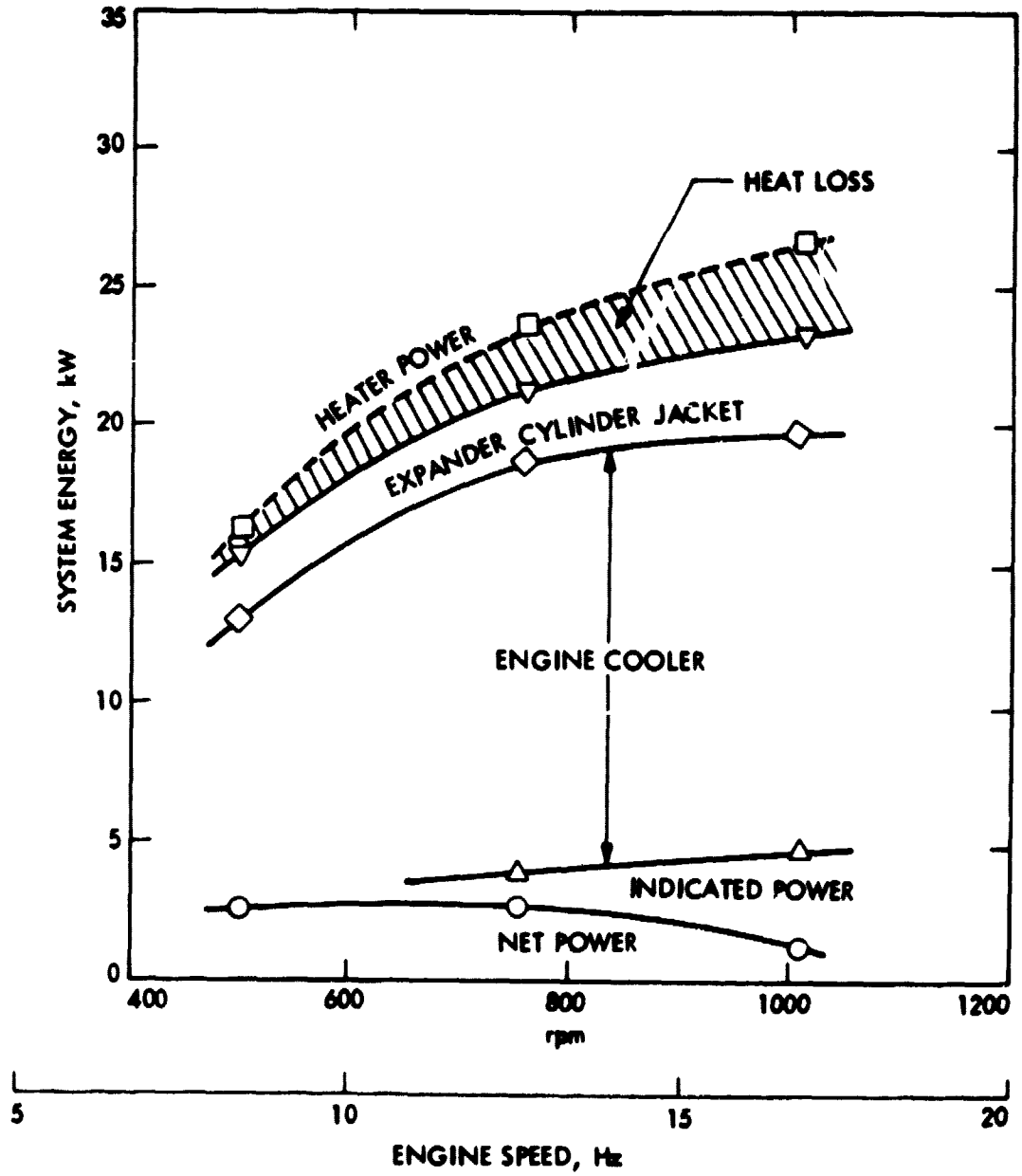

Figure 26. Typical Energy Distribution for SLRE

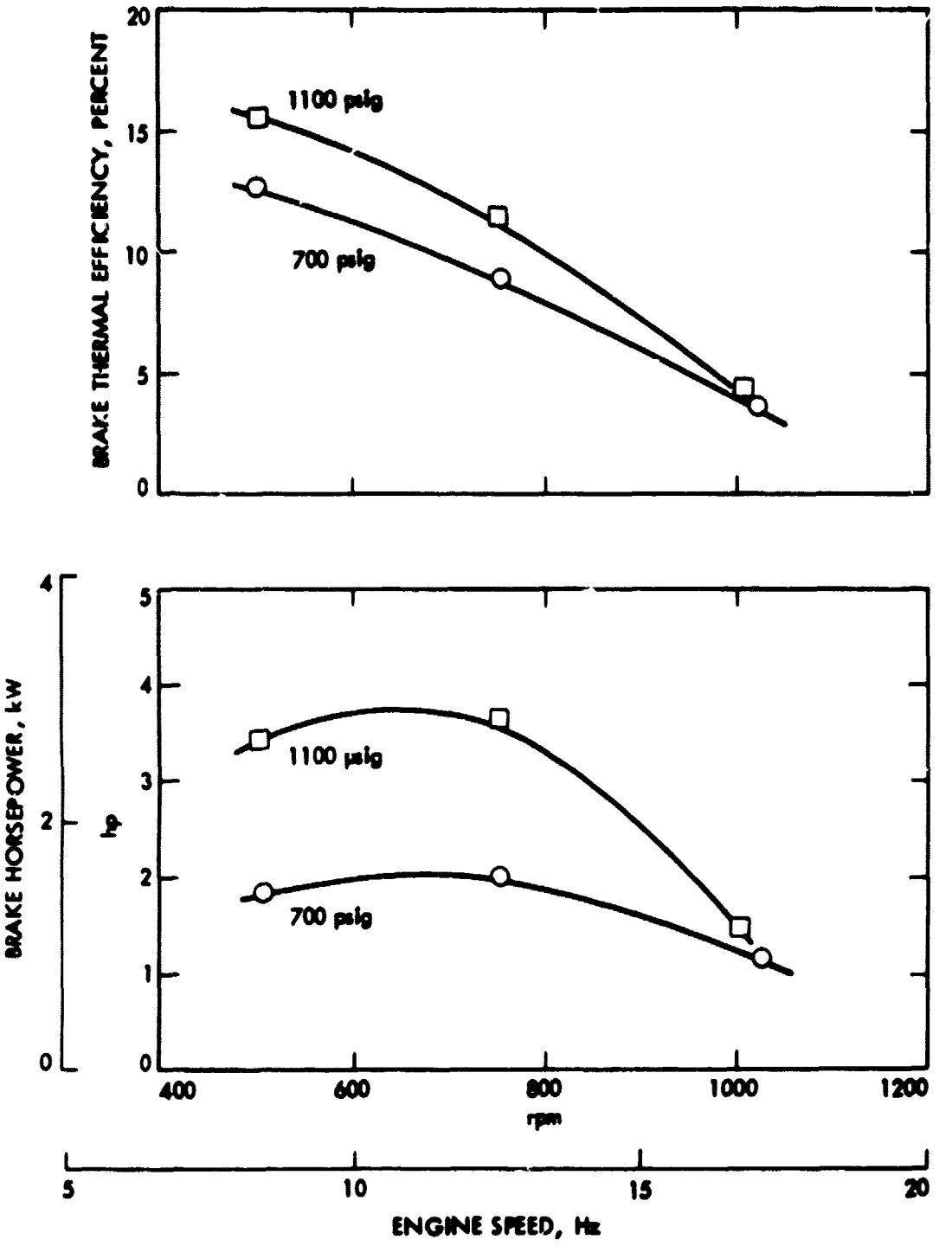

Figure 27. Engine Performance as a Function of Speed

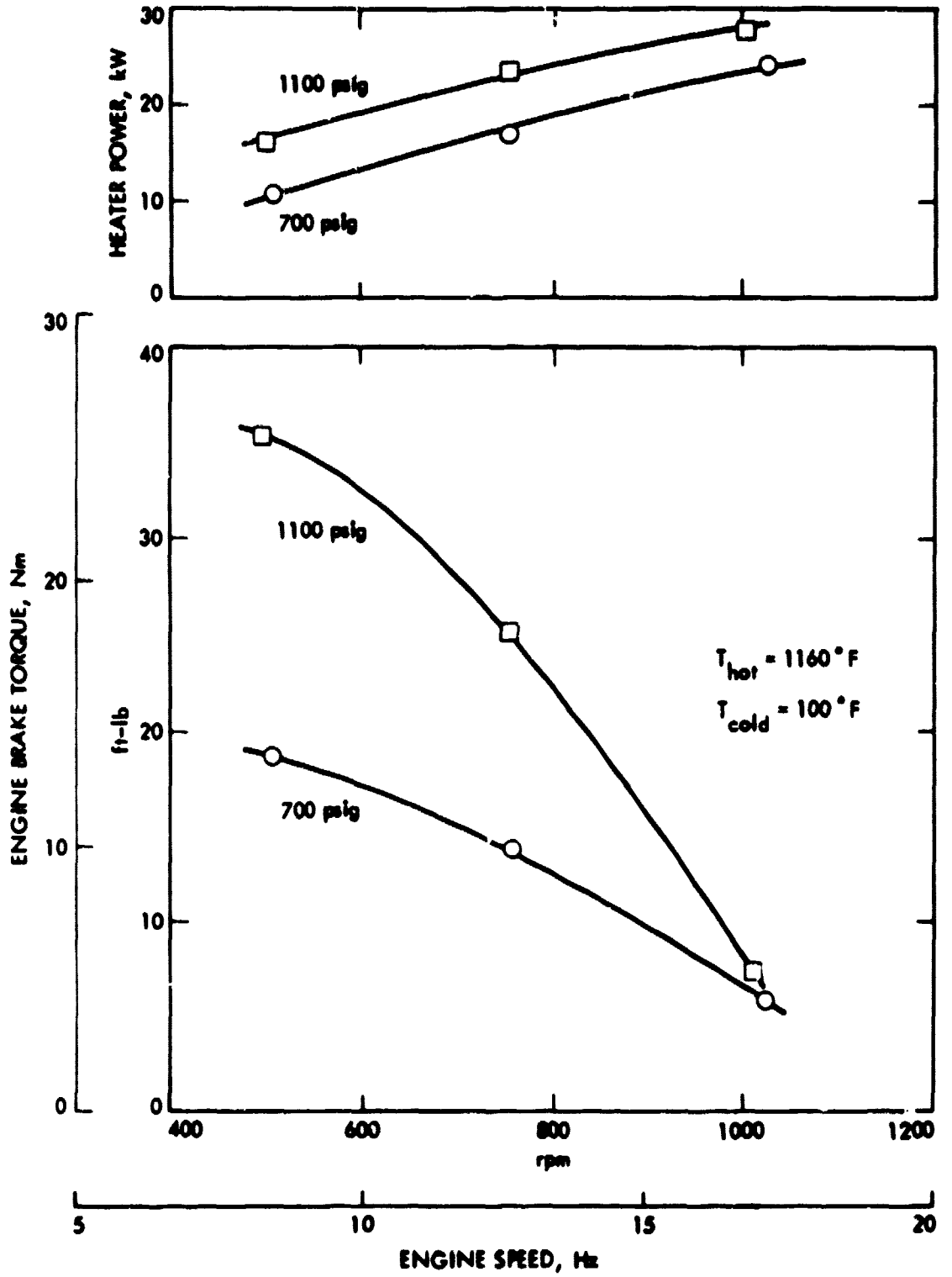

Figure 28. Performance Results with Variable Engine Speed

Profiles of pressure and temperature are measured across the three basic SLRE heat exchanger components (Figure 29). The data were obtained from the two previous test conditions made at 12 Hz (750 rpm). The hot and cold gas temperatures are seen to be nearly identical for the two tests at different pressure levels. The control point for the power supply is the heater temperature measured at the outside tube wall as indicated.

2. Variable Working Pressure

Performance results for a series of SLRE tests run with variable working gas pressures at three different engine speeds are shown in Figures 30 and 31. The mean gas pressure was varied from about 3.1 to 7.6 x 10^6 N/m^2 (450 to 1100 psig) for engine speeds of 8, 12 and 17 Hz (500, 750 and 1000 rpm). Both the thermal efficiency and brake horsepower results show similar trends (i.e., the performance improves with increasing working pressure and decreasing engine speed). The first result is typical of Stirling engines while the second appears contrary to that normally observed for fully developed engines.

In order to explain this apparent anomaly, a plot of heater input power and the differential gas temperature across the regenerator matrix is shown in Figure 31. For this example, all of the data (same tests as Figure 30) can be correlated with a single line. These results were obtained with an essentially constant mean gas temperature on the hot side of the matrix. The following observations were made concerning these data:

(1) The highest regenerator effectiveness is associated with those tests yielding maximum regenerator ΔT and requiring minimum input power.

(2) Regenerator effectiveness increases with decreasing engine speed due to longer residence time for heat transfer to occur between the matrix and working gas.

(3) Engine performance (brake horsepower and thermal efficiency) increases with increasing regenerator effectiveness (at constant pressure).

These observations suggest that the performance characteristics relate directly to regenerator effectiveness. Verification of this interim conclusion is a subject of further investigation.

3. Variable Gas Temperature

The test plan was designed to give visibility to the separate effects of variations in both the hot and cold gas temperatures. As discussed earlier, the hot gas temperature is controlled by the electrical energy supplied to the heater head, while the cold gas temperature is regulated by the cooling water flow.

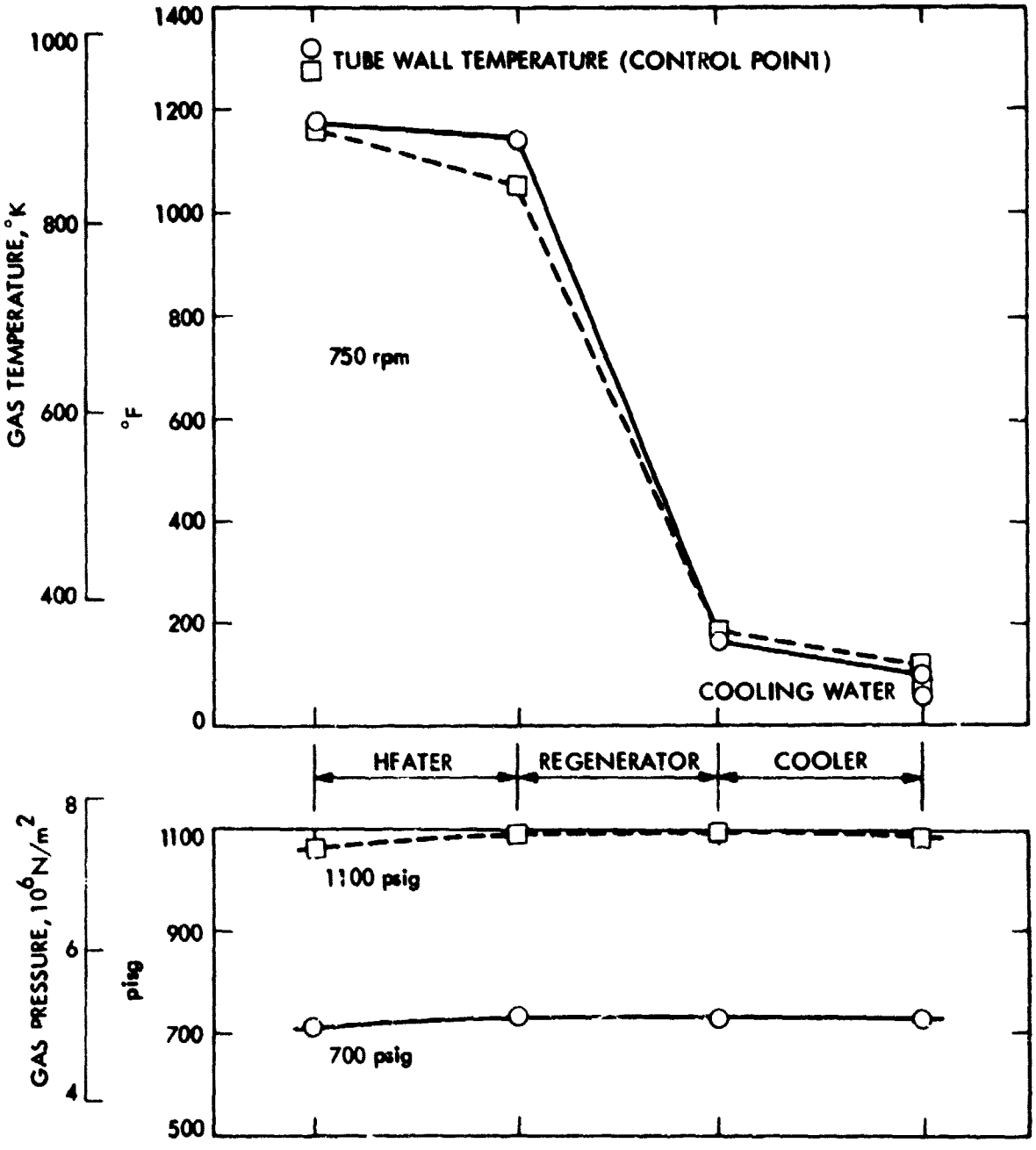

Figure 29. Working Gas Temperature and Pressure Profiles

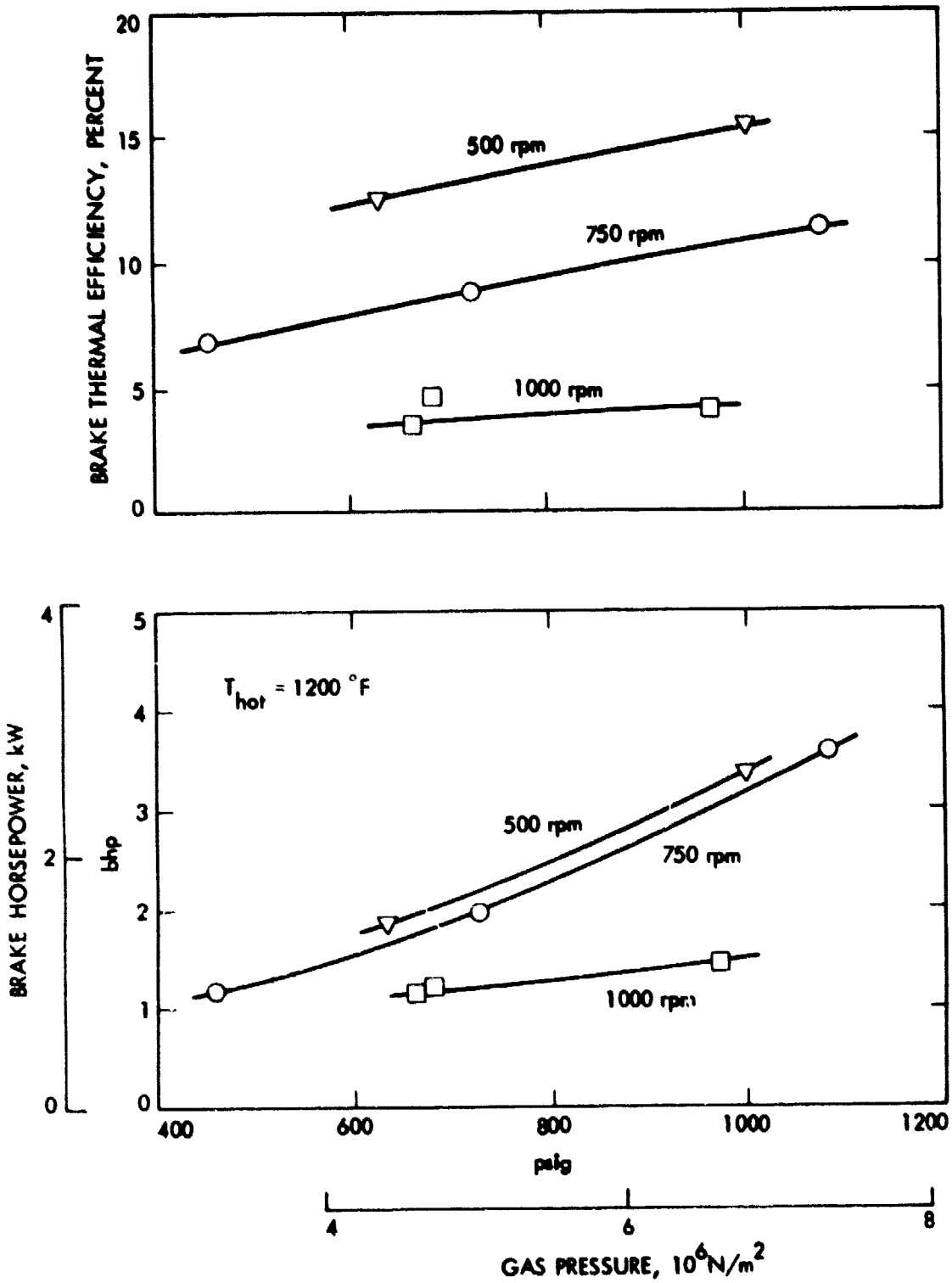

Figure 30. Brake Performance as a Function of Working Gas Pressure

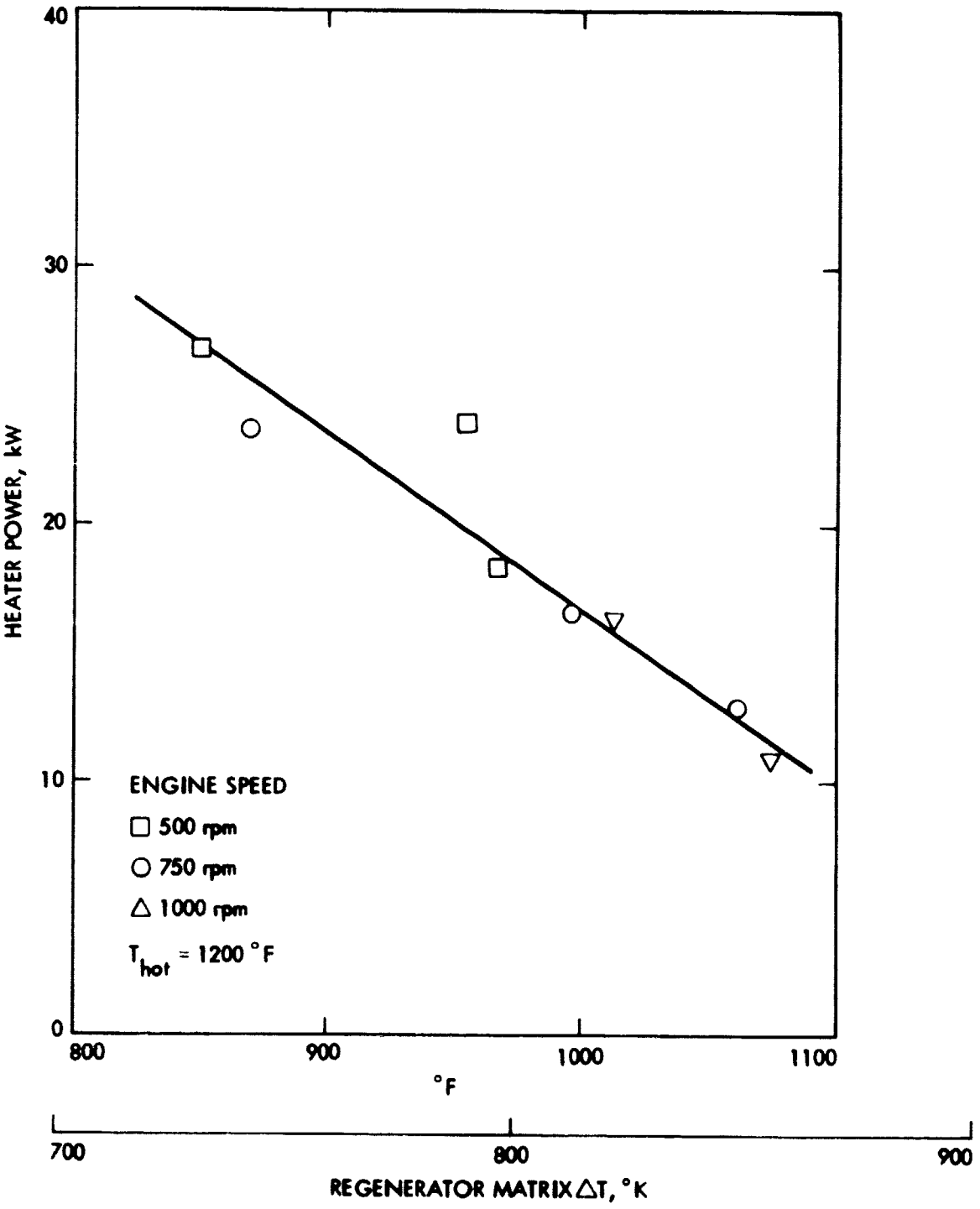

Figure 31. Data Correlation in Terms of Regenerator Performance

The SLRE mean hot gas temperature was measured by a closed sheath thermocouple installed in the helium working gas between the expansion space and heater head. The experimental data, obtained at a constant speed of 12 Hz (750 rpm) for two different working pressures are shown in Figure 32 for a range of hot gas temperatures from 810 to 950°K (1000 to 1250°F). The brake horsepower is seen to be about equally sensitive to changes in temperature for both levels of working gas pressure. Extrapolation of this temperature to 1034°K (1400°F) yields a predicted increase in BHP of about 36%. Thermal efficiency appears less responsive to temperature changes at reduced pressure levels.

The cold gas temperature was measured in the working gas at the interface between the engine cooler and the compression space. The results of three tests with variable cold gas temperatures is shown in Figure 33. As expected, performance of the SLRE decreases with increasing cold gas temperatures. The hottest temperature achieved in the compressor-end gas was about 370°K (205°F).

4. Variable Phase Angle

The last test variable studied was phase angle, and data obtained over a 1.2 to 1.9 rad (70 to 110°) change are presented in Figure 34. Although the optimum phase angle was not determined during this limited test series, examination of these results suggests that it approaches 1.6 rad (90°).

E. ENGINE INDICATED PERFORMANCE

In addition to obtaining overall engine performance, data were recorded which permitted the calculation of indicated performance. As described in Section IV.B, fast response (cyclic) pressure data were recorded on magnetic tape and then computer-processed to produce pressure-volume diagrams. The indicated performance results, obtained from the integration of these diagrams, are tabulated in Table 8. A data acquisition problem limited these results to those tests run at speeds greater than 8 Hz (500 rpm). A typical set of computer processed data obtained for a single test point is shown in Appendix B. A discussion of the indicated performance results follows.

1. Variable Engine Speed

Horsepower and engine efficiency test results are shown in Figure 35 for three different engine speeds. For a constant working pressure of about 5.0×10^6 N/m^2 (720 psig), the brake performance (horsepower and thermal efficiency) are both shown to decrease with increasing speed. These observations are similar to those seen previously in Figure 28. The maximum brake thermal efficiency for these particular tests is 8.9% at 13 Hz (755 rpm); the corresponding indicated efficiency is 19.7%. Mechanical efficiency for the preprototype SLRE decreases from about 45% to only 13% for these particular tests. This relatively poor efficiency contributes to the low brake performance measured at higher engine speeds. The highest mechanical efficiency point recorded for the entire test series (see Table 8) was about 58% and corresponds to a maximum brake power output of about 3.0 kW (4.0 hp).

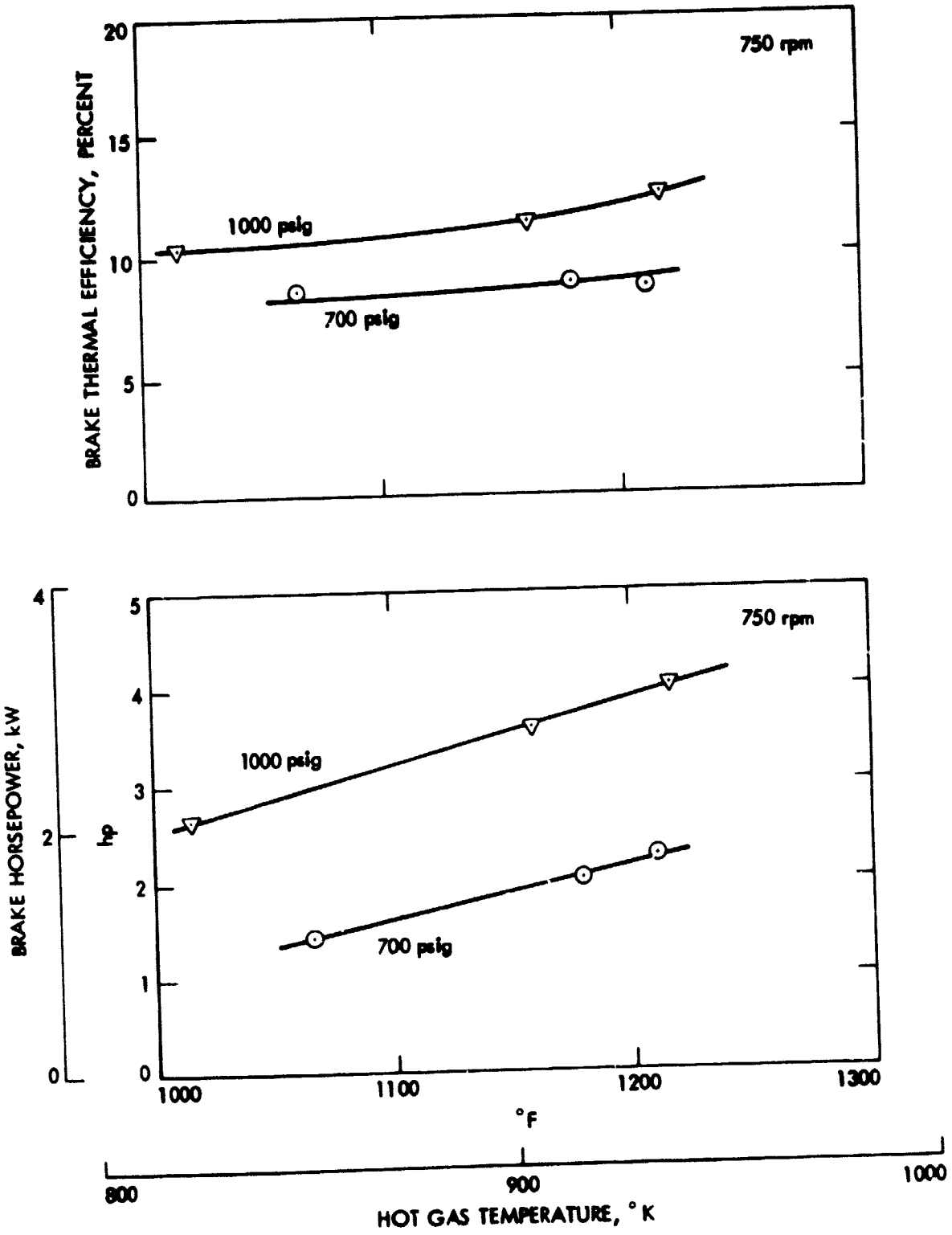

Figure 32. Brake Performance as a Function of Hot Gas Temperature

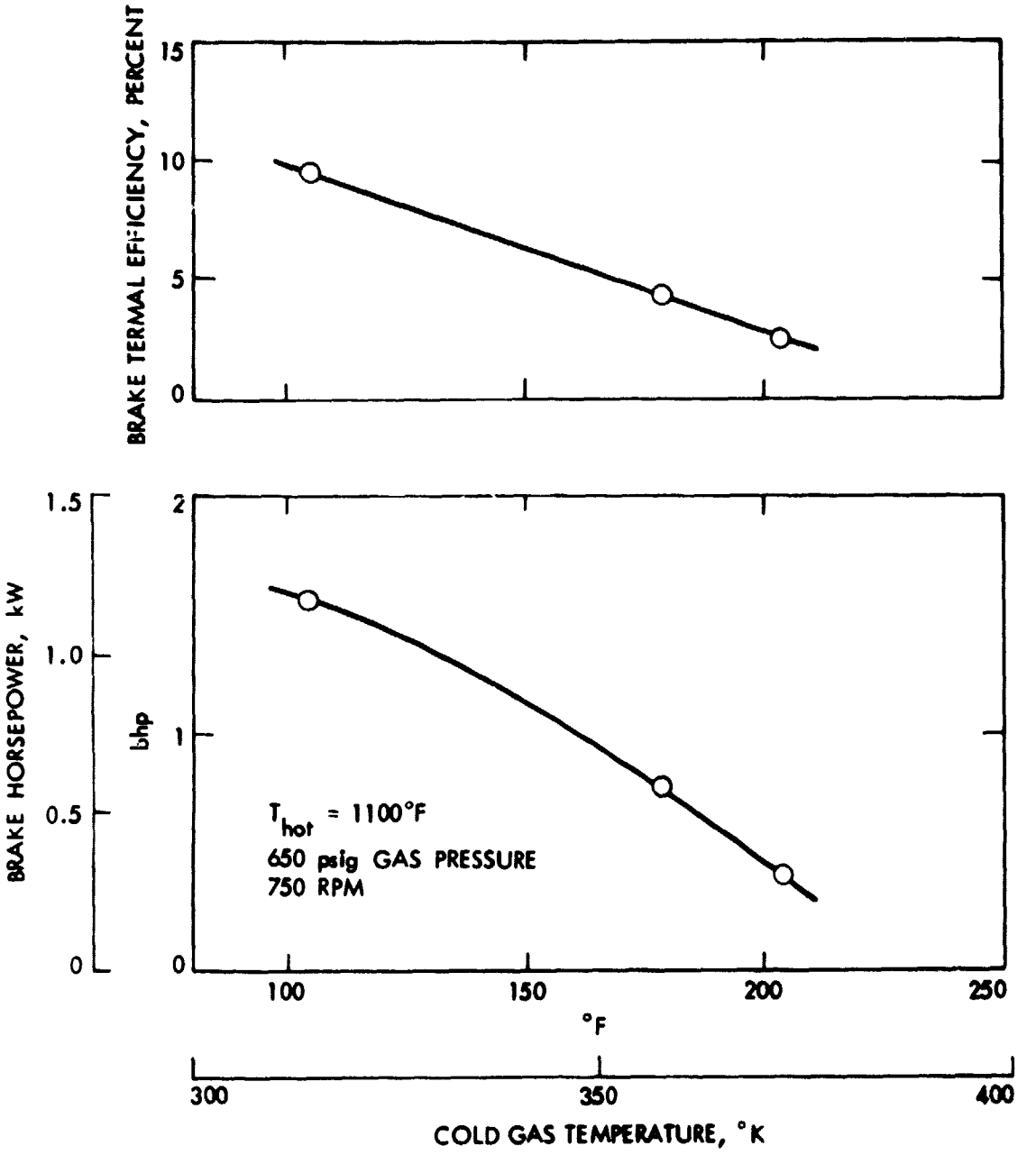

Figure 33. Brake Performance as a Function of Cold Gas Temperature

Table 8. Indicated Performance Summary - Test 9

Test Point	Expander Power, hp	Compressor Power, hp	Net Indicated Power, hp	Thermal Eff., %	Mechanical Eff., %	Net Indicated Torque, ft-lb	Ideal Ihp[a]
1	11.52	-8.90	2.62	24.1		13.68	7.21
2	12.03	-8.68	3.35	12.8		17.40	7.85
3	12.56	-8.46	4.10	13.1	12.9	21.15	8.03
4	12.73	-8.14	4.60	14.3	24.4	23.64	8.29
5	12.56	-7.55	5.01	14.7	30.6	25.69	8.40
6	8.88	-5.22	3.66	22.6	38.0	25.60	5.52
7	9.83	-5.46	4.37	19.7	45.1	30.38	5.81
8	9.65	-5.12	4.54	17.9	48.6	31.51	6.16
11	11.07	-6.83	4.24	18.4	33.7	25.41	7.11
12	12.15	-7.51	4.64	18.7	25.7	24.28	8.15
13	13.22	-7.92	5.31	20.8	50.0	37.05	8.40
14	14.92	-8.43	6.49	20.2	55.9	45.12	9.46
15	14.77	-7.83	6.94	21.8	57.8	48.14	9.41
18	16.15	-11.36	4.79	16.3	19.0	25.10	10.17
19	16.49	-11.30	5.19	14.1	27.6	27.02	11.35
20	13.18	-7.19	5.99	18.8	60.6	41.64	8.35
21	6.83	-4.07	2.76	32.1	35.2	19.41	4.06
22	6.68	-3.72	2.96	17.1	39.7	20.79	4.07

[a]Based upon idealized Schmidt cycle analyses.

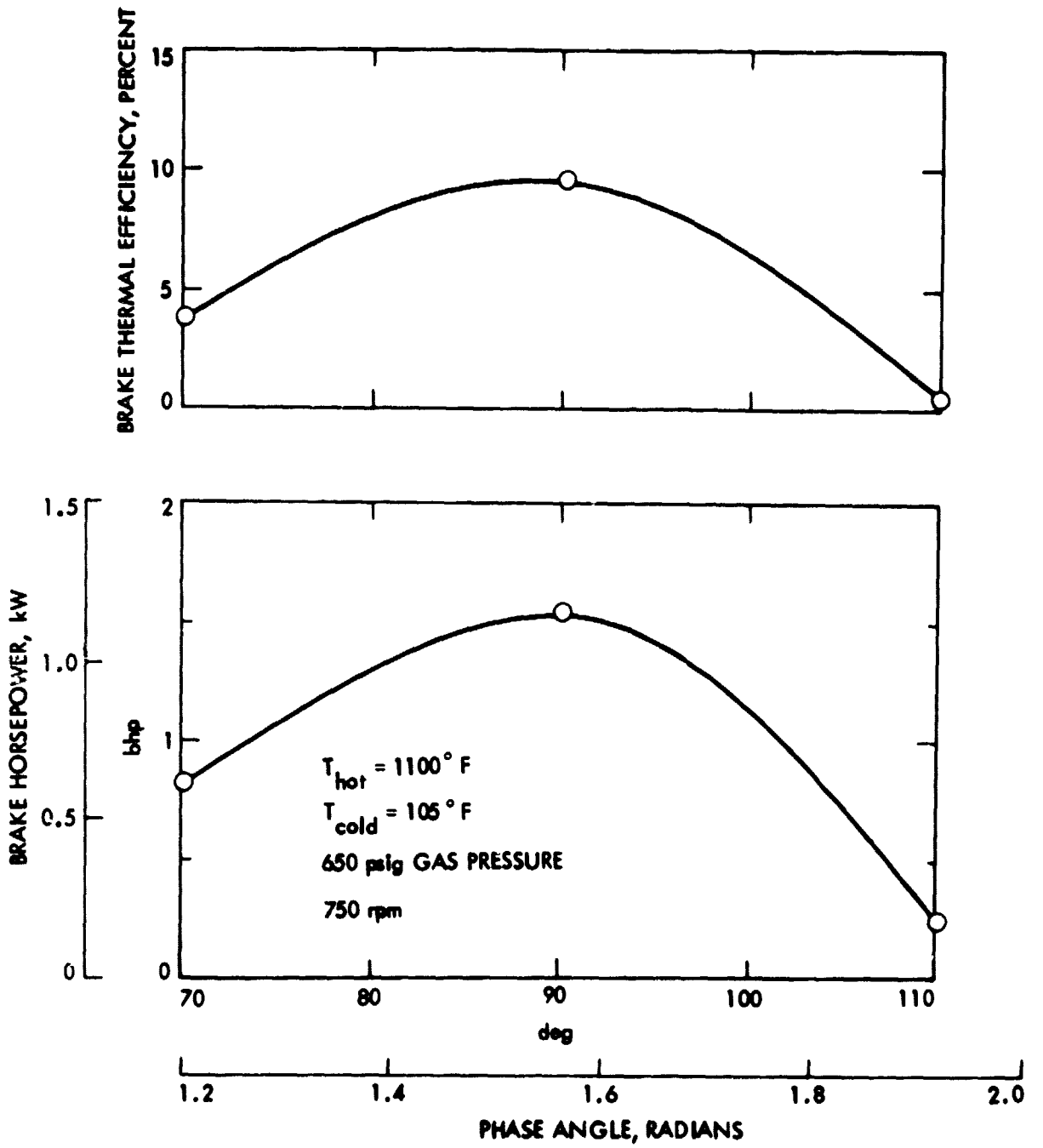

Figure 34. Brake Performance as a Function of Phase Angle

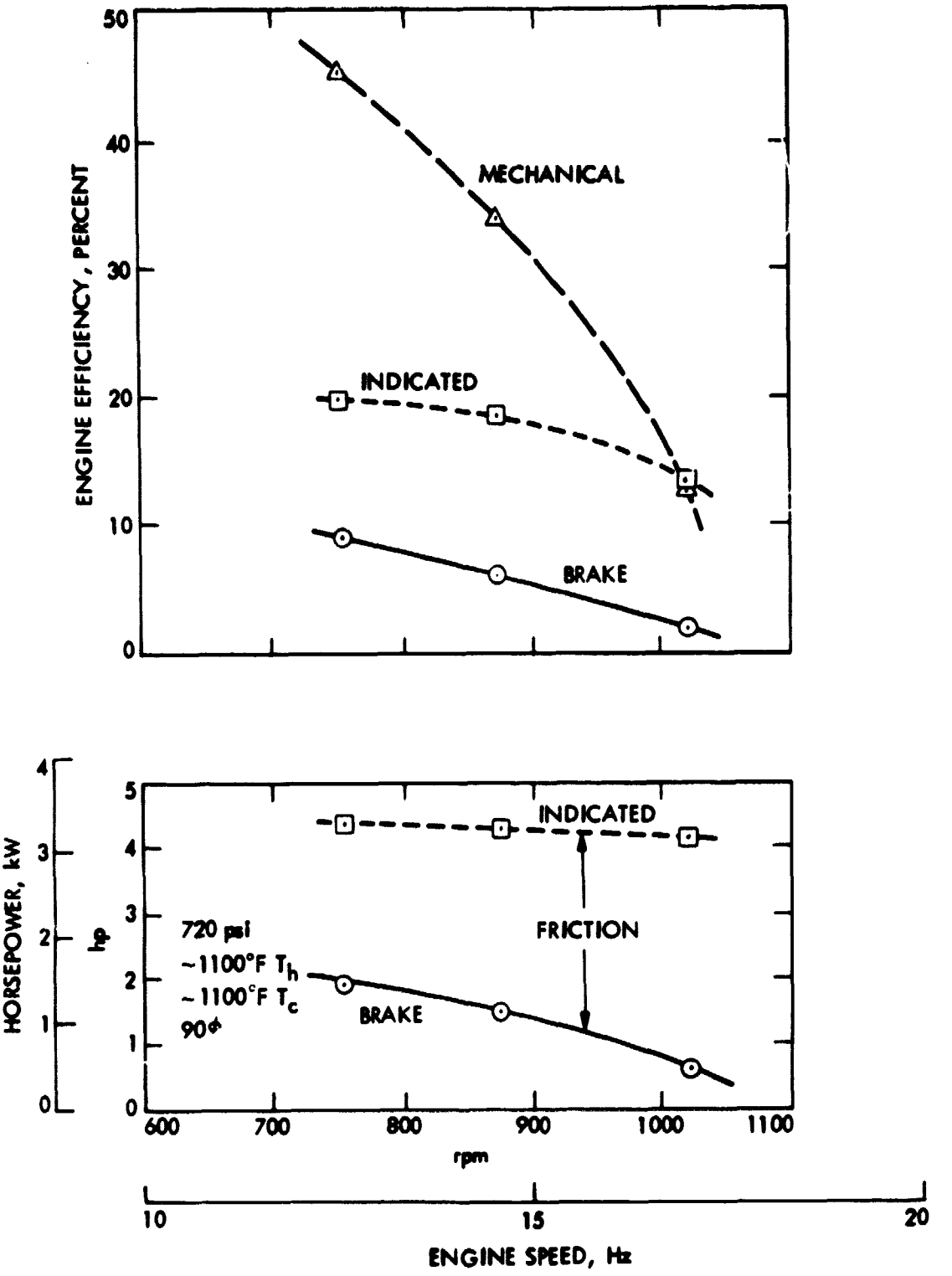

Figure 35. Indicated Performance with Variable Engine Speed

As indicated in Figure 35, the difference between the brake and indicated horsepower data represents the friction horsepower (FHP). These data are also shown in Figure 36, together with mechanical friction data obtained during an earlier motoring test (see Figure 20). As shown, the motoring test results are 10-20% higher than that calculated from the indicated performance data. Several factors could contribute to this difference. First, the higher motoring data could reflect some measure of engine pumping losses even though care was taken to minimize these effects. In addition, the running friction data could be lower (because of high engine operating temperatures) due to gas density effects upon fluid friction, and oil viscosity effects upon mechanical friction.

2. Variable Hot Gas Temperatures

Similar results were obtained at constant speed an variable hot gas temperature (see Figure 37). For this case, the mechanical efficiency increases from about 38 to 49% with a corresponding increase in gas temperature from 847 to 927°K (1065 to 1209°F). This trend confirms the previous observation.

3. Comparison with Analytical Predictions

Typical experimental indicator diagrams are shown in Figures 38 and 39. Included are diagrams calculated (predicted) from the idealized Schmidt theory. Separate diagrams for the compression and expansion spaces are shown in Figure 38; the dashed lines represent the Schmidt predictions. Agreement is seen between the two diagrams drawn for the SLRE expansion space. For the compression space, the Schmidt model under-predicts the cycle work, probably because of higher fluid frictional losses in the experimental preprototype engine.

These two diagrams are combined into a single system indicator diagram shown in Figure 39. The net result is a predicted higher value for indicated horsepower than that actually achieved by experiment. However, the agreement between theory and experiment must be considered as good in view of the oversimplifications incorporated into the Schmidt cycle model. A summary of the predicted Schmidt IHP values can be found in Table 8.

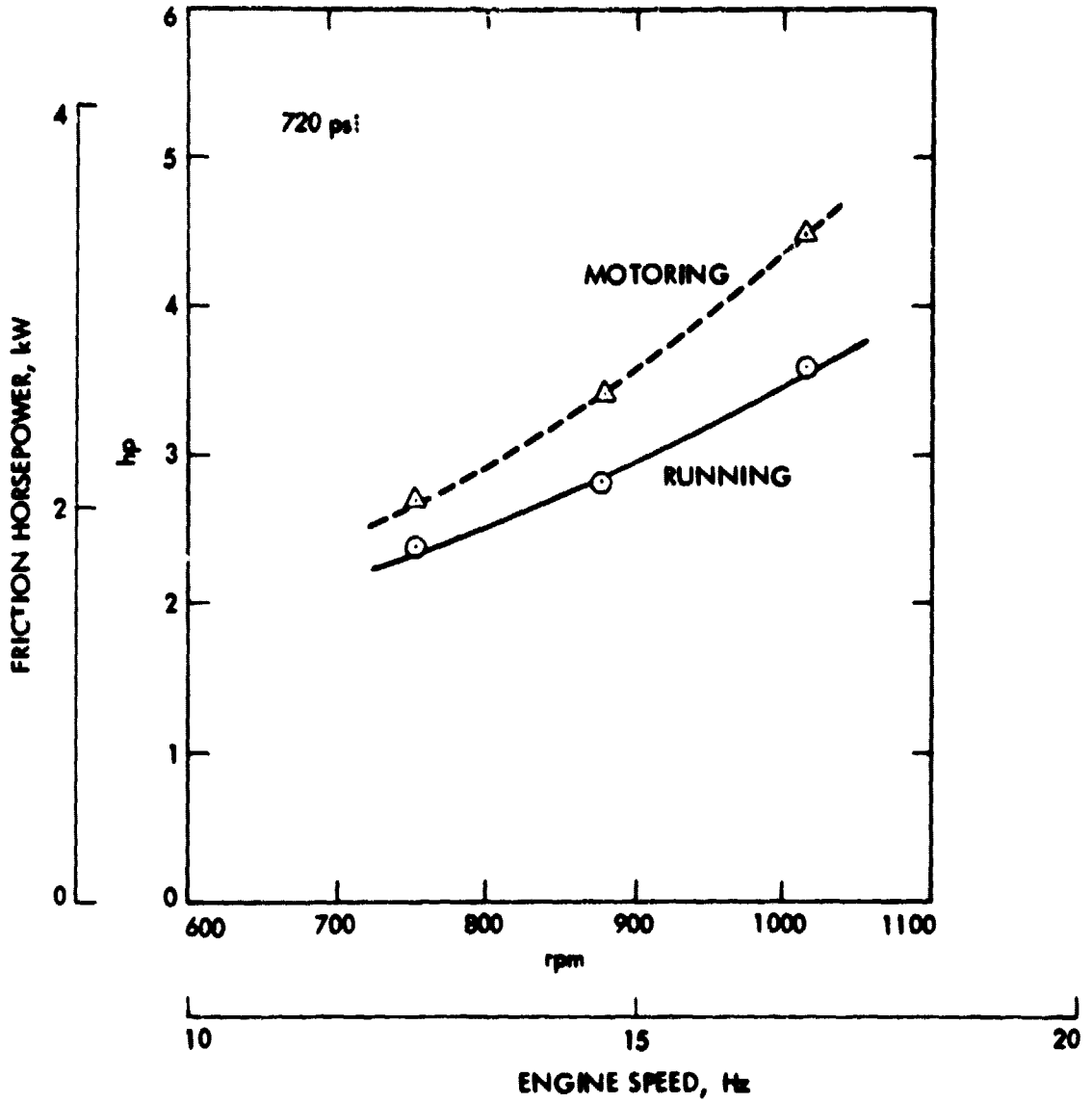

Figure 36. Comparison of Motoring and Running Friction Horsepower

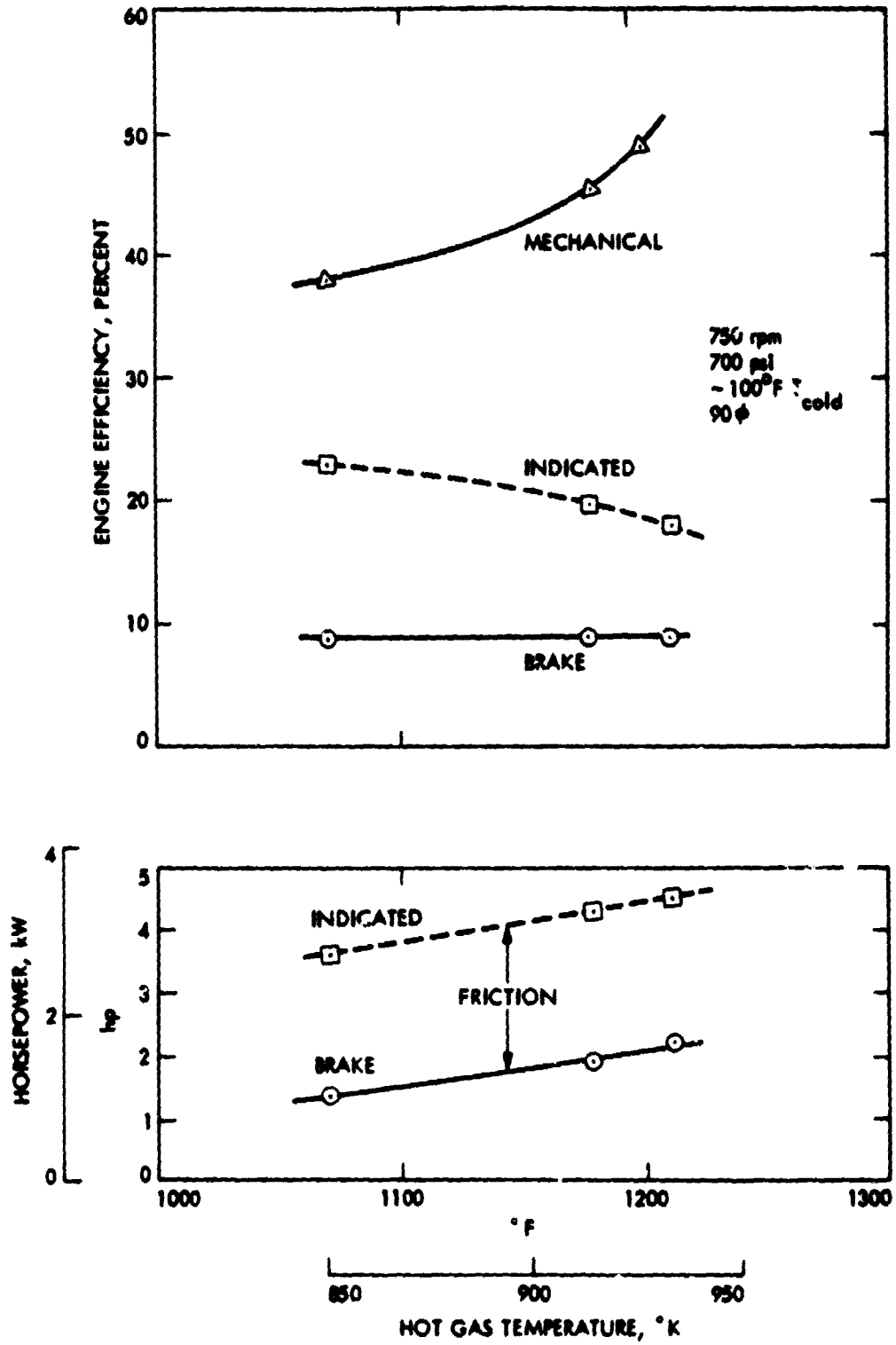

Figure 37. Indicated Performance as a Function of Hot Gas Temperatures

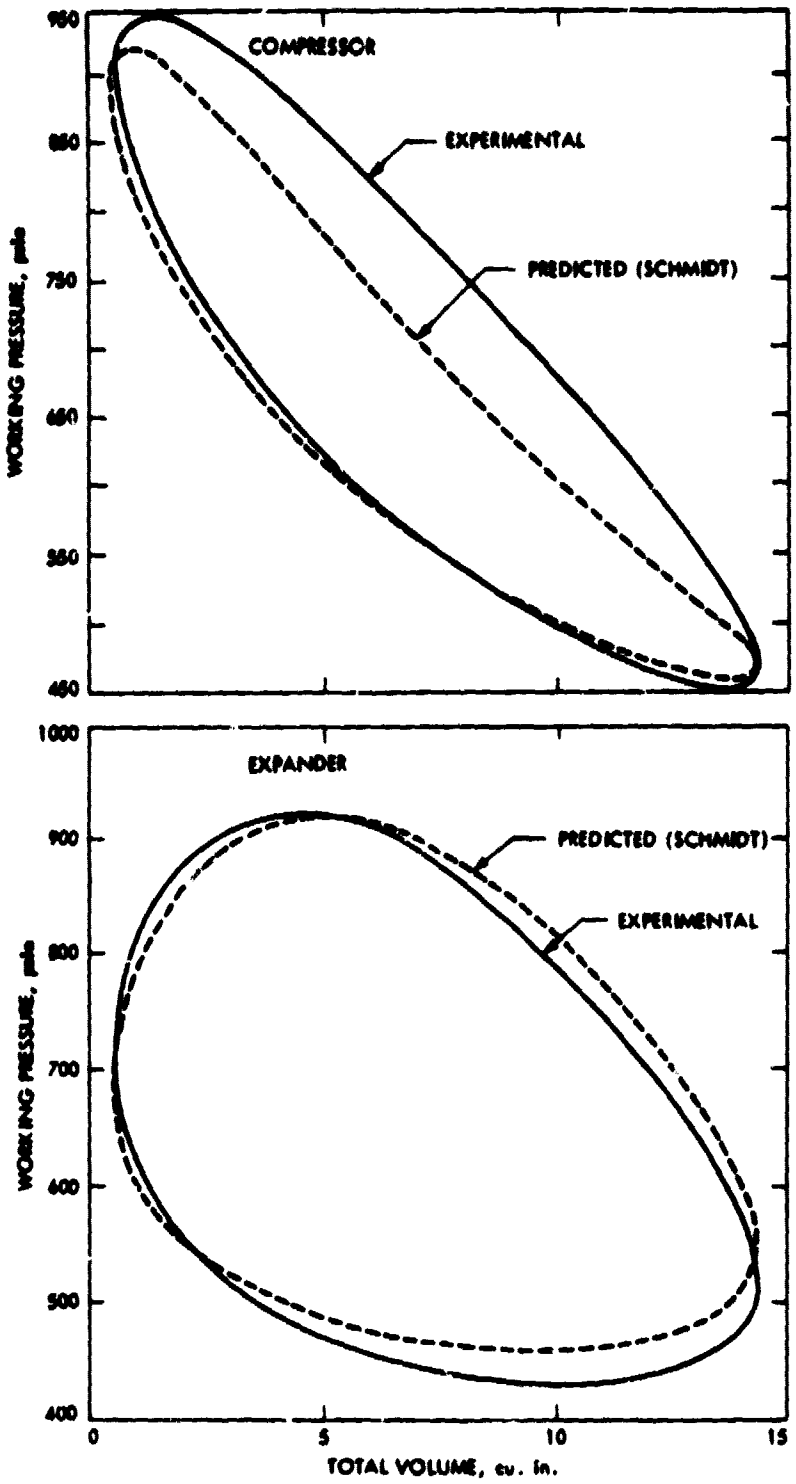

Figure 38. Indicator Diagrams for Compression and Expansion Spaces

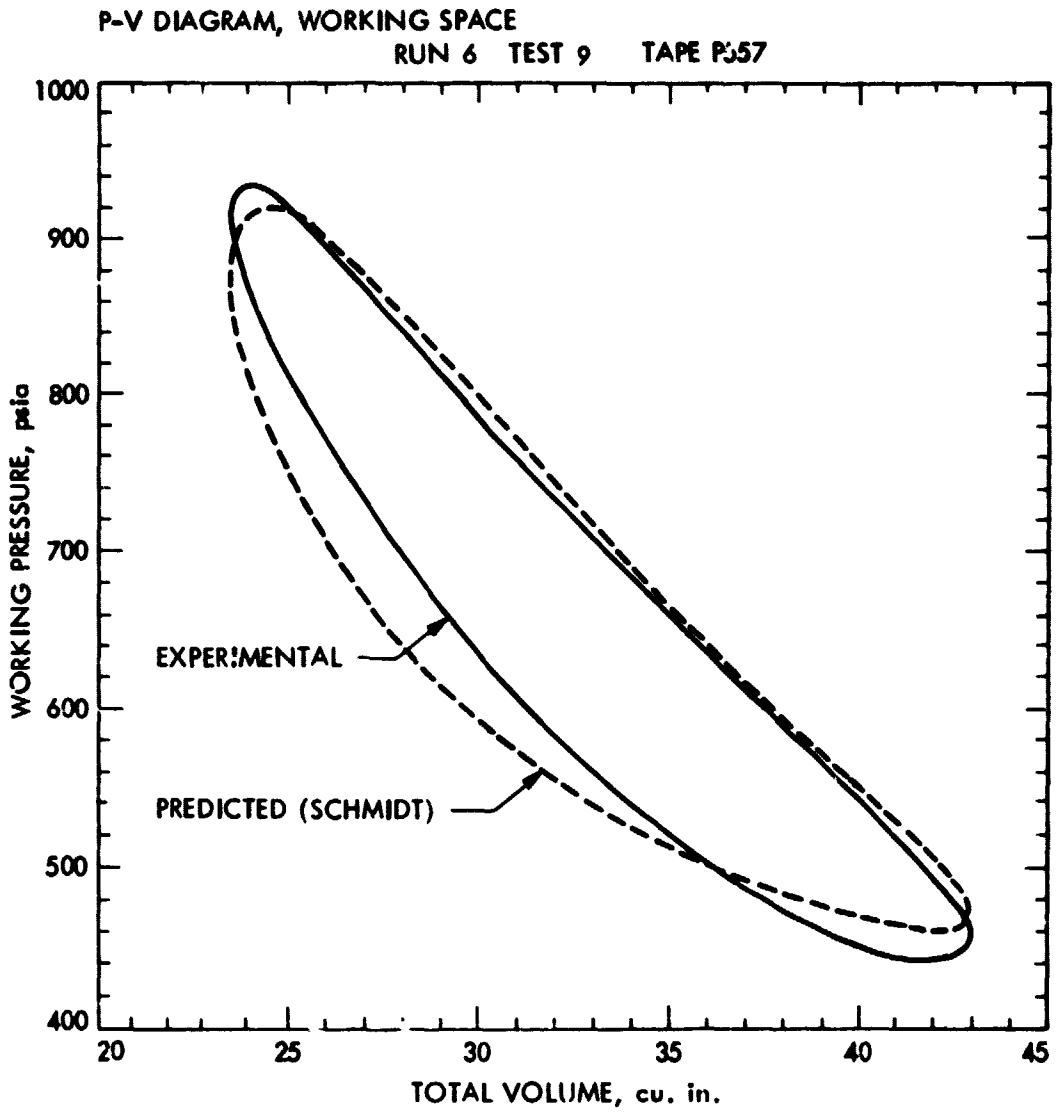

Figure 39. Typical Indicator Diagram for Total Working Space

VI. CONCLUSIONS AND RECOMMENDATIONS

This effort was accomplished independently of foreign technology and has validated the concept of a simple laboratory research engine to support basic Stirling cycle research. This section discusses specific conclusions based on the findings of this work:

First, the design concept of modular construction and interchangeable components was proven during actual operation of the preprotype engine. The method of electrical heating using a heater head with special resistance elements was successfully demonstrated.

Second, based upon a limited number of experimental test cases, the SCCM program has not been entirely successful in its attempt to model the flow dynamics of the SLRE. The initial results yielded either a uniform pressure throughout the engine or a binary valued distribution with a discontinuous pressure change occuring near the center of the regenerator. These predicted results did not yield accurate mass flow calculatons upon which more elaborate and realistic heat transfer and pressure drop calculations could be made. The SCCM program successfully demonstrated, however, the flexibility and utility of the modular approach in developing an analytical Stirling computer model. This feature allows a large variety of designs to be simulated to various levels of desired accuracy or refinement with a minimum of effort on the part of the user, and without involving changes in the program logic and structure.

Third, a significant interest was shown by the surveyed technical community in acquiring test engines of this type to support both fundamental Stirling cycle research and component developments for various commercial applications. University participation in research activities will almost certainly require some type of supporting grant or other subsidy.

Fourth, initial test results with the preprototype SLRE have demonstrated engine operation at its design temperature and pressure levels within a limited speed range. High engine performance was not a primary goal of the preprototype engine task. It is expected, however, that significant improvements could be achieved by the appropriate R&D efforts.

The following options were identified as possible sources of engine performance improvements:

(1) Use improved regenerator matrix.

(2) Increase engine working pressure.

(3) Reduce heat loss to cylinder jackets.

(4) Increase engine speed.

(5) Increase operating temperature.

(6) Change working gas to hydrogen.

Based upon the results obtained with the preprototype SLRE, interest shown by the technical community, and a general lack of fundamental understanding in Stirling engines, it is recommended that this effort be continued and a next generation engine design be accomplished. In a report to Congress by the Department of Energy (Ref. 9), it was stated that there remains a basic lack of knowledge by the technical community in the Stirling engine and that specifically designed laboratory-type engines should be considered for university use. This goal is consistent with the intent of the SLRE project.

It is proposed that the detailed design be accomplished by an outside contractor(s) to take advantage of expertise in engine fabrication techniques to reduce the unit cost. Three prototype engine builds are recommended, two would be delivered to universities for comparative performance validation tests. It is further recommended that the new prototype engines, as well as the present JPL preprototype engine, be used to support basic Stirling cycle research. The following are suggested research objectives:

(1) Increase U.S. understanding of Stirling machines.

(2) Create and expand a public U.S. Stirling technology base.

(3) Create a cadre of U.S. Stirling research experts.

(4) Create a supply of Stirling-trained engineering graduates.

(5) Fully exploit the energy saving capabilities of Stirling cycle machines.

(6) Hasten the introduction of stirling engines into the commercial market.

The program could initially focus on the thermodynamics of the Stirling cycle to:

(1) Gain a better understanding of the transient fluid dynamics and heat transfer.

(2) Develop a methodology for optimizing the thermodynamic cycle of a real engine.

(3) Develop cyclic analytical models of engine components and systems.

VII. REFERENCES

1. Walker, G., "Stirling Engines," University of Calgary, September 1978.

2. van Giessel, R., and Reinink, F., "Design of the 4-215 D.A. Automotive Stirling Engine," SAE Paper 770082, presented at the International Automotive Engineering Congress, Detroit, Michigan, February 1977.

3. Schmidt, G. "Theore der Geschlossen Calorischen Maschine Laubroy and Schwatskopff in Berlin," Z ver Oster Ing., 1861.

4. Finegold, J. G., and Vanderbrug, T. G., Stirling Engines for Undersea Vehicles, JPL Report 5030-63, NASA, March 1977.

5. Jet Propulsion Laboratory, California Institute of Technology, "Should We Have a New Engine? An Automotive Power Systems Evaluation," JPL SP43-17, August 1975.

6. Hoehn, F. W., Stirling Laboratory Research Engine: Report on the Design and Fabricaton of the Preprototype Configuration, JPL Interim Report 5030-178, NASA, January 1979.

7. Anderson, J. W., and Hoehn, F. W., Stirling Laboratory Research Engine Survey Report, JPL Publication 79-86, NASA, September 1979.

8. McDougal, Allan R., "Phase-Angle Controller for Stirling Engines," United States Patent Number 4,240,256, December 23, 1980.

9. First Annual Report to Congress on Automotive Technology Development Program, DOE, August 1979.

VIII. APPENDICES

Appendix A - Standard Instrumentation List

Symbol	Parameter Location	Units	Range
TRQ	Engine Torque	lb-ft	±50
PDC	Compressor-Cooler Pr*	psig	2000
PCR	Cooler-Regenerator Pr	psig	2000
PRH	Regenerator-Heater Pr	psig	2000
PHE	Heater-Expander Pr	psig	2000
PDB	Compressor Buffer Pr	psig	2000
PDL	Compressor End Lube Pr	psig	2000
PEL	Expander End Lube Pr	psig	2000
PSC	Seal Cavity Pr	psig	2000
PWC	Cooler Water Inlet Pr	psig	100
ACC-X	Accelerometer, X-Axis	g	
ACC-Y	Accelerometer, Y-Axis	g	
ACC-Z	Accelerometer, Z-Axis	g	
PHTR	Heater Power	kW	40
PHANG	Phase Angle	deg	±180
RPM	Engine Speed	rpm	4000
TCR	Cooler-Regenerator Temp	°F	1000
TS	Heater Sheath Temp	°F	1500
TRH	Regenerator-Heater Temp	°F	1500
THE	Heater-Expander Temp	°F	1500
TDC	Compressor-Cooler Temp	°F	500
TDL	Compressor End Lube Temp	°F	500
TEL	Expander End Lube Temp	°F	500
TBS	Buffer Space Temp	°F	500
TWC	Delta Cooling Temp	°F	3
FCW	Cooler Water Flowrate	gpm	50
FEW	Expander Water Flowrate	gpm	50

* The dash signifies that the measurement is made at the interface between the compression space and cooler, etc.

Appendix B - Typical Indicated Performance Data

Test Number 9

Test Point 15

Work done on expander-side of engine:	643.79 ft-lb
Work done on compressor-side of engine:	-341.35 ft-lb
Net work done by engine:	302.44 ft-lb
Average expander power:	14.77 hp
Average compressor power:	-7.83 hp
Average net power:	6.94 hp
Average expander-side torque:	102.46 ft-lb
Average compressor-side torque:	-54.33 ft-lb
Average engine torque:	48.13 ft-lb
Average expander working space pressure:	1073.8 psia
Average compressor working space pressure:	1094.0 psia
Average buffer space pressure:	962.8 psia
Average working space pressure:	1083.9 psia

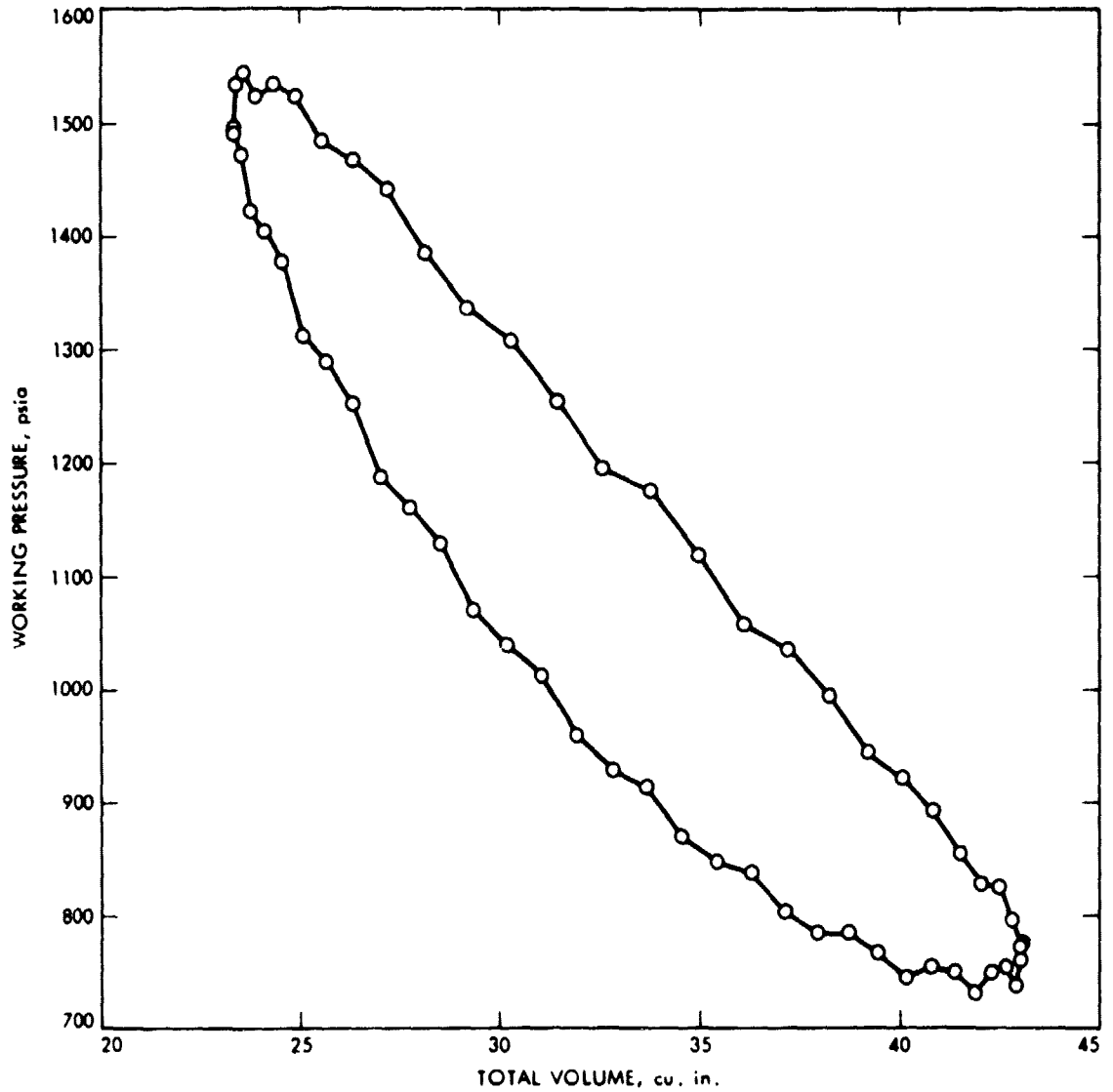

Figure B-1. Pressure-Volume Diagram for Total Working Space

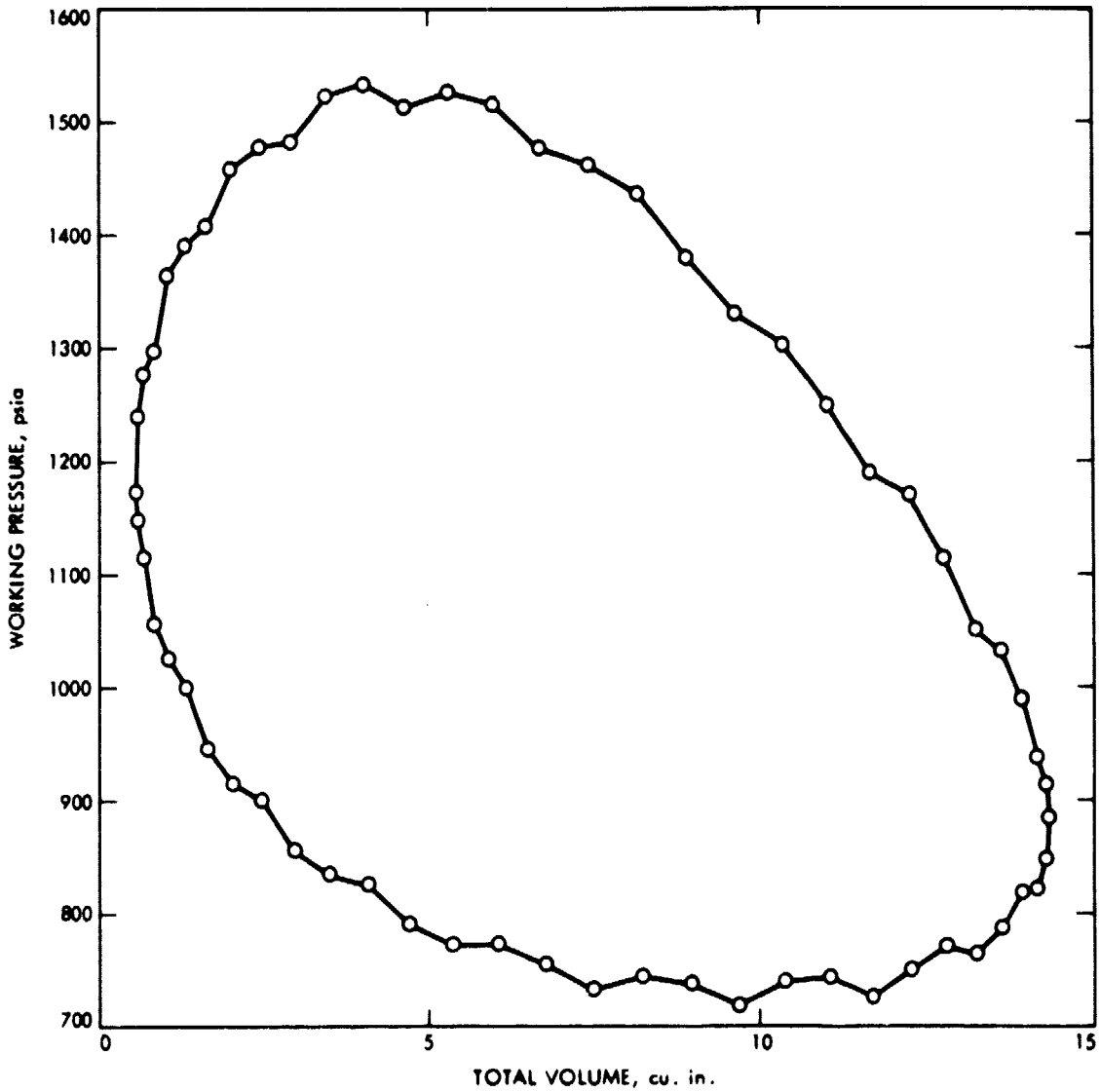

Figure B-2. Pressure-Volume Diagram for Expansion Space

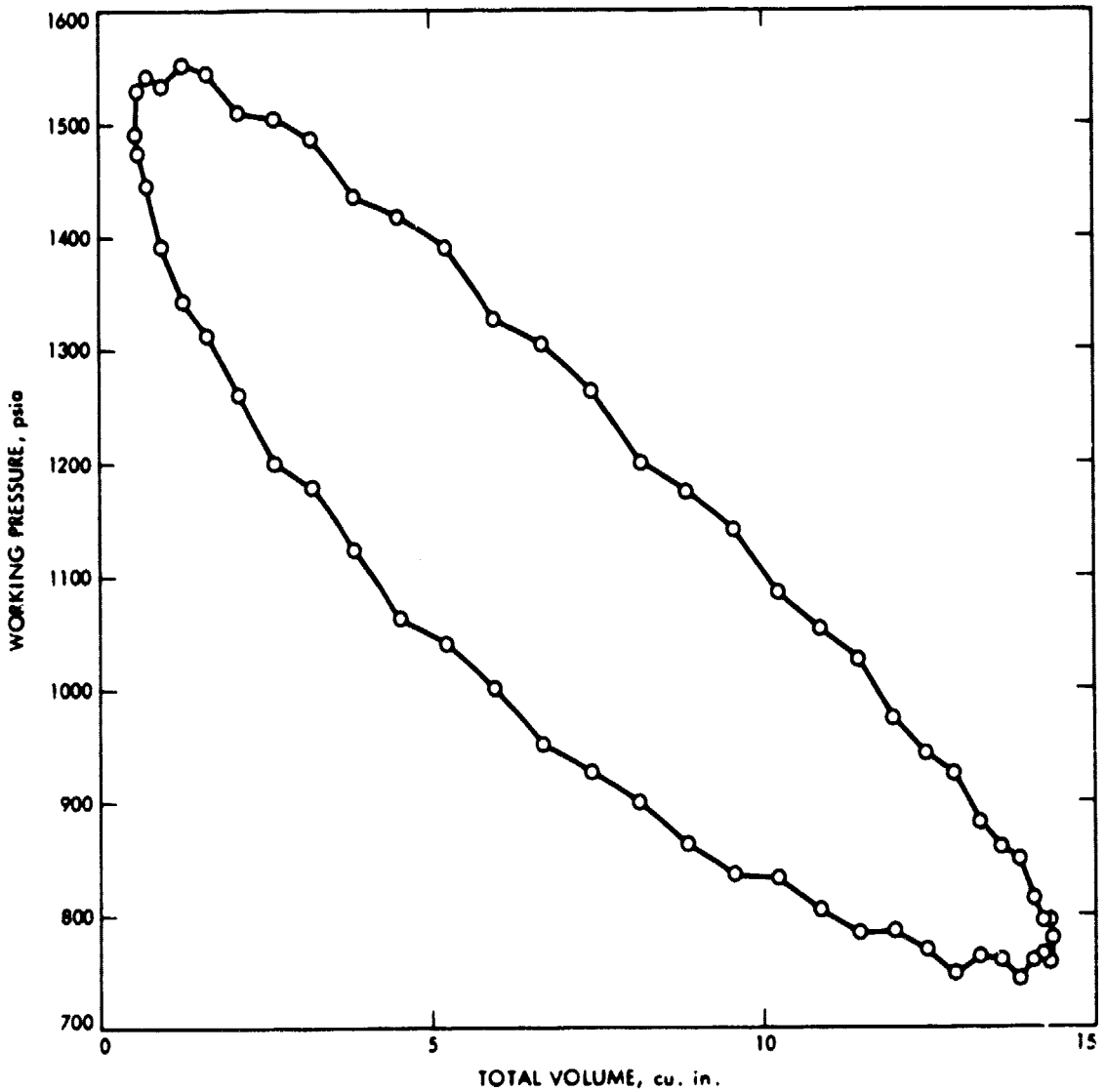

Figure B-3. Pressure-Volume Diagram for Compressor Space

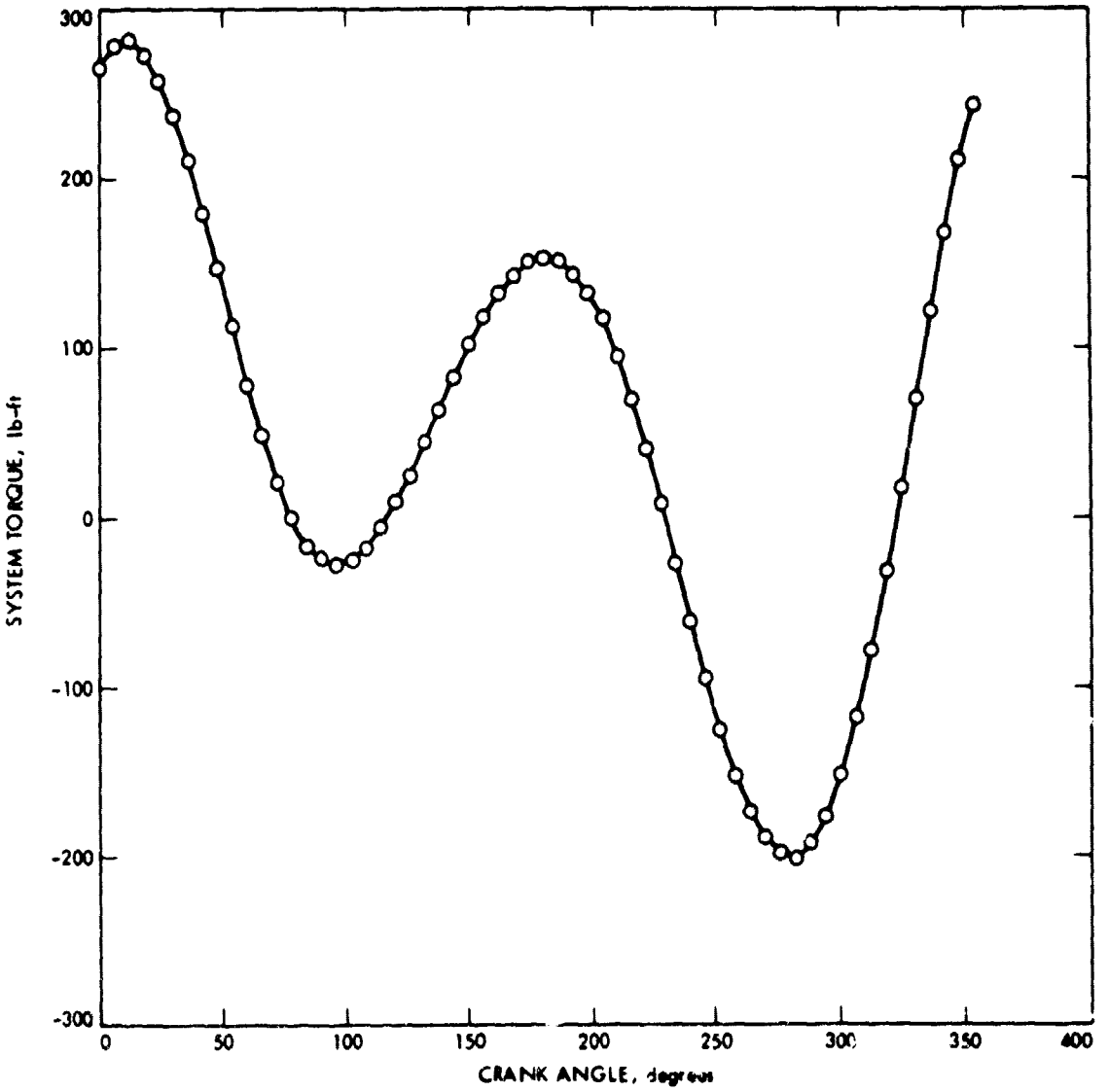

Figure B-5. Indicated Torque for Total Engine System